1957

Structures of some polynuclear metal carbonyls

Lawrence Frederick Dahl
Iowa State College

STRUCTURES OF SOME POLYNUCLEAR METAL CARBONYLS

by

Lawrence F. Dahl

A Dissertation Submitted to the
Graduate Faculty in Partial Fulfillment of
The Requirements for the Degree of
DOCTOR OF PHILOSOPHY

Major Subject: Physical Chemistry

Approved:

Signature was redacted for privacy.

In Charge of Major Work

Signature was redacted for privacy.

Head of Major Department

Signature was redacted for privacy.

Dean of Graduate College

Iowa State College
1957

TABLE OF CONTENTS

INTRODUCTION

Metal carbonyls and their derivatives represent an almost unique class of compounds in the field of transition metal complexes in that their composition in most cases appears to be governed not by consideration of the stable coordination numbers of the metals, but primarily by the tendency of the metal to form closed electronic shells. Although metal carbonyls may be regarded as coordination complexes between zerovalent transition metals and electron donor carbon monoxide molecules, they have the striking physical properties of being electrically neutral and diamagnetic. Chemically metal carbonyls are a reactive class and form a number of very interesting and unusual types of compounds.

The physical and chemical properties of the metal carbonyls have been extensively determined largely through the work of W. Hieber and his school. In Table 1 are summarized some of the physical properties of the known metal carbonyls. However, neither the properties nor the chemical reactions of the metal carbonyls seem to give an insight into their structural aspects.

The metal carbonyls can be subdivided into two classes: (a) volatile mononuclear molecules which are very soluble in

Table 1. Known metal carbonyls and their properties

Metal(atomic number)	Mononuclear Carbonyls	Polynuclear Carbonyls
Cr(24)	$Cr(CO)_6$ colorless, sublimes	
Mn(25)		$Mn_2(CO)_{10}$ golden yellow m.p. 154-155°C.
Fe(26)	$Fe(CO)_5$ yellow m.p. -20°C., b.p. 103°C.	$Fe_2(CO)_9$ golden yellow decomposes 100°C. $[Fe(CO)_4]_3$ dark green decomposes 140°C.
Co(27)		$Co_2(CO)_8$ orange, m.p. 51°C. $[Co(CO)_3]_x$ black, decomposes 60°C.
Ni(28)	$Ni(CO)_4$ colorless m.p. -25°C., b.p. 43°C.	
Cu(29)		$[Cu(CO)_3]_2$* white, sublimes
Mo(42)	$Mo(CO)_6$ colorless, sublimes	
Tc(43)		

*Only qualitative evidence.

Table 1. (Continued)

Metal(atomic number)	Mononuclear Carbonyls	Polynuclear Carbonyls
Ru(44)	$Ru(CO)_5$ colorless, m.p. -22°C.	$Ru_2(CO)_9$ orange, sublimes $[Ru(CO)_4]_3$* green
Rh(45)		$Rh_2(CO)_8$ orange, decomposes 76°C. $[Rh(CO)_3]_x$ deep red, sublimes 150°C. $Rh_4(CO)_{11}$ black, decomposes 200°C.
Pd(46)		
Ag(47)		
W(74)	$W(CO)_6$ colorless, sublimes	
Re(75)		$Re_2(CO)_{10}$ colorless, m.p. 177°C.
Os(76)	$Os(CO)_5$ colorless, m.p. -18°C.	$Os_2(CO)_9$ bright yellow, m.p. 224°C.
Ir(77)		$Ir_2(CO)_8$ greenish yellow, sublimes
Pt(78)		
Au(79)		

non-polar solvents and (b) relatively non-volatile polynuclear molecules (i.e. containing more than one metal atom per molecule) which usually are sparingly soluble in non-polar solvents.

The mononuclear carbonyls have been studied in great detail by electron diffraction, X-ray diffraction, and Raman and infrared analysis. Their structural features are given in Table 2. Each CO ligand can be regarded as contributing two bonding electrons to the metal atom; thus an increase of two in the atomic number of the metal decreases the number of ligands by one. Some of the carbonyls of the first row transition metals and their derivatives found in Table 3 well illustrate that the coordination number of most of the mononuclear carbonyls results from the attainment of an effective atomic number for the metal equal to that of the next inert gas, in this case 36. For all of the mononuclear carbonyls the M-C-O grouping is linear. The bond hybridization and structures of the mononuclear carbonyls have been readily explained with Pauling's theory of directed valence (1).

The only polynuclear carbonyl whose molecular structure has been determined by diffraction methods is $Fe_2(CO)_9$. An X-ray analysis of $Fe_2(CO)_9$ by Powell and Ewens (2) in 1939 showed it to exist in the solid as discrete $(CO)_3Fe(CO)_3Fe-(CO)_3$ units with an approximate molecular symmetry D_{3h}.

Table 2. Structural features of mononuclear carbonyls as determined by diffraction methods

Metal Carbonyl	Molecular Symmetry	Method (ref.)	M-C Distance (Å)	C-O Distance (Å)	Calculated M-C Distance (8)
$Cr(CO)_6$	Octahedral	Eln. D.* (3) X-ray D. (4)	1.92 ± 0.04 ~1.80	1.16 ± 0.05 ~1.15	1.943
$Fe(CO)_5$	Trigonal Bipyramidal	Eln. D. (5)	1.84 ± 0.04	1.15 ± 0.04	1.936
$Ni(CO)_4$	Tetrahedral	X-ray D. (6) Eln. D. (7)	1.84 ± 0.03 1.82 ± 0.03	1.15 ± 0.03 1.15 ± 0.02	1.920
$Mn(CO)_6$	Octahedral	Eln. D. (3) X-ray D. (4)	2.08 ± 0.04 ~2.13	1.15 ± 0.05 ~1.15	2.062
$W(CO)_6$	Octahedral	Eln. D. (3) X-ray D. (4)	2.06 ± 0.04 ~2.13	1.13 ± 0.05	2.070

*Eln. D. = Electron Diffraction.

Table 3. Coordination number and effective atomic number of some first row transition metal carbonyls and their derivatives

Transition metal(atomic number)	Carbonyl	Number of Electrons Donated to Metal	Effective Atomic Number
Cr(24)	$Cr(CO)_6$	12	36
	$Cr(CO)_3Py_3$	12	36
Mn(25)	$Mn(CO)_5Cl$	11	36
Fe(26)	$Fe(CO)_5$	10	36
	$Fe(CO)_4I_2$	10	36
	$Fe(CO)_4H_2$	10	36
	$Fe(CO)_3(NH_3)_2$	10	36
	$Fe(CO)_2(NO)_2$	10	36
	$Fe(CO)_2$(o-phen)I_2	10	36
Co(27)	$Co(CO)_4H$	9	36
	$Co(CO)_3NO$	9	36
	Co(CO)(NO)(o-phen)	9	36
Ni(28)	$Ni(CO)_4$	8	36
	$Ni(CO)_2$(o-phen)	8	36

The structure can be viewed as two octahedra joined at a face, such that the iron atoms are linked by three bridge carbonyl groups. The data were based on single crystal oscillation and zero-layer line Weissenberg photographs around the a_o and c_o axes of thin, hexagonal, crystal plates. The space group was determined to be C $6_3/m$ with two molecules per unit cell, and lattice constants a_o = 6.45 Å, c_o = 15.98 Å. The molecular axis lies along the c_o axis. The interatomic distances and angles found are:

	Fe-Fe	2.46 Å
	Fe-C (in -C ≡ O)	1.9 Å
	Fe-C (in >C = O)	1.8 Å
	-C ≡ O	1.15 Å
	>C = O	1.3 Å
terminal	C-Fe-C angle	94°
bridge	C-Fe-C angle	78°
bridge	Fe-C-Fe angle	87°

This structure has two very important features. First, two types of carbonyl bonds are formed: (a) terminal carbonyl bonds, which, similar to those of the mononuclear carbonyls, contribute two electrons each to the metal atom and (b) bridge carbonyl bonds which contribute one bonding electron to each metal atom. Second, in order to account for the

observed diamagnetism of the molecule the short Fe-Fe distance was interpreted to mean a direct metal-metal bond. Unfortunately, no absorption correction was made for the irregular shape of the crystal (the experimental error reported was ± 0.05 Å). This might account for the fact that the terminal Fe-C bonds, which supposedly possess double bond character, were reported to be longer than the bridge Fe-C bonds which were interpreted as single bonds.

In 1950 a spectral study of $Fe_2(CO)_9$ by Sheline and Pitzer (9) suggested that the stretching frequency of bridge carbonyl groups lies in the same spectral region of about 1800 cm.$^{-1}$ as organic ketonic groups, whereas terminal carbonyl groups absorb around 2000 cm.$^{-1}$. In fact their partial vibrational analysis was found, perhaps fortuitously, to be in agreement with the solid spectrum of $Fe_2(CO)_9$.

The type of vibrational analysis employed by Sheline and Pitzer (9) consists of determining by group theory the number of infrared active and Raman active normal frequencies involving mainly the carbonyl stretching or the metal carbon stretching for the different internuclear structures, and comparing the results with the observed data. The assumption is that the masses and interactions of the atoms are such that the observed frequencies are characteristic of "atom-pair" vibrations. This method neglects forces between

Table 4. Infrared-active carbonyl stretching frequencies of various metal carbonyls

Metal Carbonyl	(state)	Terminal Carbonyl Frequencies ($cm.^{-1}$)	Bridge Carbonyl Frequencies ($cm.^{-1}$)	Ref.
$Cr(CO)_6$	(gas)	2000		10,11
$Fe(CO)_5$	(gas)	2033, 2012		12
$Fe(CO)_5$	(gas)	2028, 1994		9
$Ni(CO)_4$	(gas)	2050		13
$Ni(CO)_4$	(gas)	2060		12
$Ni(CO)_4$	(solution)	2047		12
$Ni(CO)_4$	(solution)	2045		14
$Mo(CO)_6$	(gas)	2000		10
$W(CO)_6$	(solid)	1997		15
$Fe_2(CO)_9$	(solid)	2080, 2034	1828	9
$Fe_2(CO)_9$	(solid)	2082, 2019	1829	16
$Co_2(CO)_8$	(gas)	2079, 2053, 2037	1876	12
$Co_2(CO)_8$	(gas)	2077, 2054, 2034	1859	17
$Mn_2(CO)_{10}$	(C_6H_{12})	2050, 2010, 1988		18
$Mn_2(CO)_{10}$	(CS_2)	2061, 2027, 1998		19
$Mn_2(CO)_{10}$	(solid)	2060, 2014, 1989		19
$Mn_2(CO)_{10}$	(gas)	2068, 2039, 2006		19
$Re_2(CO)_{10}$	(CCl_4)	2078, 2015, 1973		18
$Re_2(CO)_{10}$	(CS_2)	2065, 2006, 1968		19
$Re_2(CO)_{10}$	(gas)	2070, 2019, 1985		19
$[Fe(CO)_4]_3$	(solution)	2052, 2029	1860, 1830	1,20
$[Co(CO)_3]_n$	(C_7H_{16})	2058, 2030	1873	12
$[Co(CO)_3]_n$	($n\text{-}C_6H_{14}$)	2067, 2037	1866	1

non-bonding atoms and interaction effects between bonds and therefore should be much more valid in the gaseous state than in the solid or in solution. Characteristic carbonyl frequencies for the metal carbonyls which have been studied are listed in Table 4.

Further application of this type of vibrational analysis to $Co_2(CO)_8$ has been made by Cable, Nyholm, and Sheline (17) and Friedel, Wender, Shufler, and Sternberg (12). The former postulated three structures which satisfy the spectrum. The first model is obtained by the junction of two trigonal bipyramids at an equatorial edge with the molecular symmetry D_{2h}, resulting in two bridge carbonyl groups (Figure 1a). Another model satisfying the data is a trans-square pyramid structure of C_{2h} symmetry (Figure 1b) which was viewed as less likely from precedent. The third structure proposed, which also possesses C_{2h} symmetry (Figure 1c) is a trans configuration of two trigonal bipyramids joined at an edge such that apical and equatorial carbonyls are shared as bridge carbonyls. The third structure was postulated by Friedel et al. (12) as the most probable structure, since they rejected the D_{2h} structure on the basis of intramolecular distances. A cobalt-cobalt bond again was assumed to account for the observed diamagnetism. It was also pointed out (12) that although it appeared reasonably certain that the band

Figure 1. Proposed structures of $Co_2(CO)_8$

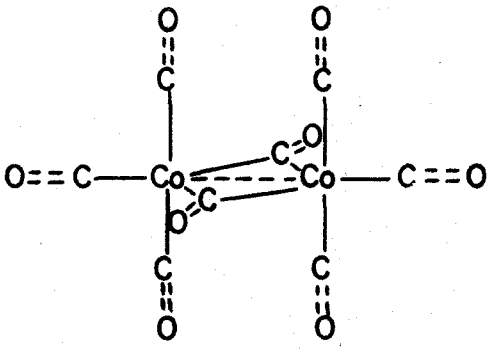

FIG. 1a

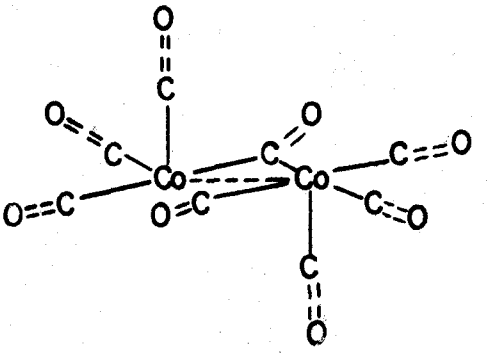

FIG. 1b

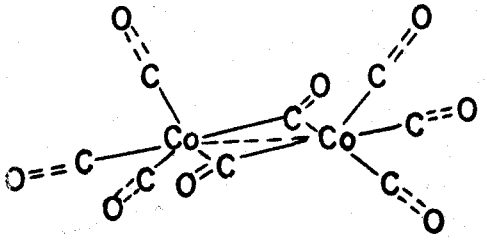

FIG. 1c

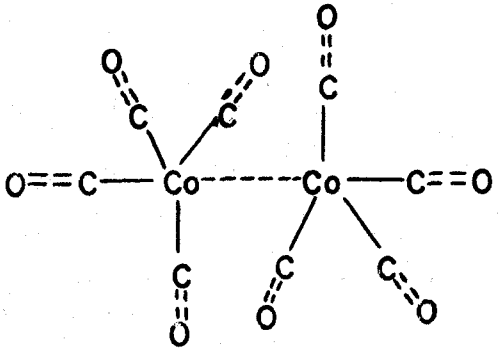

FIG. 1d

at 1876 cm.$^{-1}$ is a bridge carbonyl stretching frequency, a structure such as shown in Figure 1d, in which the dimerization is obtained directly by a cobalt-cobalt bond only, should not be excluded solely on the basis of infrared data. Both the staggered (D_{3d} symmetry) and the eclipsed form (D_{3h} symmetry) of this model predict three bands in the carbonyl region, and the one due to the apical carbonyls can be assigned as the 1876 cm.$^{-1}$ "bridge carbonyl" band.

None of the dinuclear carbonyls of the heavier transition metals have been studied structurally. Cable and Sheline (1) felt that $Ru_2(CO)_9$ and $Os_2(CO)_9$ are isomorphous with $Fe_2(CO)_9$ though they were less certain about $Rh_2(CO)_8$ and $Ir_2(CO)_8$ being similar to $Co_2(CO)_8$.

Structural predictions for the more polymerized carbonyls are open to more doubt. Cobalt tricarbonyl was reported from freezing point measurements (21) to be a tetramer. However, Cable and Sheline (1) from an infrared vibrational analysis predicted a dimeric molecule, such as that shown in Figure 2, in which two cobalt molecules in a square planar configuration are joined at an edge. Support for this possibility is given by the isoelectronic ion $Ni(CN)_3^{=}$ which is dimeric, with square planar nickel and bridge cyano groups (Figure 3). They found no tetrameric structure to fit the infrared data.

Figure 2. Proposed structure of $\left[Co(CO)_3\right]_n$

Figure 3. Structure of $Ni(CN)_3^{-2}$ dimer

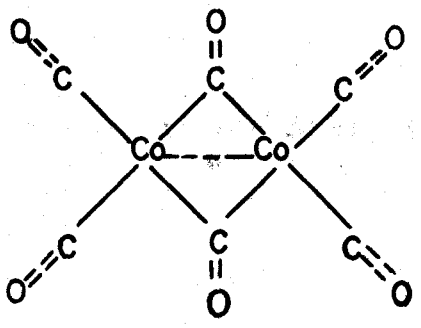

FIG. 2

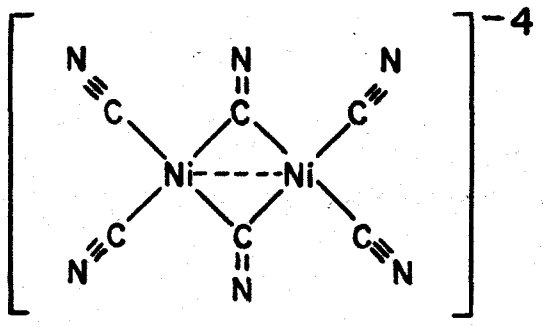

FIG. 3

In 1956 Cotton, Liehr, and Wilkinson (19) suggested that a third type of carbonyl group, involving a pseudo-ring of carbon monoxide ligands lying between the metal atoms, can occur in polynuclear metal carbonyls with a characteristic infrared absorption band around 2000 cm.$^{-1}$. This postulate was applied to $Mn_2(CO)_{10}$ and $Re_2(CO)_{10}$ which show no absorption in the 1800 cm.$^{-1}$ region characteristic of bridging carbonyl groups. On the other hand Brimm et al. (18) and Cable and Sheline (1) have interpreted the spectral data of $Mn_2(CO)_{10}$ and $Re_2(CO)_{10}$ in terms of a structure involving only direct metal-metal bonding.

Thus there exists a great need to bridge the gap between the conflicting postulates concerning the polynuclear metal carbonyl structures and the nature of their bonding. Only then can a clearer formulation be put forth to explain a number of their unusual properties. Therefore, the structural determinations of $[Fe(CO)_4]_3$, $Re_2(CO)_{10}$, and $Mn_2(CO)_{10}$ were undertaken in an attempt to obtain a better understanding of the polynuclear carbonyls.

STRUCTURE OF IRON TETRACARBONYL

Review of Literature

Iron tetracarbonyl is a dark green crystalline compound which decomposes at 140°C. (22; p. 144). The crystals are somewhat unstable in air and decompose slowly. Iron tetracarbonyl is hydrophobic and slightly soluble in non-polar solvents. Magnetic susceptibility measurements showed the compound to be diamagnetic (23, 24, 25). From freezing point measurements in $Fe(CO)_5$ Hieber and Becker (26) found the molecular weight to correspond to a trimeric structure; hence the formula is given as $[Fe(CO)_4]_3$.

Assuming the molecular configuration to be a combination of octahedral and tetrahedral symmetry, Hieber and Becker (26) postulated three arrangements as the probable structures for $[Fe(CO)_4]_3$.

The first (Figure 4a) is structurally similar to $Fe_2(CO)_9$ and is formed by the junction of two octahedra at the opposite faces of an octahedron such that the central iron atom is octahedrally coordinated by six bridge carbonyls (molecular symmetry D_{3d}). The other two configurations involve both tetrahedral and octahedral symmetry: one (Figure 4b) has each terminal iron surrounded by six CO

Figure 4. Proposed structures of $[Fe(CO)_4]_3$

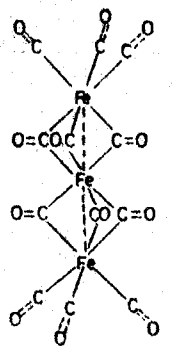

FIG. 4a

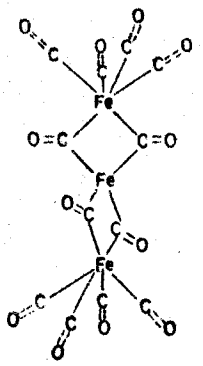

FIG. 4b

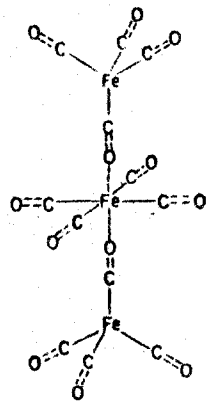

FIG. 4c

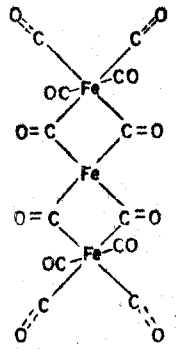

FIG. 4d

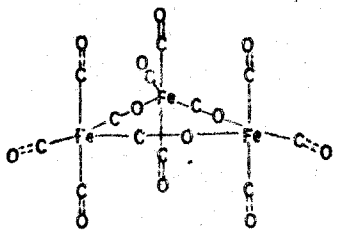

FIG. 4e

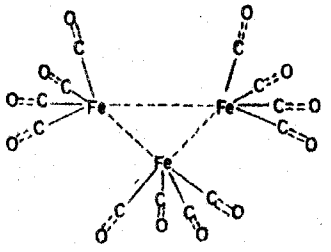

FIG. 4f

groups with the central iron tetrahedrally coordinated to four bridge carbonyl groups (D_{2d} symmetry); the other (Figure 4c) has two terminal iron groups which are both tetrahedrally linked to an octahedrally coordinated central iron by a CO group.

A preliminary X-ray investigation was made in 1931 by Brill (27) who reported $[Fe(CO)_4]_3$ to be a monoclinic, prismatic crystal belonging to the space group C 2/c (C^6_{2h}). The unit cell dimensions he reported are a_B = 13.00 Å; $b_B = c_B$ = 11.41 Å; β_B = 94° 24.9', with twelve $Fe(CO)_4$ species per unit cell. In addition a morphological examination by Brill (27) of the face angles of the prismatic crystals with an optical goniometer indicated C_{2h} symmetry. The c_B and b_B axes are located at right angles to one another across the face diagonals of the base of the prism with the a_B axis inclined upon the base. From the goniometric measurements the axial ratios $a_B:b:c_B$ = 1.136:1:1 with the monoclinic angle β_B = 93° 29.9' were obtained. The axes here have been relabeled to correspond to the X-ray work. Of the three structural formulas suggested by Hieber and Becker (26), Brill, from the pseudo-tetragonal symmetry of the crystal, favored the one with D_{2d} symmetry as the most likely molecular structure.

The electronic structures for the arrangements proposed by Hieber and Becker (26) were further analyzed by Klemm, Jacobi, and Tilk (28). They found it difficult to understand the trimolecular character of $[Fe(CO)_4]_3$ since they expected it to possess a square planar configuration similar to the isoelectronic ion $Ni(CN)_4^{=}$ which is also diamagnetic. They felt that the D_{3d} structure proposed by Hieber and Becker (26) is magnetochemically not very probable. Also they reasoned that with such a molecular configuration one would expect hexagonal symmetry for the crystal. They postulated as the most probable structure one in which each terminal iron is surrounded octahedrally by six CO groups with the inner four CO groups forming a square around the central iron (Figure 4d).

In 1951 a spectral study of the compound was interpreted by Sheline (20) to favor the D_{2d} structure as the one most compatible with the diamagnetic susceptibility, X-ray diffraction, and spectral data. The presence of a very weak band at 1833 $cm.^{-1}$ was attributed to bridge carbonyl groups similar to those in the $Fe_2(CO)_9$ structure. This band was later resolved into two bands at 1830 and 1860 $cm.^{-1}$ by Cable and Sheline (1). Differences between the solubility of $[Fe(CO)_4]_3$ and $Fe_2(CO)_9$ in non-polar solvents, together with a weak electronic transition at 2835 $\mathring{A}$ supposedly

characteristic of ketone carbonyls, were also given by Sheline as support for this structure. In 1956 Cable and Sheline (1) elaborated on the electronic configuration of the proposed D_{2d} molecule in which the central iron atom forms four tetrahedral bonds by utilization of the d^3s hybrid orbitals while the end iron atoms form trigonal prism d^2sp^3 hybrid orbitals.

It should be noted that the central iron atom in this postulated structure would possess only thirty electrons instead of thirty-six electrons predicted by the closed electronic shell rule which is evidently followed by other "known" metal carbonyls. Also, no vibrational analysis of the D_{2d} structure was given.

Previous to the X-ray work on $Fe_2(CO)_9$ Sidgwick and Bailey (29) suggested that in the polynuclear carbonyls both the unshared pairs of electrons in the CO group were utilized to join together the metal atoms forming a linear arrangement (i.e. -M-C≡O-M-) such as that found in the structure proposed by Hieber and Becker (26). For $\left[Fe(CO)_4\right]_3$ they (29) suggested a trigonal structure involving such a link (Figure 4e).

Another trigonal structure viewed as one of the more promising ones, but rejected by Sheline (20) because of the

absence of bridge carbonyls, consists of three $Fe(CO)_4$ species linked by direct iron-iron bonding (Figure 4f).

A preliminary X-ray investigation by Florio and Rundle (30) in 1951 indicated that the space group assignment by Brill is wrong. In addition, $Fe(CO)_5$ which decomposes readily and which might complex with $[Fe(CO)_4]_3$ is a seemingly poor choice as a solvent in the molecular weight determination of $[Fe(CO)_4]_3$, and hence the existence of $[Fe(CO)_4]_3$ as a trimer is not definitely established.

Experimental Procedure and Results

Preparation and identification

Iron tetracarbonyl was first prepared by thermal decomposition of $Fe_2(CO)_9$ in CaH_2-dried toluene using vacuum techniques to prevent decomposition of the $[Fe(CO)_4]_3$. (A vacuum line was generously made available by Dr. R. Schaeffer of Iowa State College.) The $Fe_2(CO)_9$ compound was prepared from $Fe(CO)_5$ by a modification of the method of Speyer and Wolf (31), in this case utilizing an argon atmosphere and a mercury arc.

In addition to the prisms of $[Fe(CO)_4]_3$ reported by Brill (27) and Sheline (20), some very small needles were

obtained. X-ray pictures showed the two forms to have the same internal structure.

In order to obtain better crystals, $[Fe(CO)_4]_3$ was prepared directly from $Fe(CO)_5$ by oxidation with MnO_2 (32). Crystallization from different solvents yielded both crystal forms. Krylon was sprayed on the crystals to prevent decomposition. The infrared spectrum of the resulting material checked with the spectrum reported by Sheline (20). An iron analysis yielded an average of 33.74 per cent in comparison to a theoretical value of 33.26 per cent.

Diffraction data

X-ray diffraction data from small needle crystals were obtained with Cu irradiation normal to the needle axis. The Laue symmetry 2/m was indicated which placed the compound in the monoclinic class. The lattice constants and β_B angle obtained from precession and Weissenberg pictures are as follows:

$$a_B = 12.93 \text{ Å}$$

$$b_B = 11.33\ \text{Å} \qquad \beta_B = 93^\circ\ 45'$$

$$c_B = 11.44\ \text{Å (needle axis)}$$

Both Weissenberg and precession diffraction data showed the unit cell to be B-centered instead of C-centered as reported by Brill (27). The reflections observed by Brill (27) were reindexed by an interchange of the k and ℓ indices, and the results correlated very well with the author's observed reflections. Since the unit cell was found to be B-centered, a primitive monoclinic cell with half the B-centered cell volume was chosen. The index transformation from the B-centered cell to the primitive cell (Figure 5) was made with the following relationships:

$$h_p = \frac{\ell_B - h_B}{2} \qquad \ell_p = \frac{\ell_B + h_B}{2} .$$

The subscript "B" refers to the B-centered cell; the subscript "p" to the primitive cell.

Pictures of prismatic crystals were taken, and the resulting lattice constants, based on the primitive unit cell, determined from precession data are:

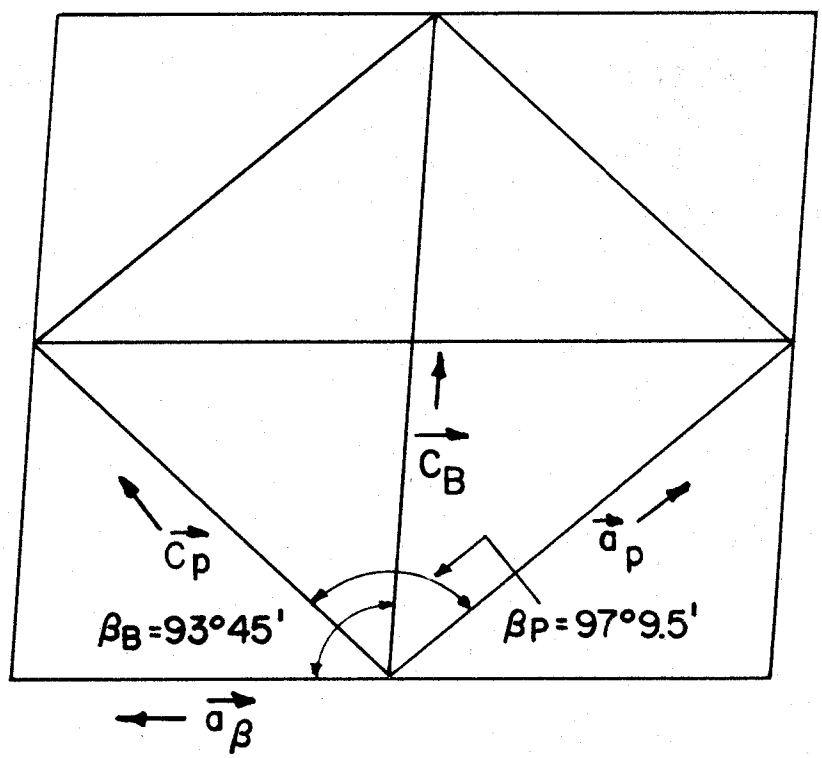

Figure 5. The unit cell of $[Fe(CO)_4]_3$

$$a_p = 8.88\ \text{Å}$$

$$b_p = 11.33\ \text{Å} \qquad \beta_p = 97^\circ\ 9.5'$$

$$c_p = 8.35\ \text{Å}$$

Six $Fe(CO)_4$ species per unit cell give a calculated density $d_{calc.}$ = 2.01 g./cc. compared with the experimental value $d_{exp.}$ = 2.03 g./cc. which was determined by the flotation method (Brill (27) reported an experimental density of 2.0 g./cc.).

The indexed data showed the occurrence of the following systematic extinctions:

1. (hkℓ) data - none, signifying a primitive lattice.
2. (0kℓ) data - k = 2n + 1 absent for (0k0) reflections observed through the 12th order.

   (hk0) data - k = 2n + 1 absent for (0k0) reflections observed through the 8th order. This signified a 2_1 screw axis in the b_p direction, or the atoms were located such that $\Delta_y \approx 30/60$.
3. (h0ℓ) data - h + ℓ = 2n + 1 absent for (h0ℓ). This strongly implied an "n" glide in the b direction

with the much less likely possibility that the atoms were oriented such that $\Delta x \approx 30/60$ and $\Delta z \approx 30/60$.

These systematic absences pointed to the centrosymmetric space group $P2_1/n$ as the most probable one, although other space groups considered included P2/n, P2/m, $P2_1/m$, and Pn.

The unit cell contains six iron atoms, twenty-four carbon atoms, and twenty-four oxygen atoms. From the symmetry positions of the space group $P2_1/n$ which are shown in Figure 6 two iron atoms were arbitrarily placed on centers of symmetry in the two-fold set (a) 0,0,0; $\frac{1}{2},\frac{1}{2},\frac{1}{2}$. The possibility of the four iron atoms occupying two of the other two-fold sets was immediately ruled out by the data. The most probable arrangement of the atoms was thus:

1. Two iron atoms in the special positions (a) with no parameters.
2. One set of iron atoms in the four-fold general set (e) with three parameters.
3. Six sets of oxygen atoms in the four-fold general set (e) with eighteen parameters.
4. Six sets of carbon atoms in the four-fold general set (e) with eighteen parameters.

Figure 6. Symmetry positions in the space group $P2_1/n$

Point positions:

2: (a) 000; $\frac{1}{2}\frac{1}{2}\frac{1}{2}$ (b) $\frac{1}{2}00$; $0\frac{1}{2}\frac{1}{2}$

(c) $0\frac{1}{2}0$; $\frac{1}{2}0\frac{1}{2}$ (d) $00\frac{1}{2}$; $\frac{1}{2}\frac{1}{2}0$

4: (e) xyz; $\frac{1}{2} + x, \frac{1}{2} - y, \frac{1}{2} + z$

$\bar{x}\bar{y}\bar{z}$; $\frac{1}{2} - x, \frac{1}{2} + y, \frac{1}{2} - z$

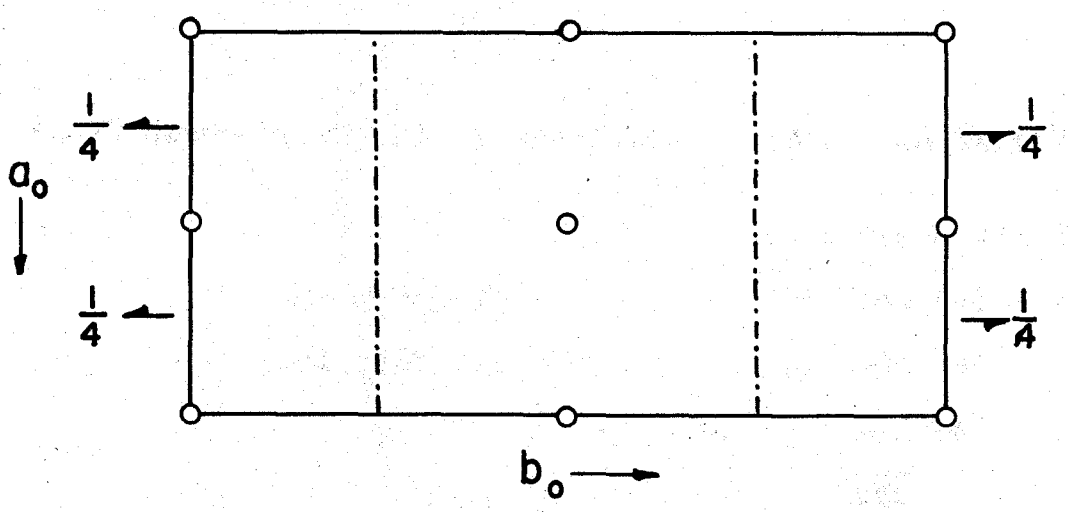
1/4
1/4
1/4
1/4
a_o
b_o

The positions of the six $Fe(CO)_4$ species in the unit cell were hence determined by thirty-nine parameters, which presented a formidable problem. The above model, with two iron atoms on centers of symmetry and the other iron atoms related in pairs by the center of symmetry, strongly suggested that the molecule exists as a linear trimer.

The following intensity data were taken with several crystals.

1. ($h0\ell$) - Precession pictures - Mo irradiation - Timed exposures.
2. ($hk0$) - Precession pictures - Mo irradiation - Timed exposures.
3. ($0k\ell$) - Precession pictures - Mo irradiation - Timed exposures.
4. ($h\ell\ell$) - Precession pictures - Mo irradiation - Timed exposures.
5. ($\bar{h}kh$) - Precession pictures - Mo irradiation - Timed exposures.
6. (hkh) - Weissenberg pictures - Cu irradiation - Multiple film.
7. ($0k\ell$) - Weissenberg pictures - Co irradiation - Multiple film.
8. ($1k\ell$), ($2k\ell$), ($3k\ell$), ($4k\ell$) - Weissenberg pictures - Co irradiation - Multiple film.

Correct indexing and intensity scaling of the data for the different zones were checked by comparing the intensities of common reflections. Since copper irradiation causes iron to fluoresce, a cobalt tube was used in obtaining Weissenberg data. Unfortunately, the intensities of the reflections from the cobalt irradiation showed considerable discrepancy on comparison with the same reflections obtained with Mo irradiation. Consequently, three-dimensional Weissenberg data involving eight layer lines around the b_p axis were obtained by the multiple film technique with Mo irradiation to minimize absorption effects as well as to provide means by which three-dimensional Patterson sections could be run.

To determine whether the crystal has a center of symmetry, as indicated by the space group $P2_1/n$, an analysis of the distribution of intensities characteristic of centrosymmetry was applied to the three principal zones (33). This method works best when the atoms are not in special positions and when there are a sufficient number of reflections for the method to be statistical. The resulting evidence supported a centrosymmetric space group or else indicated that the crystal is very nearly centrosymmetric.

The intensities of the reflections were visually estimated and corrected for Lorentz and polarization factors

(34) to give relative $F(hk\ell)^2$'s. A standard set of intensities based on one reflection was used to judge the intensities.

Patterson projections

Two-dimensional Patterson projections (35; 36, p. 150) involving the $(h0\ell)$, $(hk0)$, $(0k\ell)$, (hkh), and $(\bar{h}kh)$ data were computed using IBM equipment. These are shown in Figures 7, 8, 9, 10, and 11. It was hoped that these projections would reveal the parameters of the iron atoms from which their phases could be calculated. The inherent assumption in this method (i.e. the "heavy atom" method) is that the irons' phase angles for each reflection should give a Fourier electron-density synthesis which is a close approximation to the complete structure.

Since the diffraction photographs indicated a high temperature factor for the crystal, "sharpened" Patterson projections (36, p. 170; 37, p. 376) of the three principal zones $(h0\ell)$, $(hk0)$, and $(0k\ell)$ based on the function:

$$\left|F_M(hk\ell)\right|^2 = \left[\sum_{j=1}^{N} Z_j \Big/ \sum_{j=1}^{N} f_{oj}\right]^2 \left|F(hk\ell)\right|^2$$

were also computed (Figures 12, 13, and 14) in an attempt to resolve the iron peaks as well as to bring out more detail.

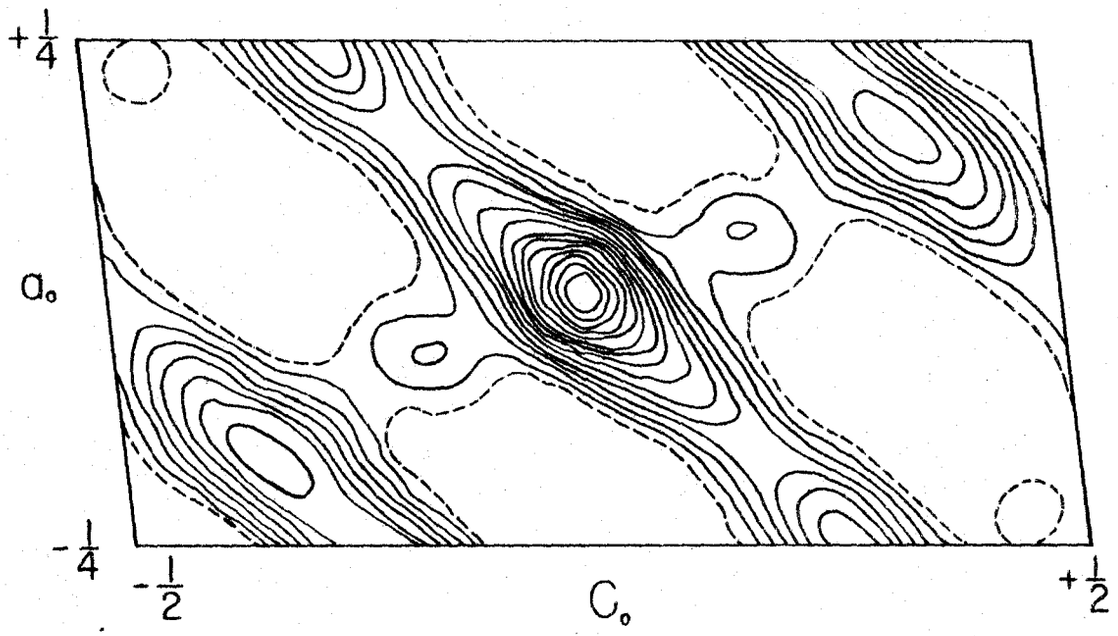

Figure 7. Patterson projection onto the (010) plane

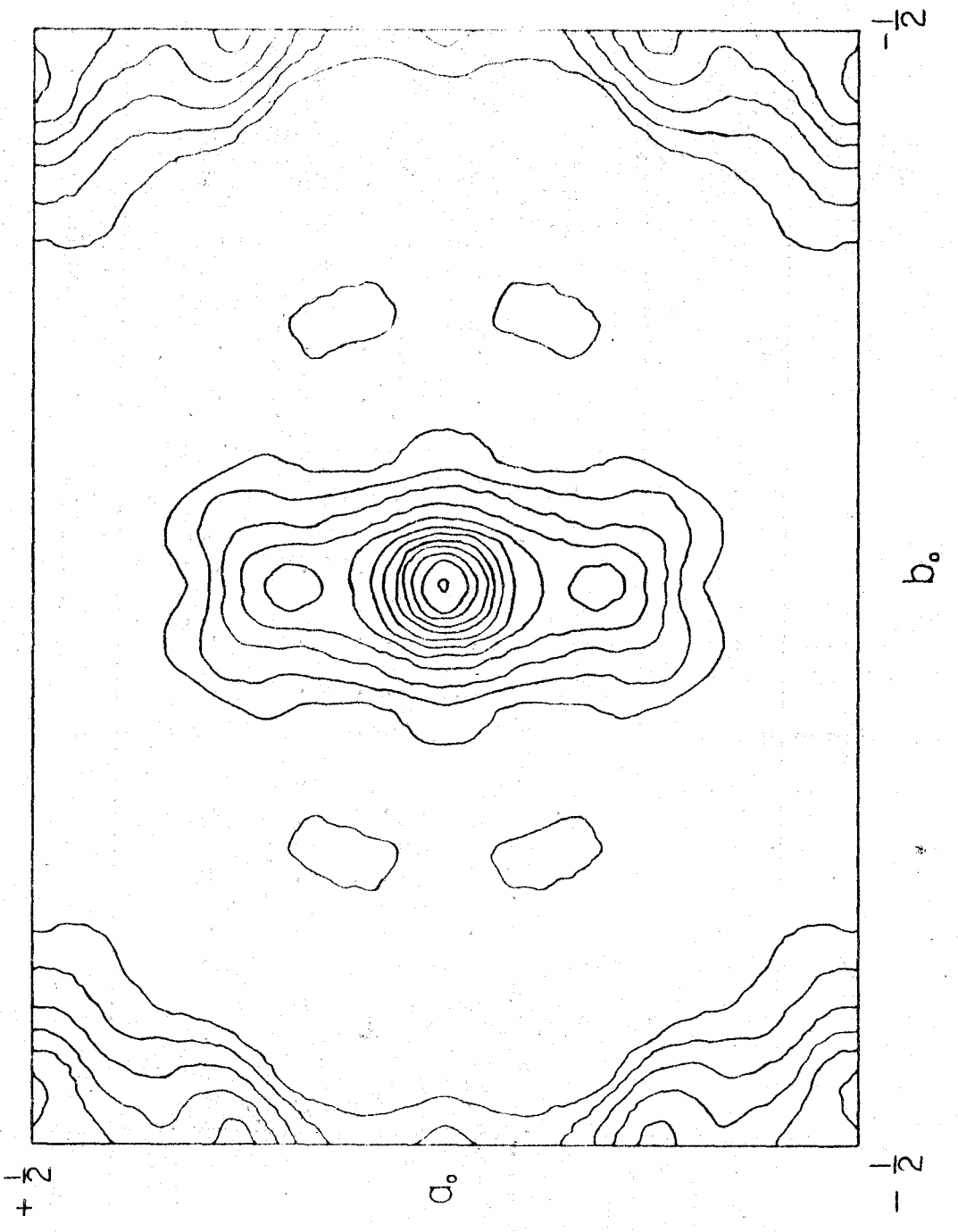

Figure 8. Patterson projection onto the (001) plane

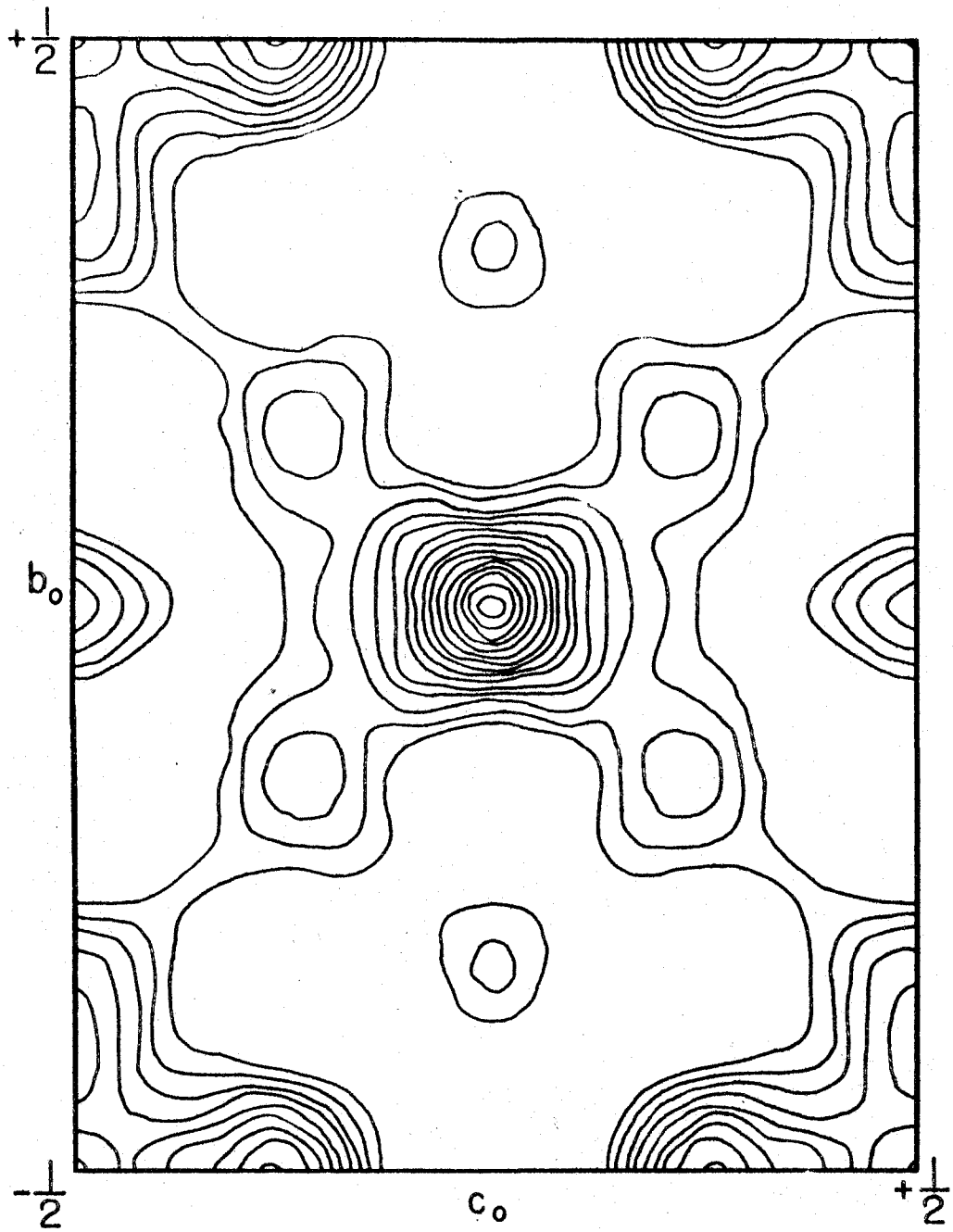

Figure 9. Patterson projection onto the (100) plane

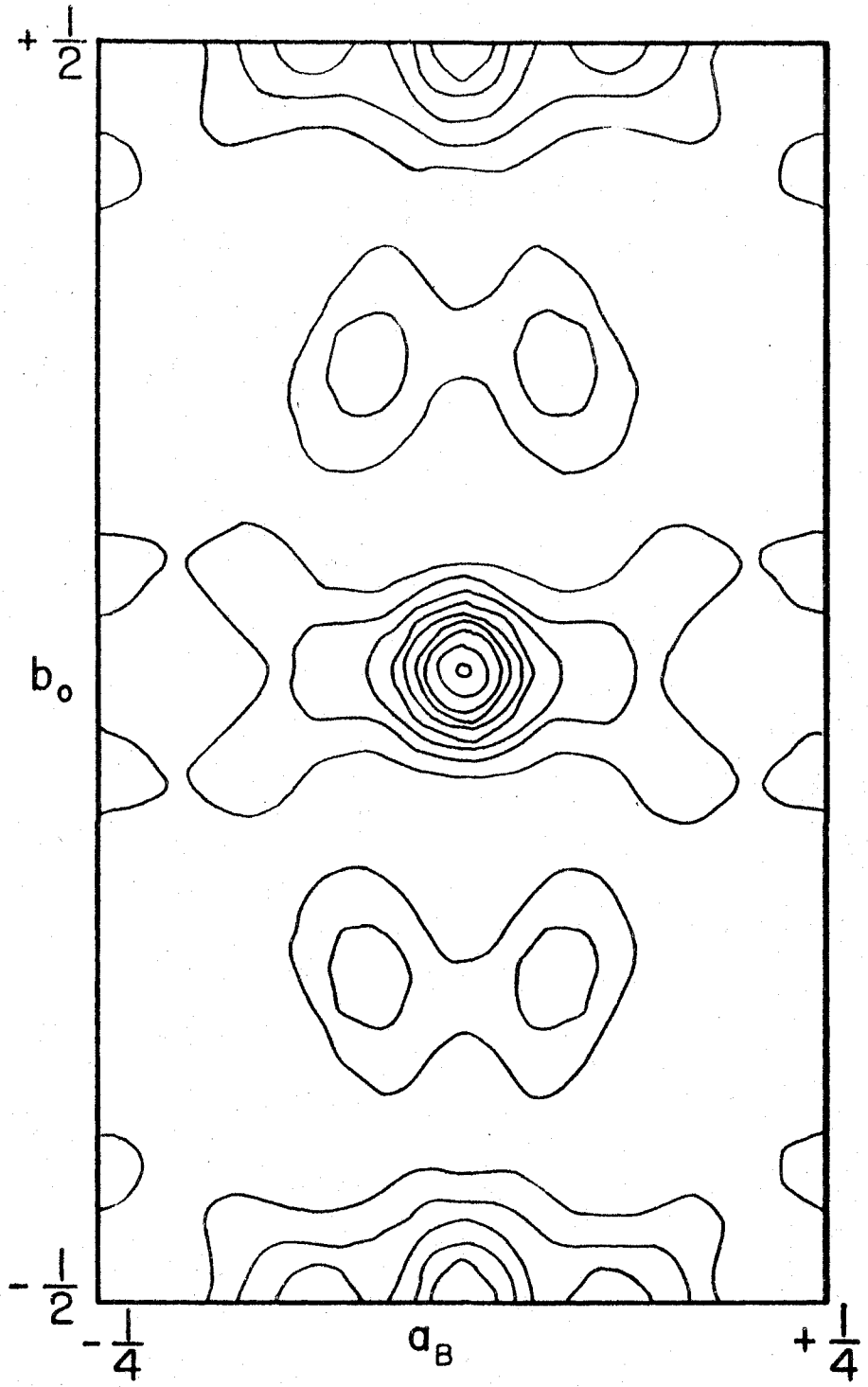

Figure 10. Patterson projection onto the (101) plane

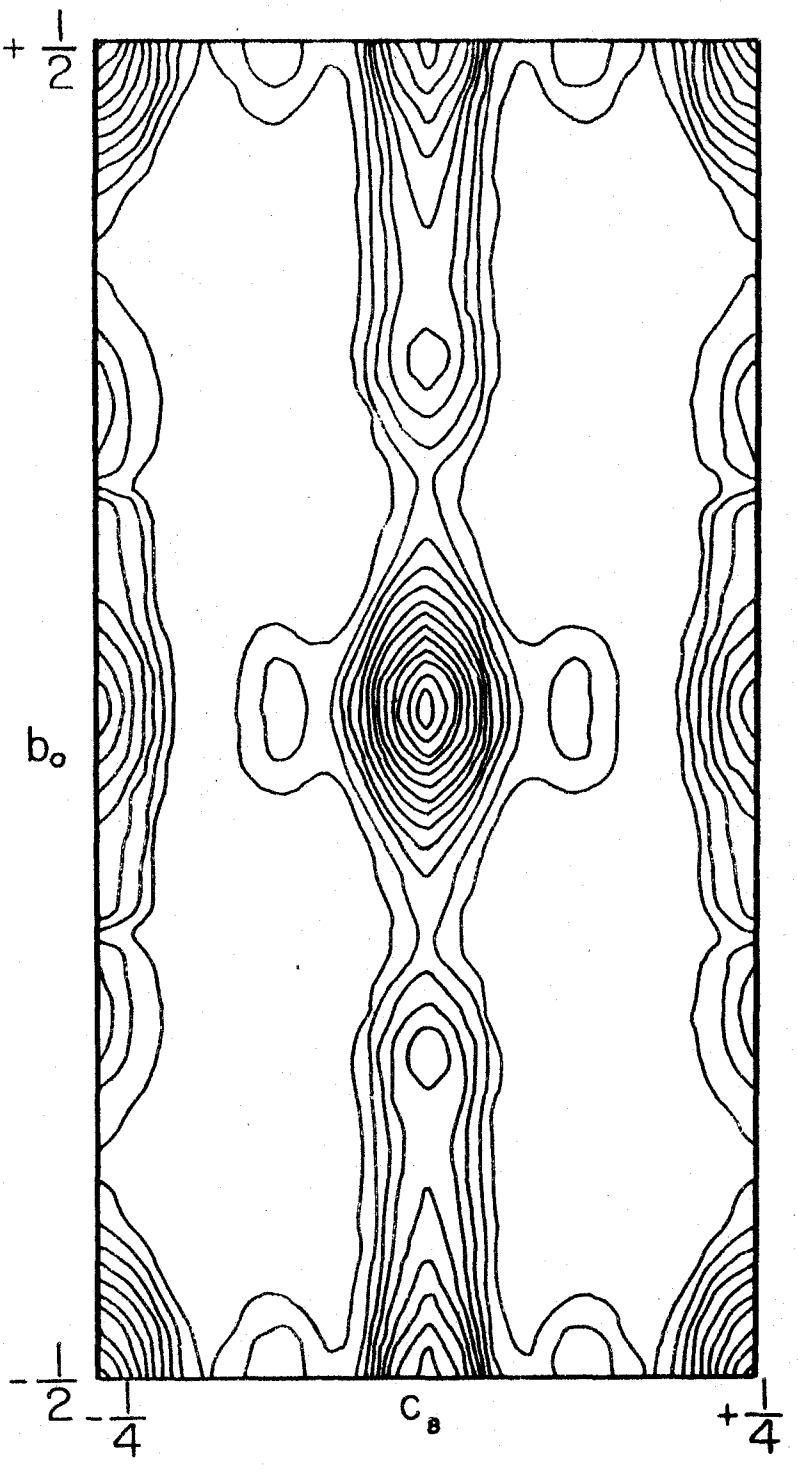

Figure 11. Patterson projection onto the ($\bar{1}$01) plane

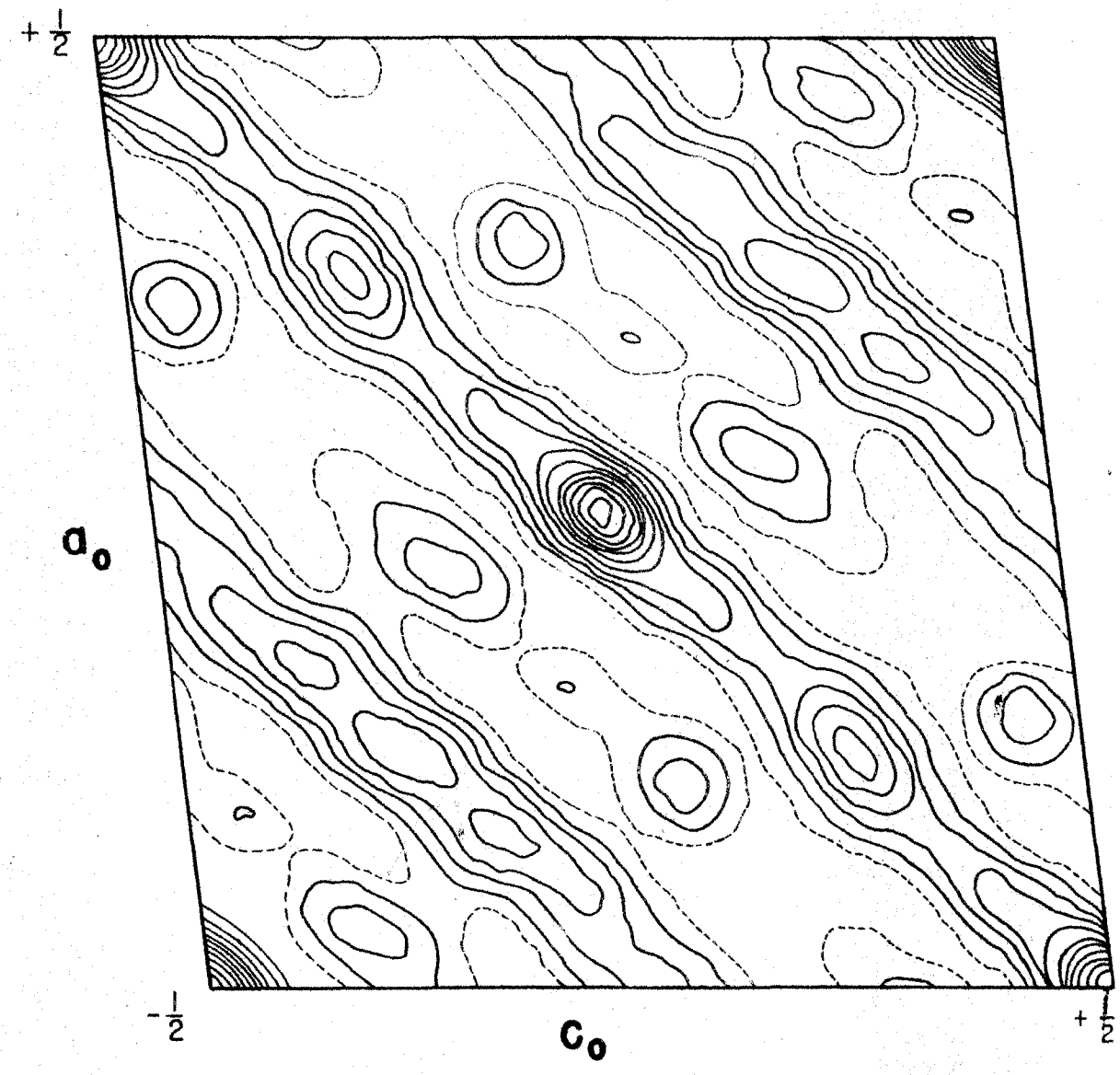

Figure 12. "Sharpened" Patterson projection onto the (010) plane

Figure 13. "Sharpened" Patterson projection onto the (001) plane

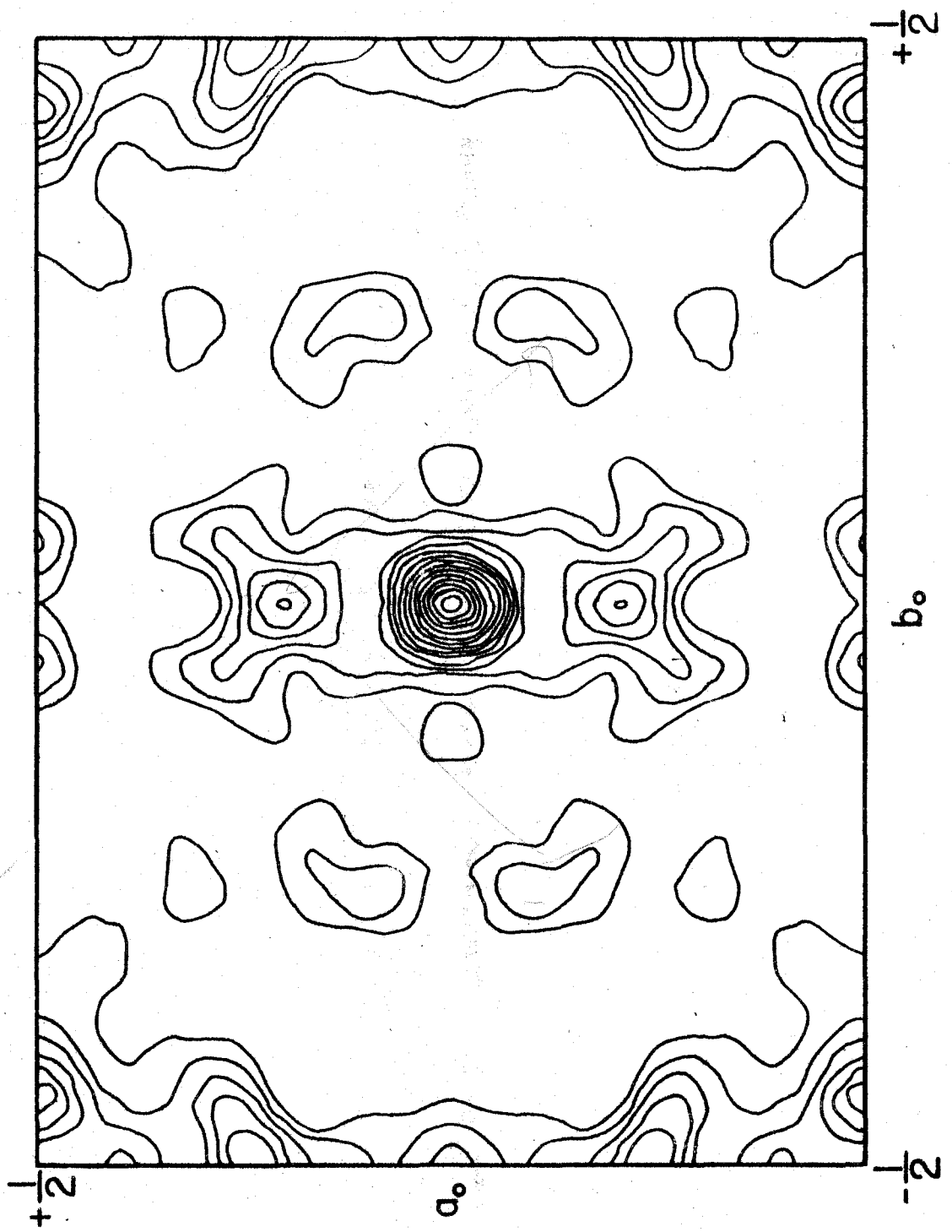
+½
b°
-½
-½
a°
+½

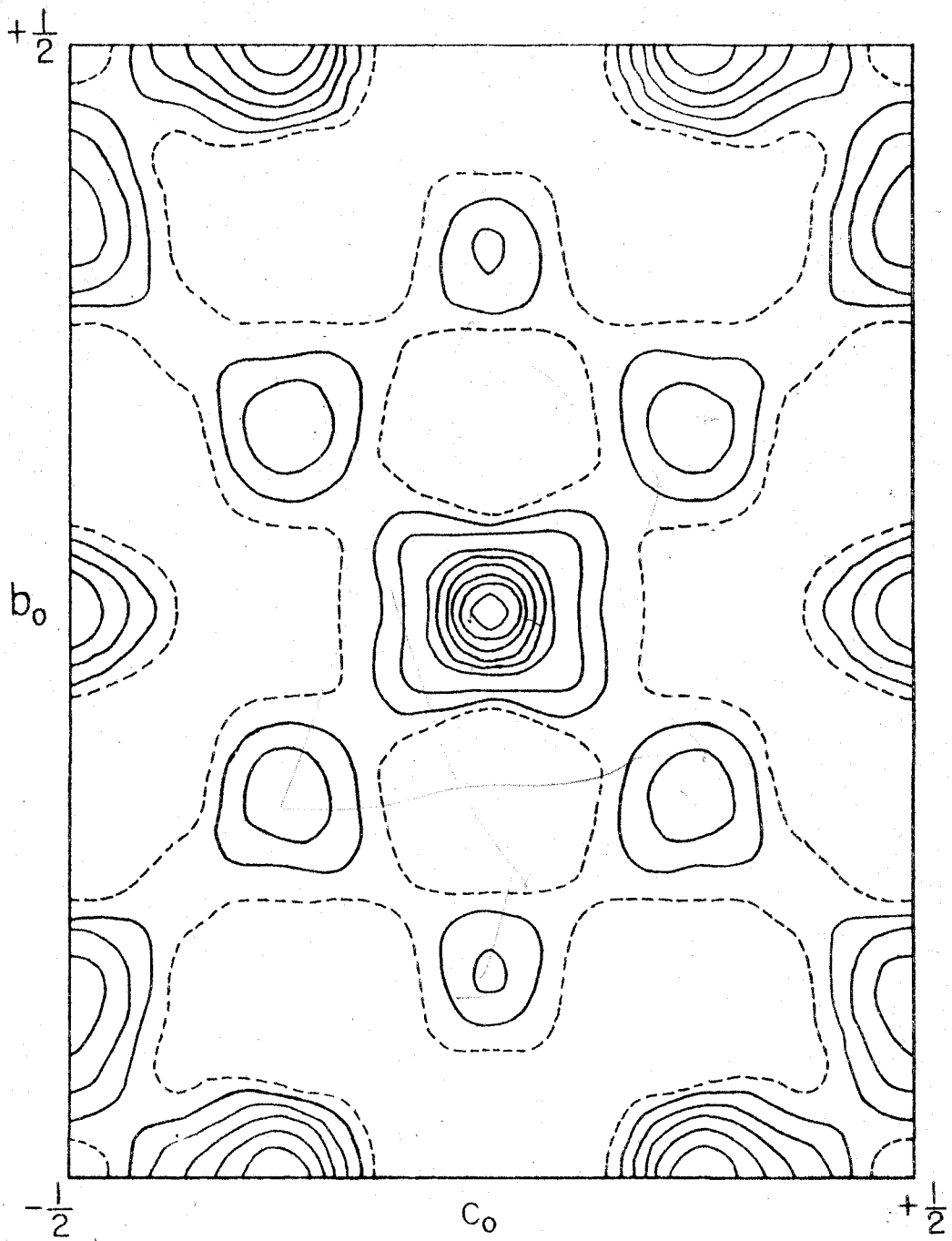

Figure 14. "Sharpened" Patterson projection onto the (100) plane

Here f_{oj} represents the atomic scattering factor, Z_j the atomic number, and $F(hk\ell)$ the observed structure factor. This type of projection depends on the modified coefficients $|F_M(hk\ell)|^2$ giving a distribution with considerably sharper maxima than those given by the regular Patterson series with the coefficients $|F(hk\ell)|^2$, although this necessarily introduces termination error, resulting in more false detail. Physically, such a method corresponds to reducing the thermal motion of the atoms.

With the assumption that two iron atoms were in the two-fold set (a) and the other four in the four-fold general set (e) given in Figure 6, the Patterson iron-iron vectors for the space group $P2_1/n$ were derived for the six iron atoms and are given as follows:

Vector	Multiplicity	Vector	Multiplicity
0,0,0	6		
$\frac{1}{2},\frac{1}{2},\frac{1}{2}$	2		
x,y,z	2	2x,2y,2z	1
$x,\bar{y},z$	2	$2x,2\bar{y},2z$	1
$\bar{x},y,\bar{z}$	2	$2\bar{x},2y,2\bar{z}$	1
$\bar{x},\bar{y},\bar{z}$	2	$2\bar{x},2\bar{y},2\bar{z}$	1

Vector (cont.)	Multiplicity (cont.)	Vector (cont.)	Multiplicity (cont.)
$\frac{1}{2} + x, \frac{1}{2} - y, \frac{1}{2} + z$	2	$\frac{1}{2} + x, \frac{1}{2} + y, \frac{1}{2} + z$	2
$\frac{1}{2} - x, \frac{1}{2} + y, \frac{1}{2} - z$	2	$\frac{1}{2} - x, \frac{1}{2} - y, \frac{1}{2} - z$	2
$\frac{1}{2} + 2x, \frac{1}{2}, \frac{1}{2} + 2z$	2	$\frac{1}{2}, \frac{1}{2} + 2y, \frac{1}{2}$	2
$\frac{1}{2} - 2x, \frac{1}{2}, \frac{1}{2} - 2z$	2	$\frac{1}{2}, \frac{1}{2} - 2y, \frac{1}{2}$	2

An interpretation of the "unsharpened" and "sharpened" Patterson projections based on the above iron vector set was unsuccessful. There appeared to be little correlation among the parameters of the big peaks of the different projections. For instance the "sharpened" (0kℓ) projection indicated a small minimum at $y = \frac{1}{2}$, $z = \frac{1}{2}$ in constrast to the (h0ℓ) projection which showed a large maximum at $x = \frac{1}{2}$, $z = \frac{1}{2}$. The above vector set unequivocally placed two iron vectors at $x = \frac{1}{2}$, $y = \frac{1}{2}$, $z = \frac{1}{2}$. The general features of these projections therefore indicated a tremendous overlap of Patterson peaks, and the problem was of such complexity that three-dimensional projections were needed to resolve the individual peaks from which an interpretation could be made.

Three-dimensional Patterson

A complete three-dimensional Patterson of $[Fe(CO)_4]_3$ involving the synthesis of thirty-one sections at intervals

of 1/60 (corresponding to ~ 0.2 Å) along the b_p axis was prepared. The general three-dimensional Patterson function is given by:

$$P(x,y,z) = c \sum_h \sum_\ell \left[\sum_k |F(hk\ell)|^2 \cos 2\pi ky \right] \cos 2\pi (hx + \ell z) .$$

The relative $|F(hk\ell)|^2$'s of approximately 400 independently observed reflections were used, and the entire procedure was carried out on IBM using punched cards. The resulting projections were plotted on paper from which tracings were made with India ink on window glass. A wood frame was constructed to hold the thirty-one glass panes; a three-dimensional scale of 1 Å = 3.6 cm. was maintained. The resulting Patterson consisted of columns of vectors arranged along the (101) direction as shown by a picture of the model in Figure 15.

The Patterson section $P(x,\frac{1}{2},z)$ is a Harker section for $P2_1/n$, and the projection of this section upon the xz plane will contain the vectors connecting the atoms symmetrically related by the operation of the two-fold screw axis. Hence, one-half of the vector from the origin to such a maximum gives directly the distance and direction of an atom from one of the screw axes of the crystal (i.e. in $P2_1/n$ there are two independent screw axes located at $x = \frac{1}{4}$, $z = \frac{1}{4}$, and $x = 3/4$, $z = \frac{1}{4}$ with the center of symmetry at the origin). Difficulties

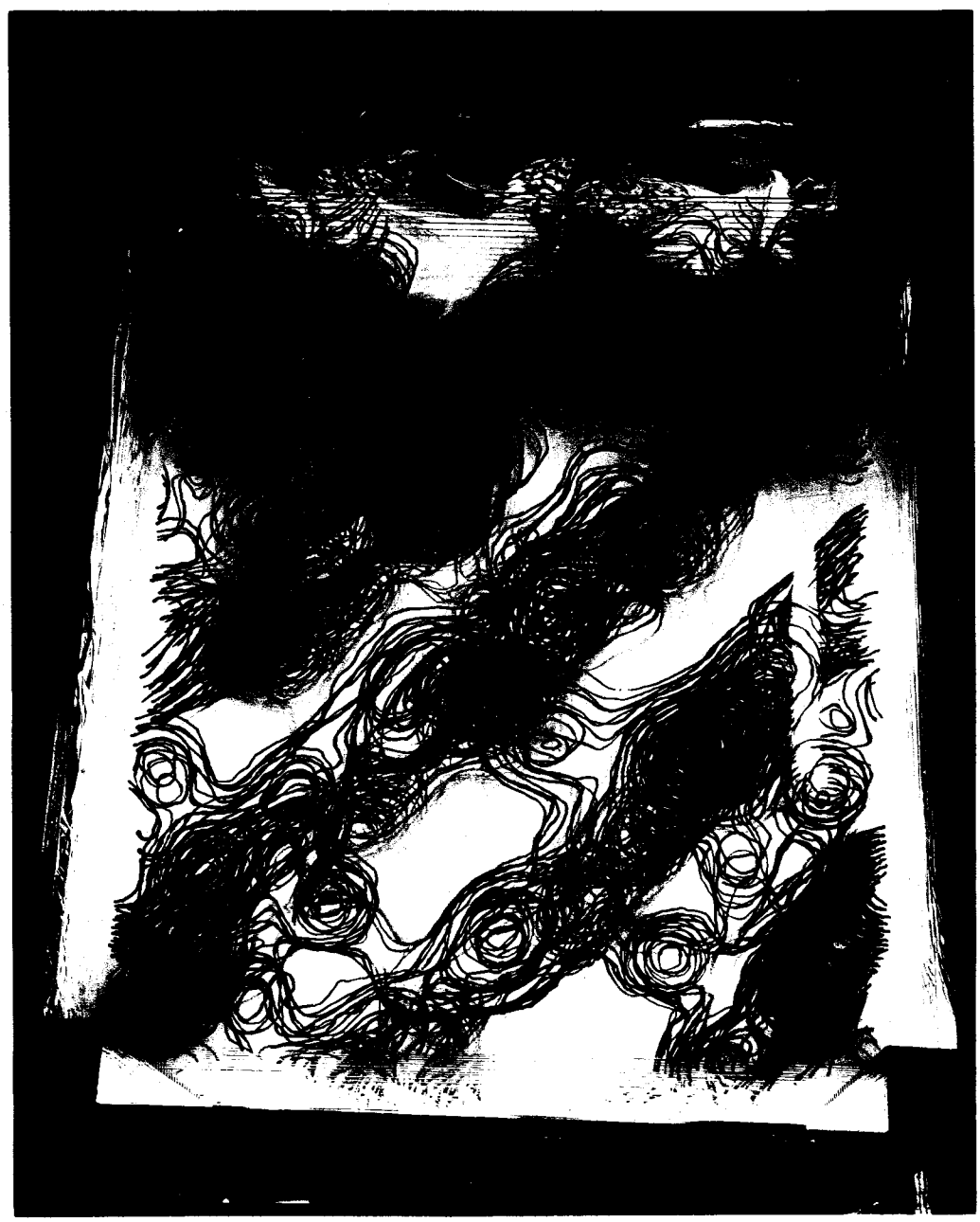

Figure 15. Model of three-dimensional Patterson

arise since such a plot also contains an equal number of peaks resulting from the inability of the function to distinguish between the two independent screw axes in the unit cell. Also, if two or more atoms lie in or near the same plane perpendicular to the two-fold screw axis, other maxima (non-Harker peaks) of twice the weight of the Harker peaks appear. The Patterson section P(x,0,z) confirmed the presence of a number of crystallographically different atoms lying in the same xz plane and showed that the non-Harker peaks were swamping the Harker peaks in the P(x,$\frac{1}{2}$,z) section.

A P($\frac{1}{2}$,y,$\frac{1}{2}$) Harker section corresponding to an "n" glide in the b_p direction was also computed (Figure 16). The results, interpreted in terms of the Harker vectors of an "n" glide, indicated a large electron-density at y $\sim$ 0/60, 15/60, and 30/60.

Generalized "sharpened" Patterson projection

In order to determine the effect on the three-dimensional Patterson sections of high order data other than (h0ℓ), an (h1ℓ) generalized "sharpened" Patterson projection (36, p. 175) was prepared, and the results shown in Figure 17, in general substantiated the three-dimensional Patterson

Figure 16. The Harker section $P(\frac{1}{2},y,\frac{1}{2})$

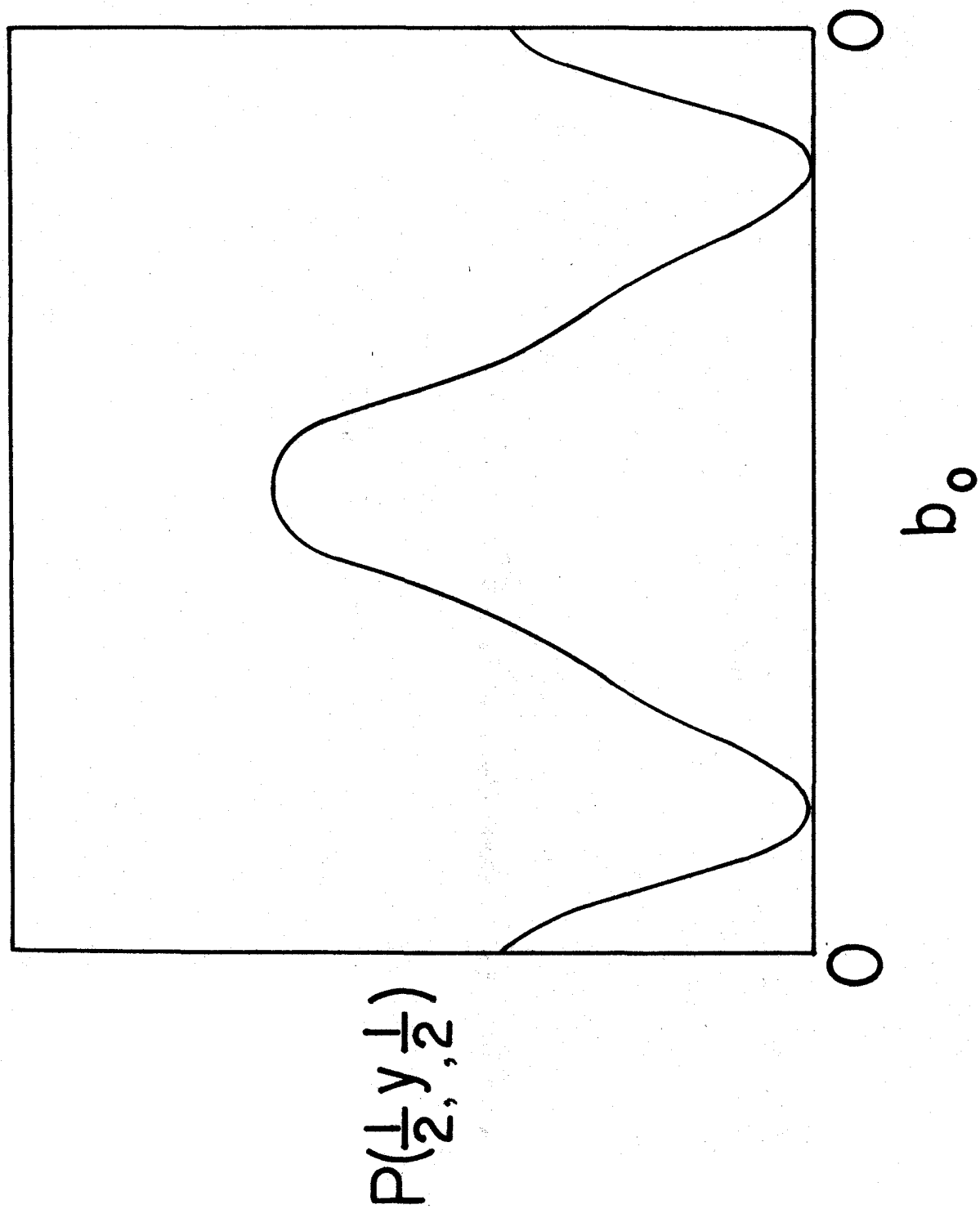
O
O
b_o
$P(\frac{1}{2}, y, \frac{1}{2})$

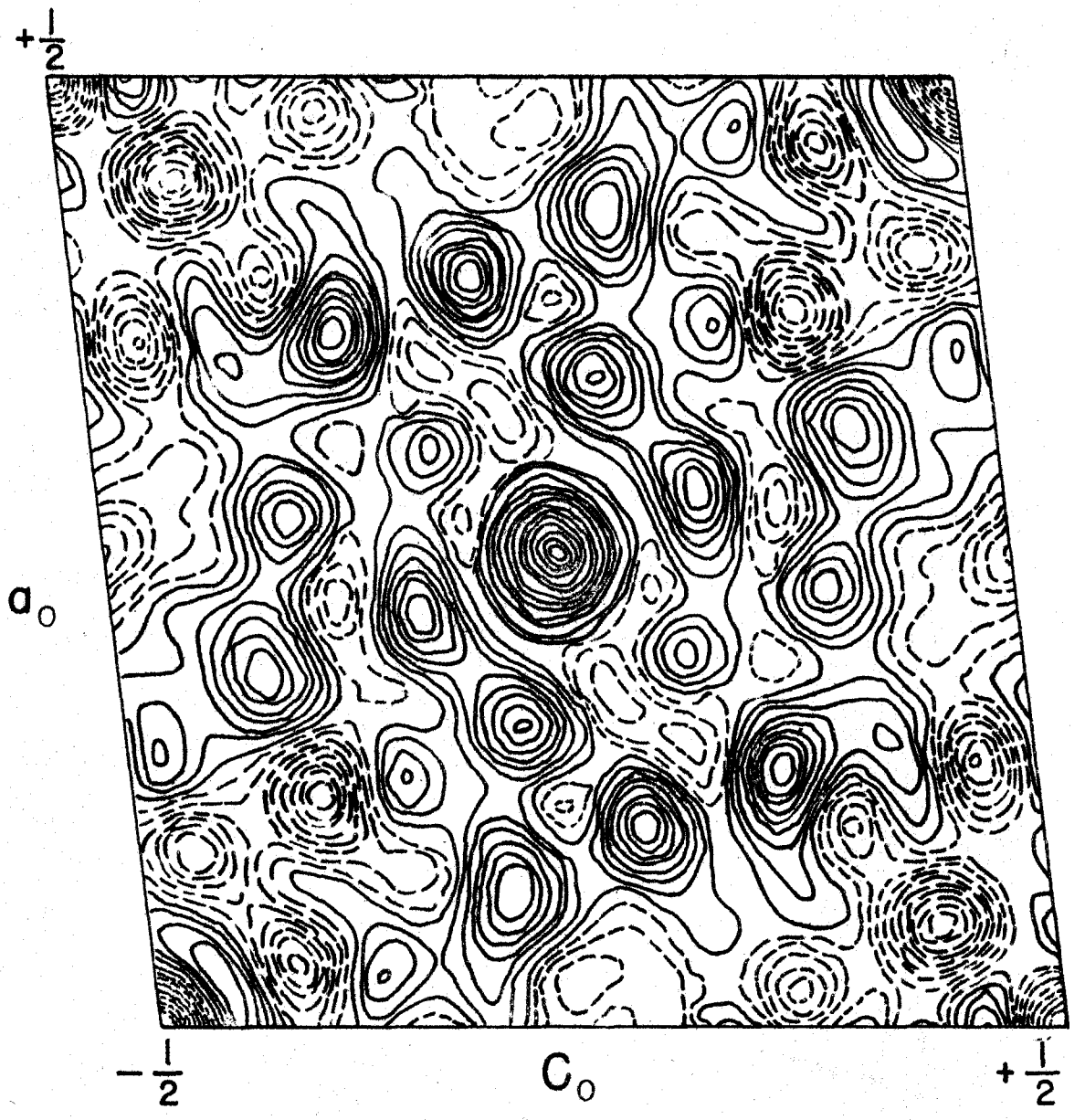

Figure 17. Generalized "sharpened" Patterson projection $P_1(xz)$ onto the (010) plane

function. Hexagonal symmetry was observed around the origin and also near $x = \frac{1}{2}$, $y = \frac{1}{2}$, $z = \frac{1}{2}$.

Three-dimensional "sharpened" Patterson

In an attempt to bring out the iron positions by sharpening the peaks, the three-dimensional "sharpened" Patterson sections $P(x,0,z)$ and $P(x,\frac{1}{2},z)$ were produced. The method of modifying the values of $|F|^2$ is an extension of that used in obtaining the two-dimensional "sharpened" Patterson projections, in which the intensities of the higher order reflections are given more weight than the lower order reflections. Scattering factors for iron (38, p. 572), carbon (39), and oxygen (39) were obtained for the three-dimensional data, and the modified $|F_M(hk\ell)|^2$ were calculated for each reflection by the formula given previously on page 29.

The resulting sections, shown in Figures 18 and 19, revealed substantial differences from the "unsharpened" Patterson sections. Consequently, seven more "sharpened" Patterson sections were produced on IBM near $y = 0/60$ and $y = 15/60$ which included the following: $P(x,2/60,z)$; $P(x,4/60,z)$; $P(x,8/60,z)$; $P(x,12/60,z)$; $P(x,14/60,z)$; $P(x,16/60,z)$; and $P(x,18/60,z)$. Plots of these sections (Figures 20-26) also showed considerable changes from the

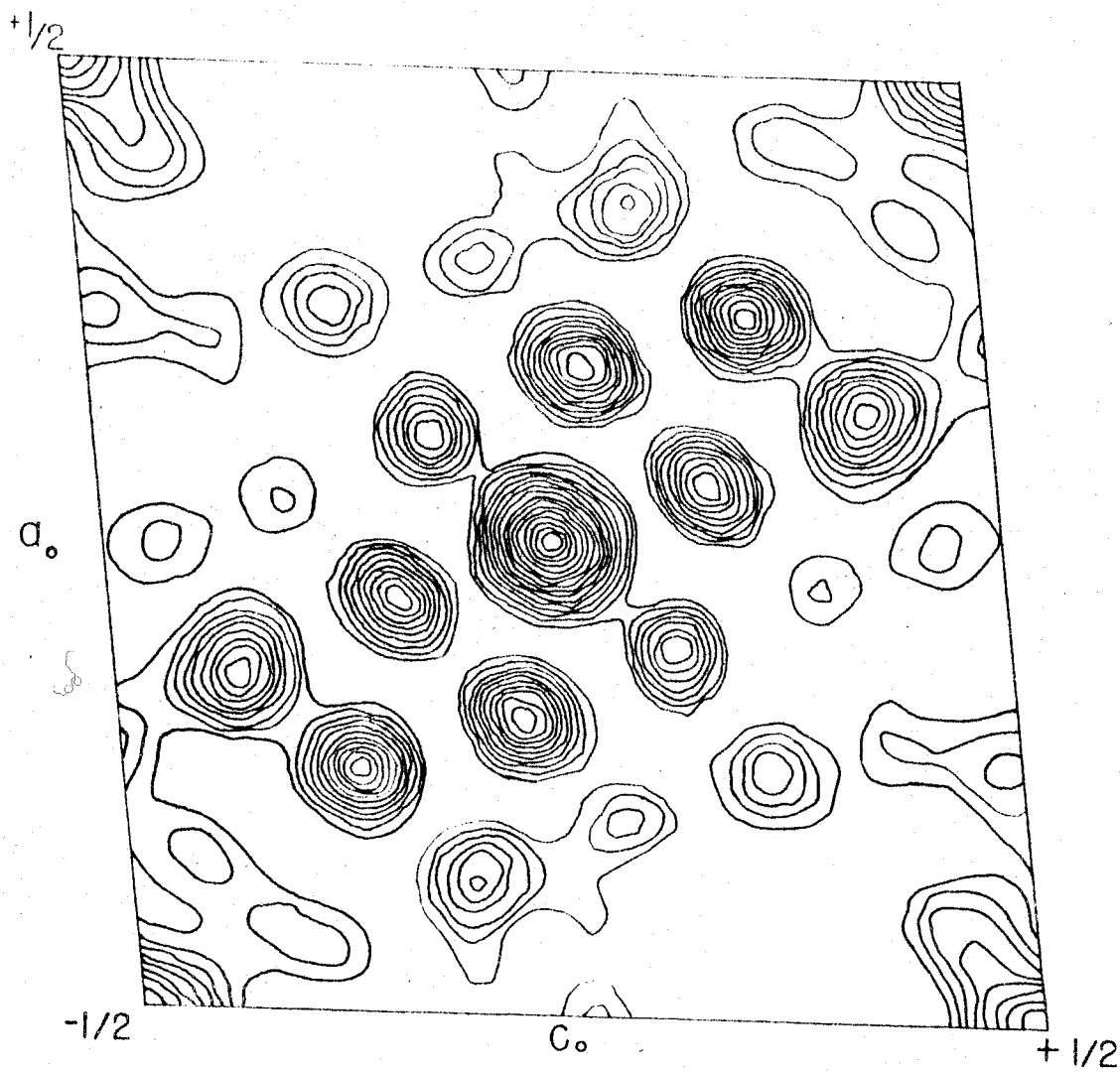

Figure 18. "Sharpened" Patterson section P(x,0,z)

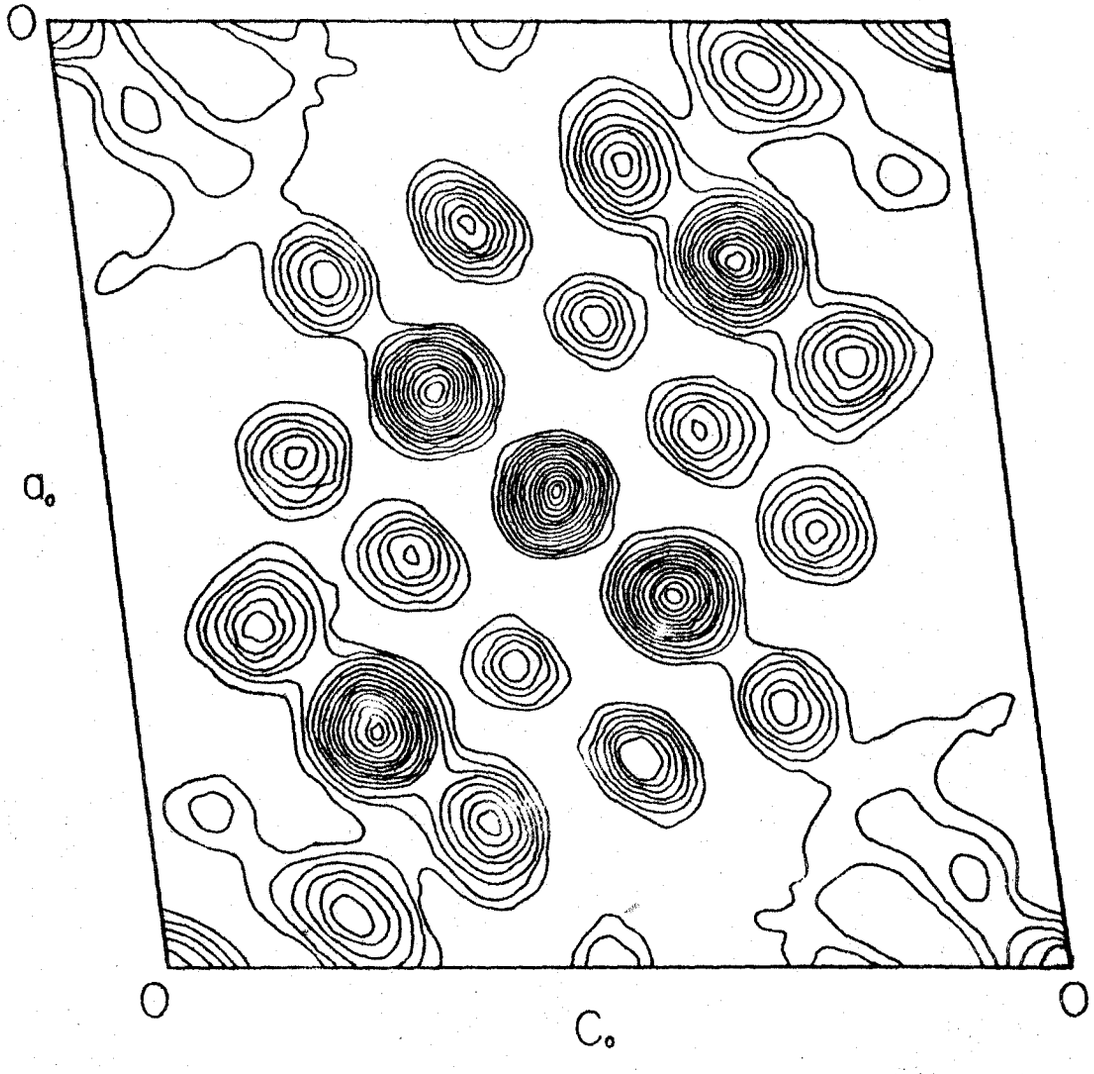

Figure 19. "Sharpened" Patterson section P(x,$\frac{1}{4}$,z)

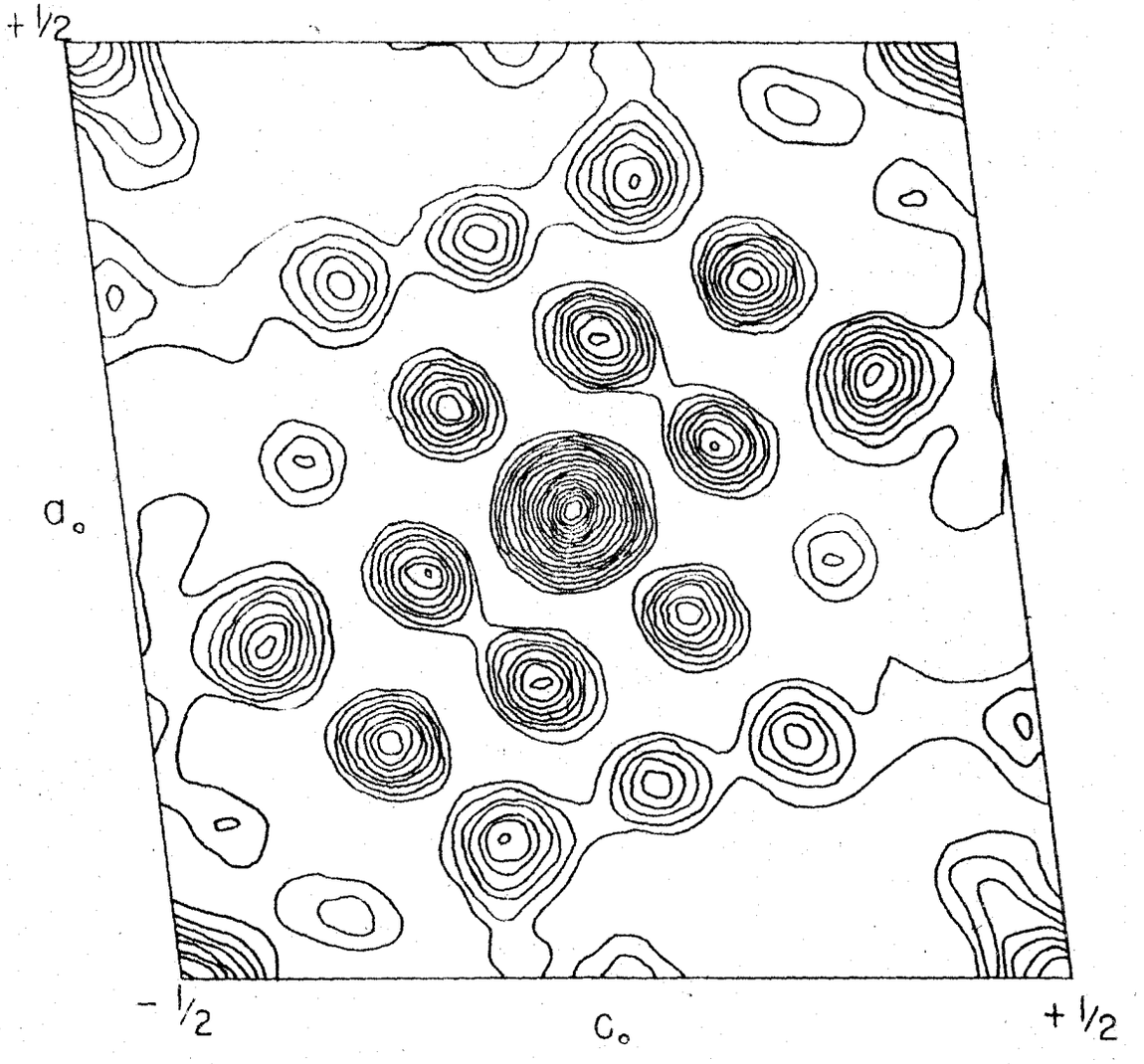

Figure 20. "Sharpened" Patterson section P(x,2/60,z)

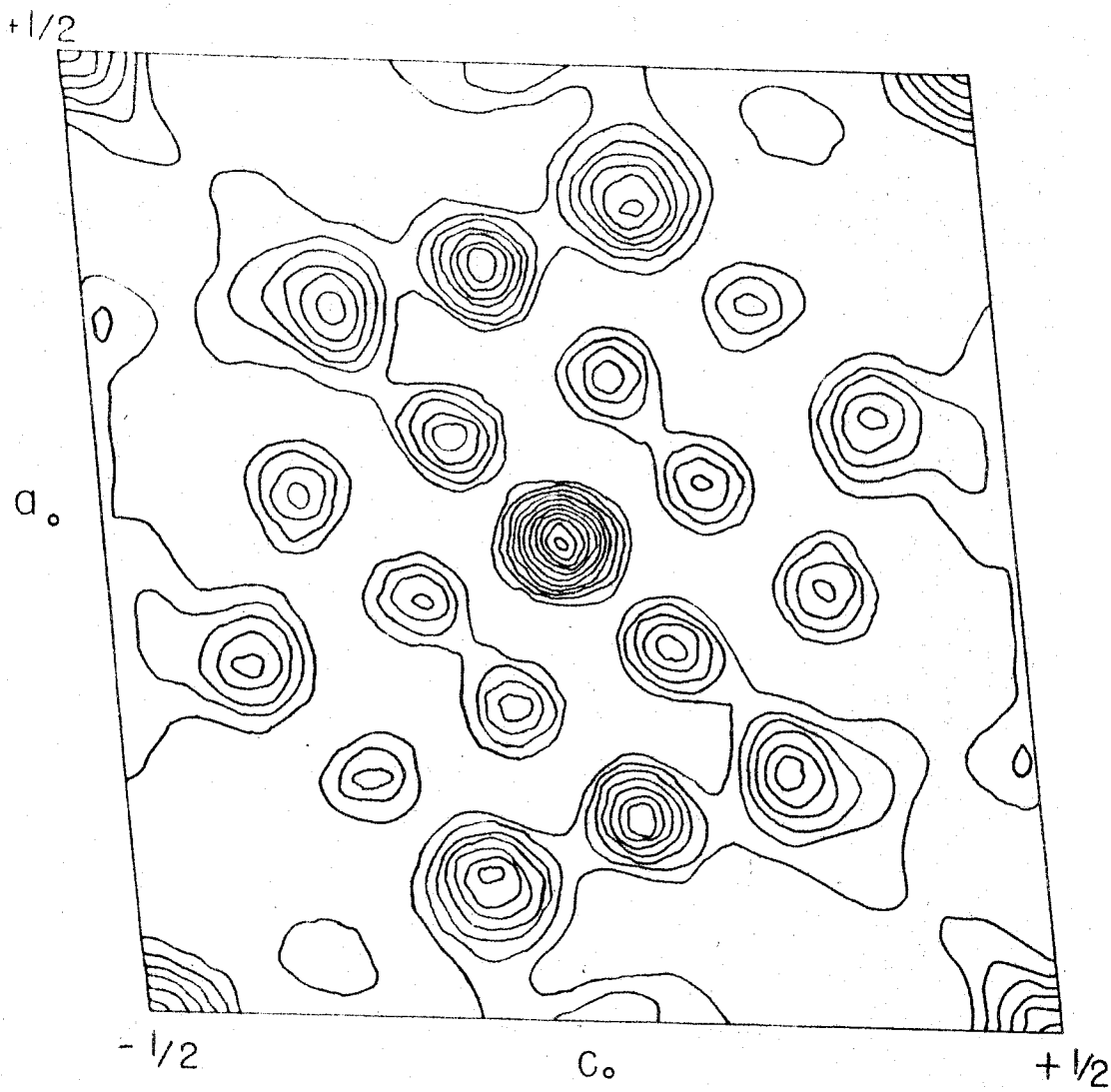

Figure 21. "Sharpened" Patterson section P(x,4/60,z)

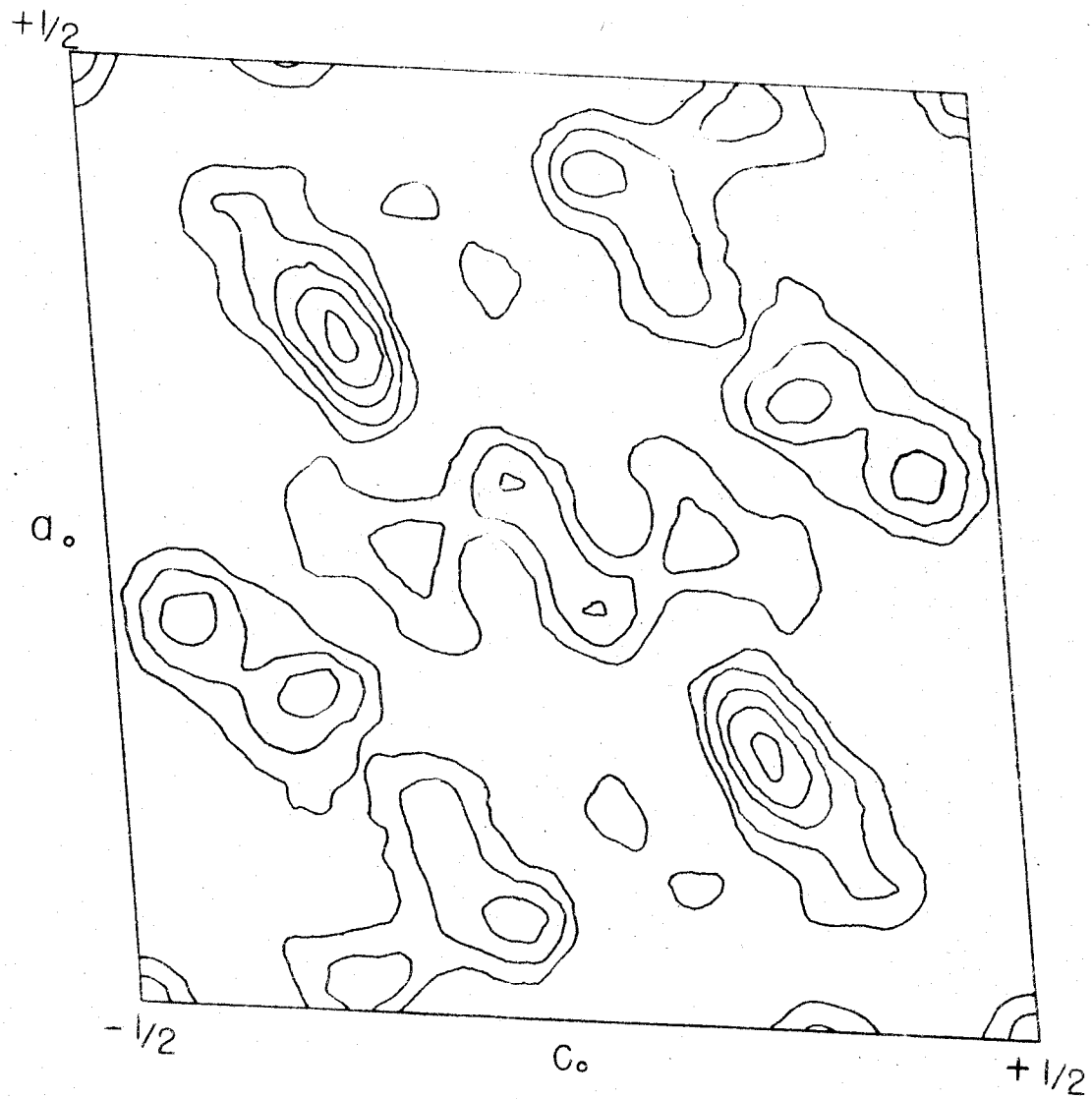

Figure 22. "Sharpened" Patterson section P(x,8/60,z)

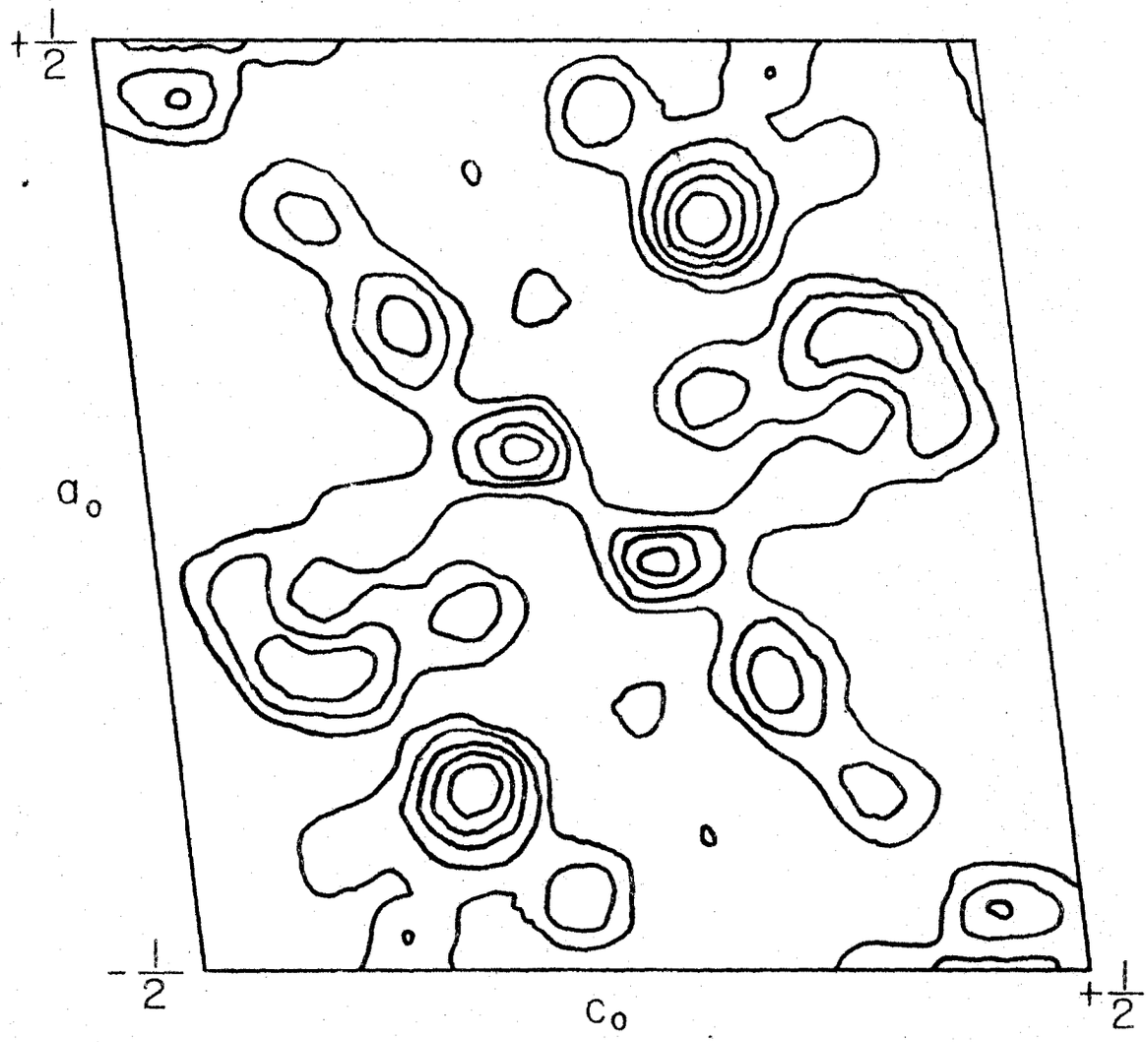

Figure 23. "Sharpened" Patterson section P(x,12/60,z)

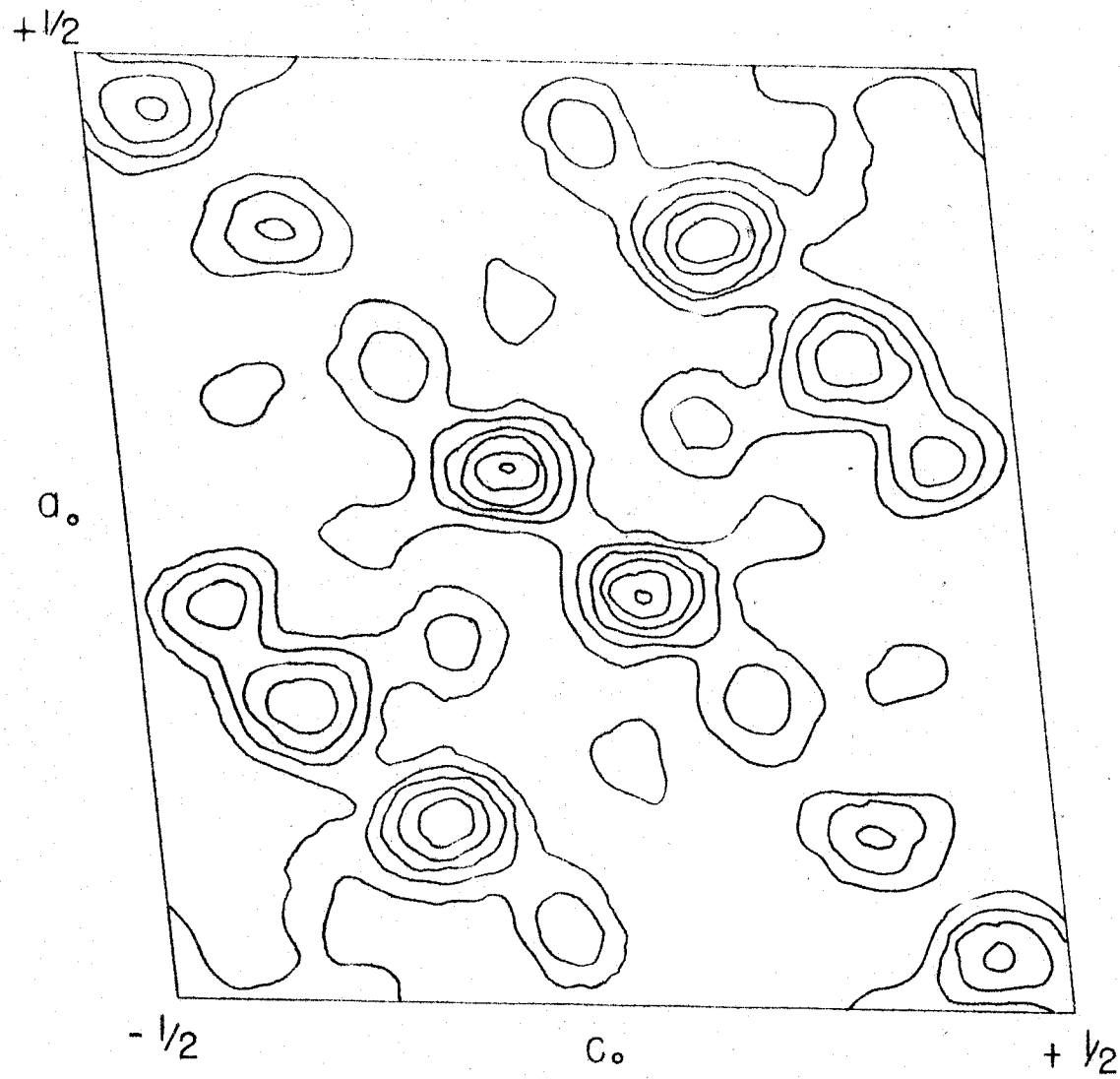

Figure 24. "Sharpened" Patterson section P(x,14/60,z)

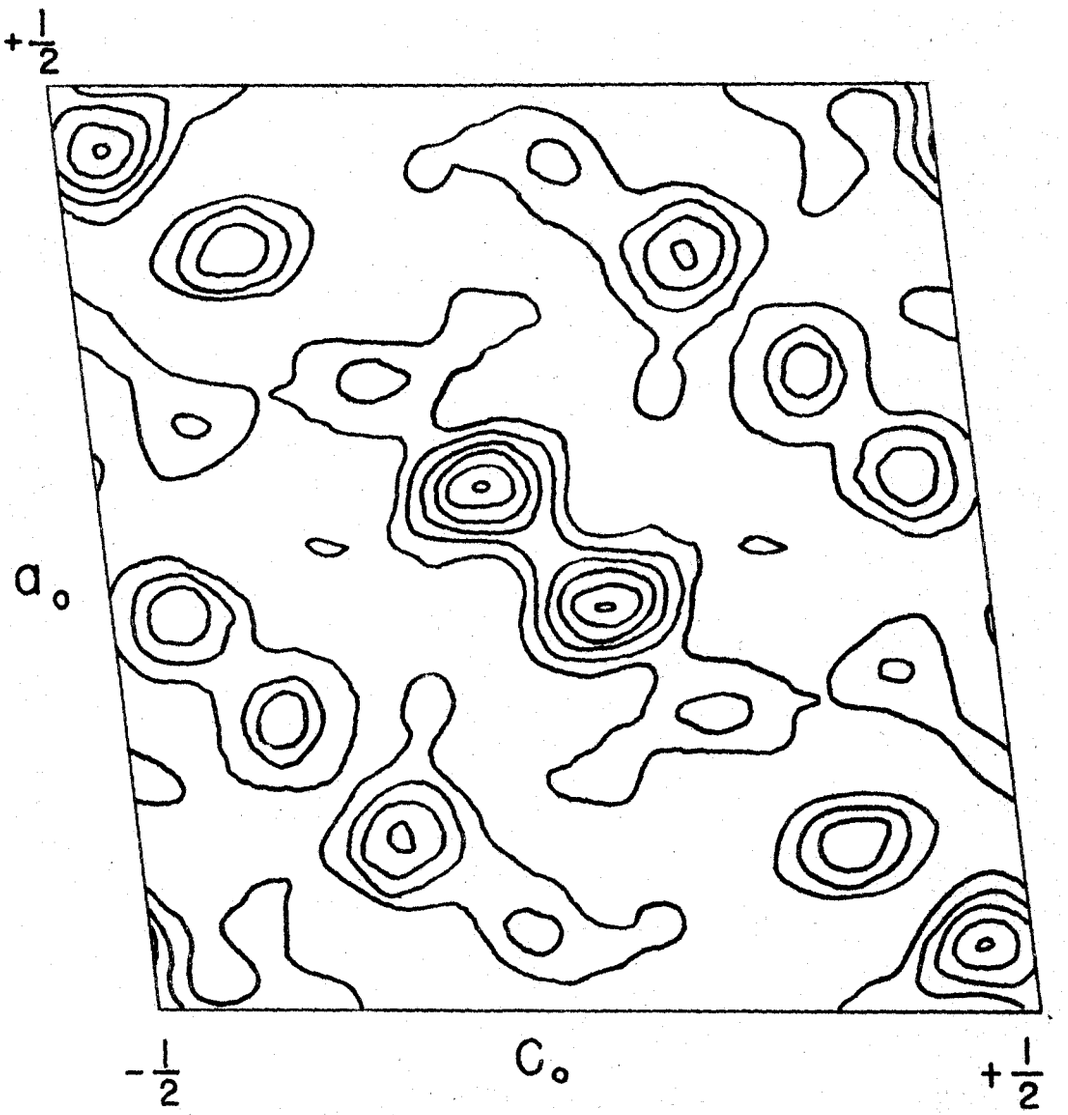

Figure 25. "Sharpened" Patterson section P(x,16/60,z)

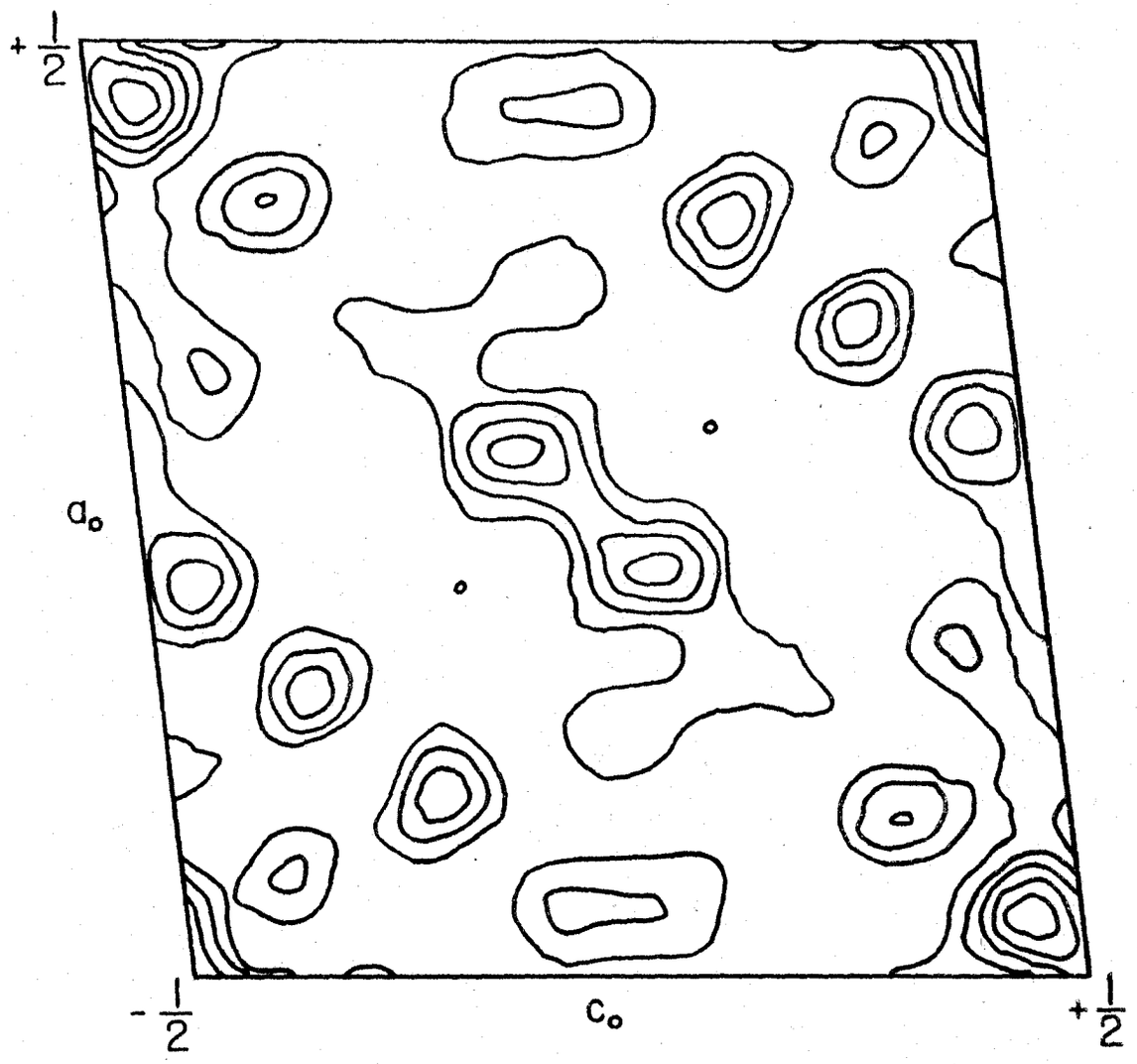

Figure 26. "Sharpened" Patterson section P(x,18/60,z)

corresponding "unsharpened" three-dimensional Patterson sections. Individual Patterson peaks appeared to be better resolved, and more detail was present. Eight more "sharpened" Patterson sections were later obtained on X-RAC (40) at Pennsylvania State University. The sections near y = 30/60, which are given in Figures 27-31, showed a concentration of large peaks of hexagonal symmetry about the point $\frac{1}{3},\frac{1}{3},\frac{1}{3}$. The $P(x,\frac{1}{3},z)$ section was included for comparison with the $P(x,\frac{1}{3},z)$ section computed on IBM equipment.

In order to determine whether the hexagon of peaks around the origin of the three-dimensional "sharpened" Patterson was partly due to diffraction ripples from the origin peak, the P(x,0,z) section was recomputed with the origin subtracted, and the resulting map shown in Figure 32 indicated strongly that the hexagon of peaks was indeed real.

Two-dimensional Fourier projections

Several Fourier electron-density projections (36, p. 199), based on different interpretations of the iron positions from the two-dimensional Patterson projections, failed to yield any interpretable information concerning the iron, carbon, and oxygen parameters.

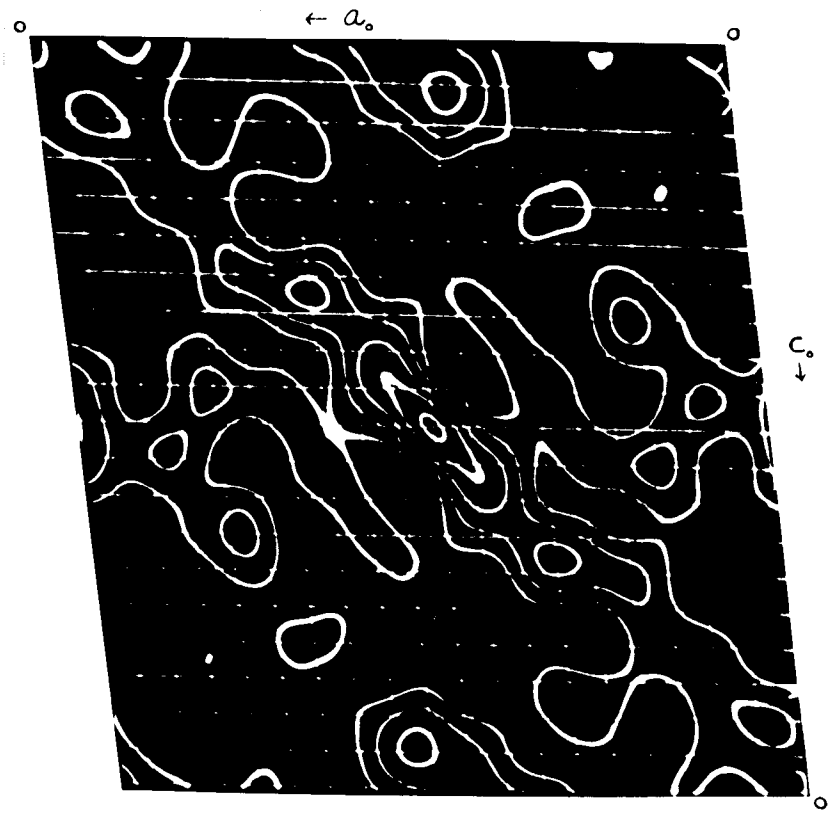

Figure 27. "Sharpened" Patterson section P(x, 22/60, z)

Figure 28. "Sharpened" Patterson section P(x, 24/60, z)

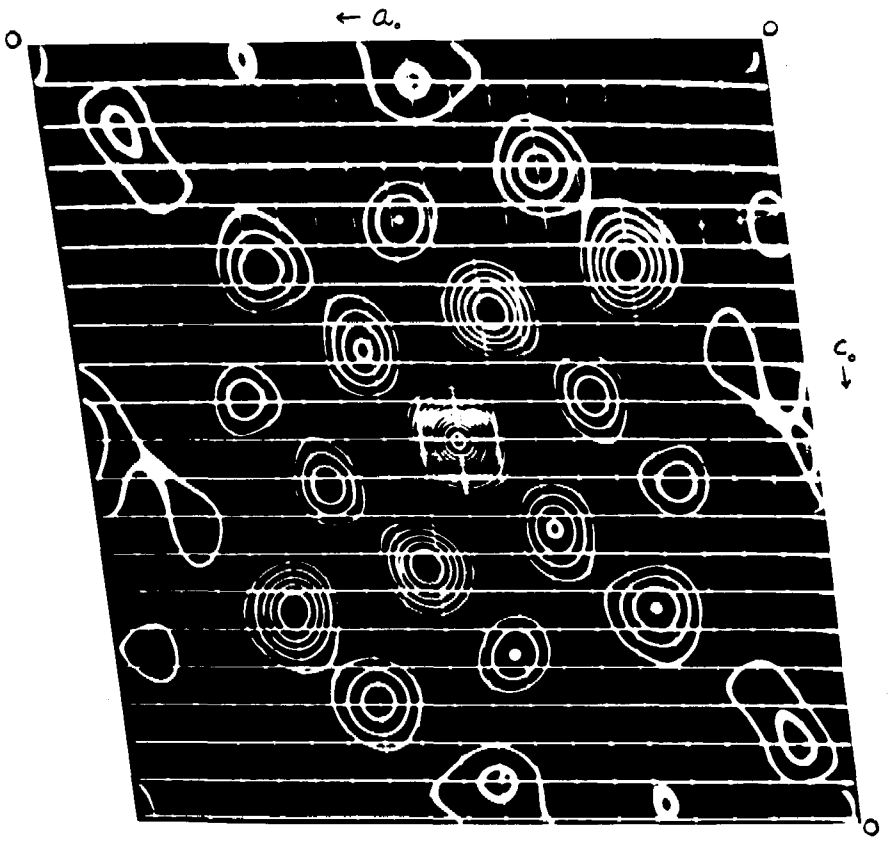

Figure 29. "Sharpened" Patterson section P(x, 26/60, z)

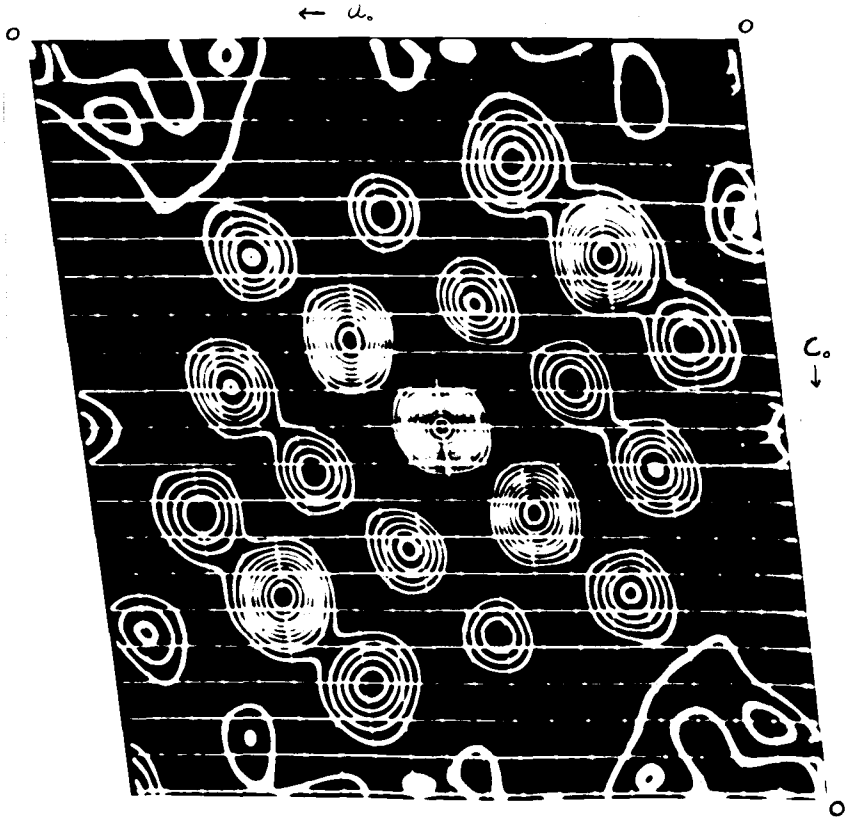

Figure 30. "Sharpened" Patterson section P(x,28/60,z)

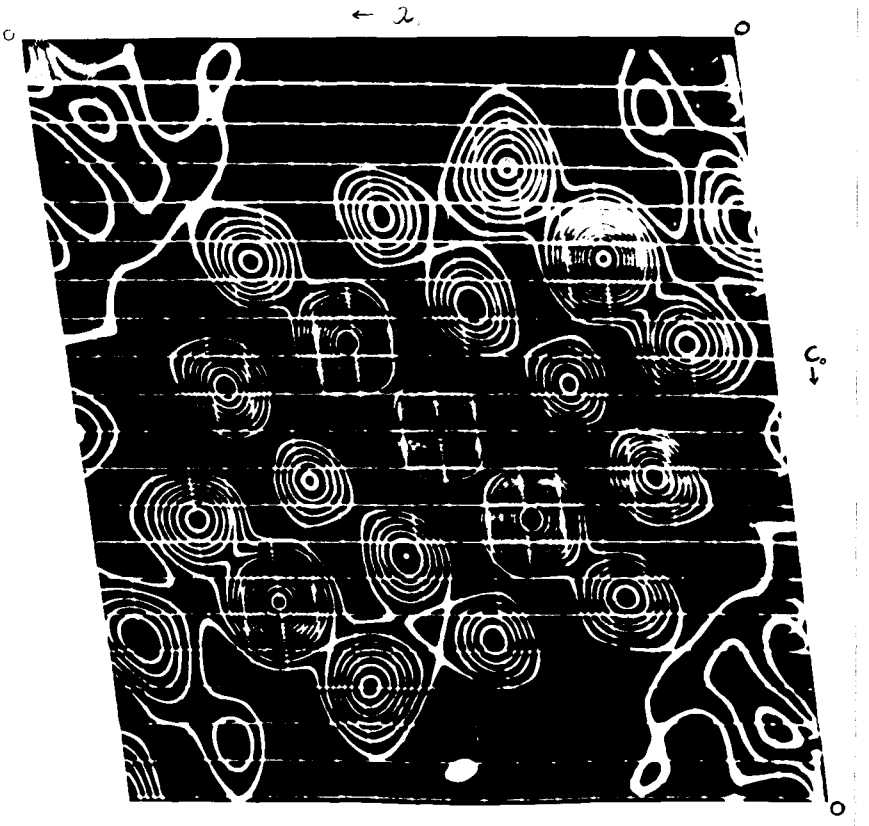

Figure 31. "Sharpened" Patterson section P(x, $\frac{1}{2}$, z)

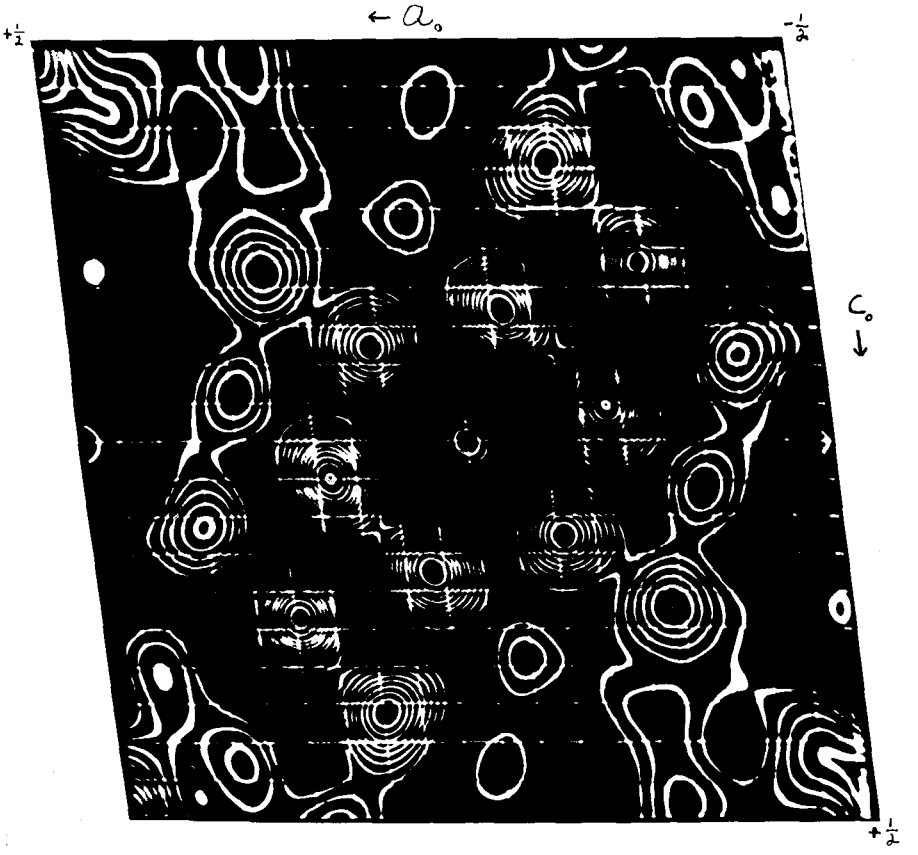

Figure 32. "Sharpened" Patterson section P(x,0,z) with the origin subtracted

Models of the D_{3d} and D_{2d} structures shown in Figures 4a and 4b, both involving collinear iron atoms, were constructed to scale, but no success in fitting the models to the "sharpened" three-dimensional Patterson was obtained.

A criterion for following the progress of the structure determination is given by the reliability index

$$R(hk\ell) = \frac{\sum_{hk\ell} \left| \left| F_{obs.} \right| - \left| F_{calc.} \right| \right|}{\sum_{hk\ell} \left| F_{obs.} \right|} .$$

The $R(hk\ell)$ value was utilized to compare the observed structure factors with those calculated for the different models.

Although absent on the $P(x,\frac{1}{2},z)$ "unsharpened" Patterson section a peak appeared on the $P(x,\frac{1}{2},z)$ "sharpened" Patterson section at $x \approx 0$, $z \approx 0$ which was interpreted analytically as an iron-iron vector due to the four-fold set of iron parameters given in Set I (Table 5).

Table 5. Trial structures involving four-fold iron parameters for $P2_1/n$

Set	Parameters		
	x	y	z
I	0.245	0.000	0.230
II	0.053	0.250	0.942

Two-dimensional Fourier projections for the (h0ℓ), (hk0), (0kℓ), (hkh), and ($\bar{h}$kh) zones based on the phases of the calculated iron structure factors obtained from the parameters in Set I (Table 5) failed again to reveal anything interpretable in terms of a molecular structure. The reiterated method of assigning the other peak positions arbitrarily as carbon and oxygen positions and recalculating structure factors to obtain new phases from which Fourier projections were again computed was followed.

Another interpretation of the Patterson sections in which the iron atoms were approximately located along the b_p axis as given by Set II (Table 5) was made. The complete hexagon of Patterson peaks around the origin and about the point $\frac{1}{3},\frac{1}{3},\frac{1}{3}$ must then be explained as coincidences of mainly iron-carbon and iron-oxygen vectors. Fourier projections of the (h0ℓ), (hk0), (0kℓ), (hkh), and ($\bar{h}$kh) zones were computed. Structure factor graphs (36, p. 138) which were made for the most intense reflections, together with known bond distances, were used to aid in shifting parameters. No interpretation of the data in terms of the above model could be made.

In order to account for the outer hexagonal array of peaks in the Patterson, a trigonal molecular structure of iron atoms in the non-centrosymmetric space group Pn was proposed (Figure 33 gives the symmetry positions for Pn) with

Figure 33. Symmetry positions for the space group Pn

Point positions:

2: xyz; $\frac{1}{2}$ + x,$\bar{y}$,$\frac{1}{2}$ + z

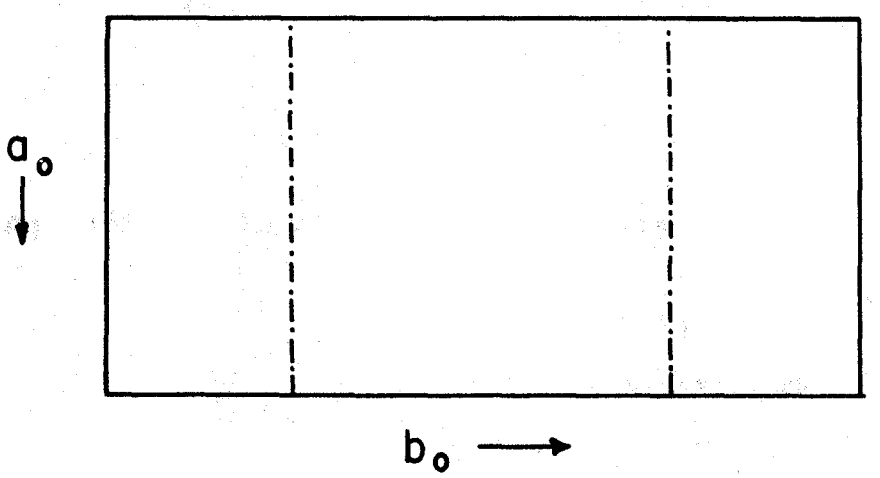
a_o
b_o

the carbonyl positions determined from spacial considerations. If the projection of molecules on the b_p axis is symmetrical about a point half-way between the glide planes, (0k0) reflections will appear only if k is even; this very type of pseudo-symmetry was observed in the structure of azulene (41, 42), in which a two-fold screw axis was at first assumed to explain the extinctions. Structure factors involving 59 parameters were calculated for the (h0ℓ) reflections, but on comparison with the observed structure factors little correlation could be made.

Since there were two possible choices of three-fold iron positions, a centrosymmetric disorder of the iron atoms corresponding to the four-fold positions of the space group $P2_1/n$ was then assumed; in each unit cell the trigonal ring was randomly placed in one of two orientations differing from each other by a rotation of approximately 60° about the three-fold axis. Iron parameters based on the above model obtained from an analysis of the three-dimensional Patterson are given in Table 6.

An iron-iron vector analysis of the three-dimensional "sharpened" Patterson was made based on the disordered trigonal model. The experimental heights of the peaks (given by the number of contours) of the different sections were found to be in fairly good agreement with the model.

Table 6. Iron positions for disordered trigonal structure

Atom	Parameters		
	x	y	z
Fe(1)	0.067	0.020	0.171
Fe(2)	0.185	0.980	0.058
Fe(3)	0.108	0.950	0.879

Within a given row in the (101) direction the multiplicities of the iron-iron vectors agreed very well. Of course, certain peaks of the experimental Patterson will be greatly enhanced by coincidences of other interatomic vectors, especially iron-carbon and iron-oxygen vectors. The complete hexagon of peaks around the points 0,0,0 and $\frac{1}{2},\frac{1}{2},\frac{1}{2}$ was thus explained.

Structure factors were calculated from the parameters in Table 6 and two-dimensional Fourier projections for the (h0ℓ), (hk0), and (0kℓ) zones were computed. Structure factor calculations were then made with the carbon and oxygen positions independently taken from each Fourier projection. The calculated structure factors for different zones involving common reflections were quite different from one another,

indicating that more accurate parameters were needed. Accordingly, it was decided to compute a three-dimensional Fourier electron-density map on X-RAC at Pennsylvania State University.

Three-dimensional Fourier sections

The electron-density Fourier series for $P2_1/n$ is given by

$$\rho(x,y,z) = 4/V_C \left[\sum_h \sum_{\substack{l \\ h+k+l=2n}} \left[C_{hl} \cos 2\pi(hx + lz) + C_{\bar{h}l} \cos 2\pi(\bar{h}x + lz) \right] + \sum_h \sum_{\substack{l \\ h+k+l=2n+1}} \left[S_{hl} \sin 2\pi(hx + lz) + S_{\bar{h}l} \sin 2\pi(\bar{h}x + lz) \right] \right]$$

where $C_{hl} = \sum_0^k F(hkl) \cos 2\pi ky$ and $S_{hl} = -\sum_0^k F(hkl) \sin 2\pi ky$.

Structure factor calculations were made from only the iron positions for over 400 reflections. Figure 34 shows the orientation of the iron atoms in the unit cell.

The method of A. J. Wilson (43) was used in an attempt to place the observed F's on an absolute scale. The observed $F(hkl)^2$ values of the three-dimensional data were arranged in several ranges of $\sin^2\theta/\lambda^2$, and a plot of

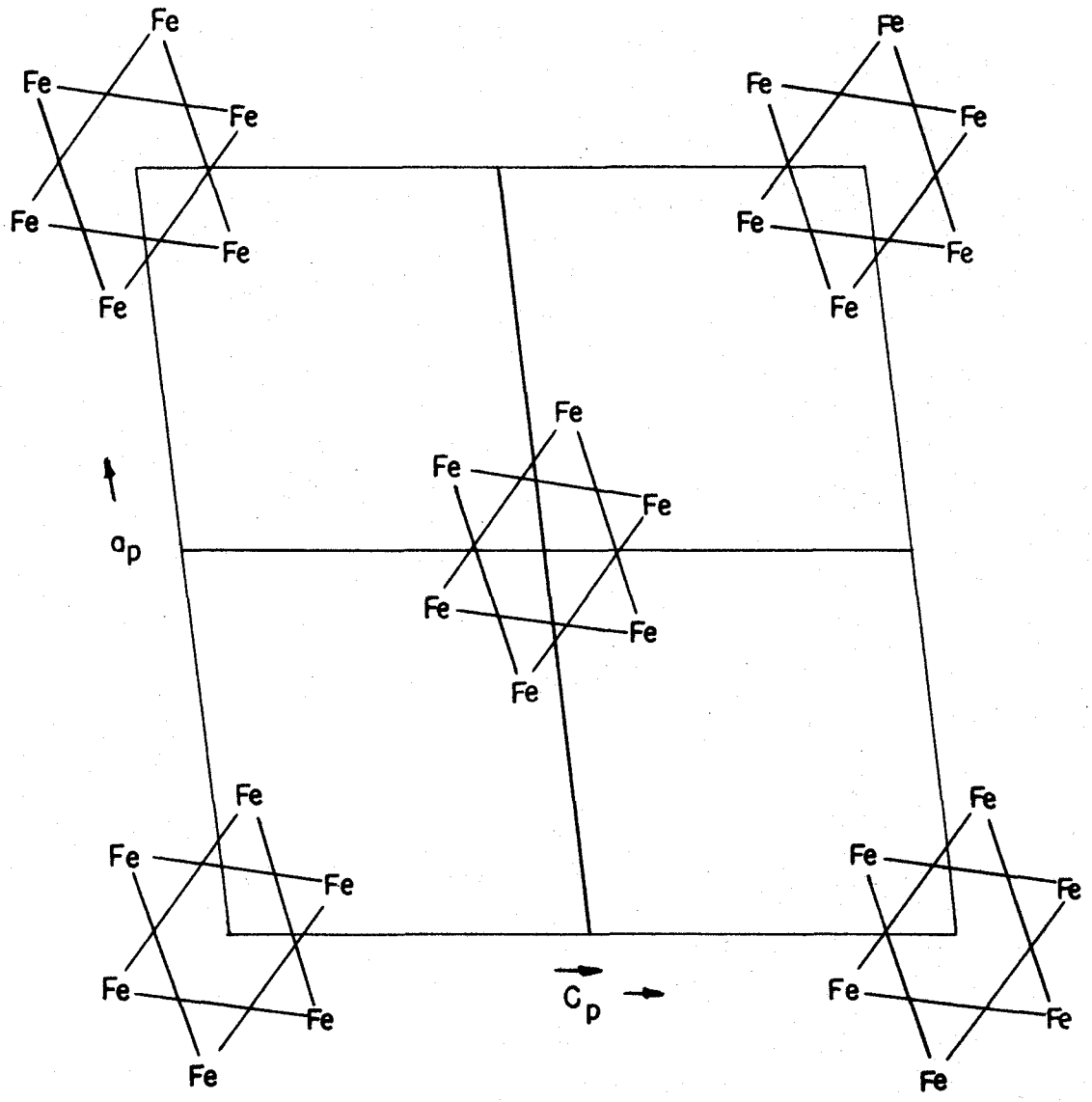

Figure 34. The arrangement of the iron atoms in the unit cell for the disordered trigonal model

$\langle F(hk\ell)\rangle^2 / \sum_n \bar{f}_n^2$ versus $\sin^2\theta/\lambda^2$ resulted in a B value of 5.73 with the scale factor k in the equation $kF_{obs.} = F_{calc.} \exp(-B\sin^2\theta/\lambda^2)$ having a value of 14.0. Unfortunately, the spread of points indicated that there was considerable error. The abnormally high temperature factor B (over half the reflections considered were accidentally extinct) might be an indication of the disordered structure proposed.

The coefficients, $C_{h\ell}$, $C_{\overline{h\ell}}$, $S_{h\ell}$, and $S_{\overline{h\ell}}$, from which the electron-density distribution for the whole unit cell could be obtained, were computed and normalized for ten sections involving the following values of y: 0/60, 1/60, 2/60, 3/60, 4/60, 6/60, 8/60, 10/60, 12/60, 14/60 (a 1/60 increment corresponded as before to 0.2 Å). These ten Fourier sections then were run at Pennsylvania State University on the X-RAC.

The shifts in the iron positions were found to be small. The x and z parameters were located by graphical measurements, and the y parameters were determined by interpolation of the peak heights of the different sections using Booth's method (44).

An interpretation of many of the other peaks of the Fourier sections as carbon and oxygen positions was made. Intramolecular Fe-C and C-O distances found for $Fe(CO)_5$ and $Fe_2(CO)_9$ were utilized in procuring the parameters. Table 7

Table 7. Four-fold sets of parameters obtained from the three-dimensional Fourier sections

Atom	Parameters		
	x	y	z
Fe(1)	.070	.178	.015
Fe(2)	.177	.053	.986
Fe(3)	.109	.833	.947
C (1)	.740	.745	~ 1/60
O (1)	.685	.615	~ 1/60
C (2)	.715	.750	~ -1/60
O (2)	.588	.700	~ -1/60
C (3)	.690	.095	~ 3/60
O (3)	.595	.200	~ 3/60
C (4)	.690	.105	~ 3/60
O (4)	.570	.105	~ 3/60
C (5)	.125	.120	.200
O (5)	.120	.120	.233
C (6)	.880	.905	.200
O (6)	.880	.875	.233

lists the parameters obtained. Since the x and z parameters determined are probably known much more accurately than the y parameters, temperature corrected structure factors for the (h0ℓ) data were calculated from the parameters in Table 7 for comparison with the observed data. A ($F_{obs.}/F_{calc.}$) versus $\sin^2\theta / \lambda^2$ plot yielded a B = 3.66 and a k = 0.725. A reliability factor of R = 44% was obtained for the observed (h0ℓ) data (Table 8). A comparison of the new phases with the old ones used in computing the three-dimensional Fourier sections showed several sign changes plus quite a few changes to the doubtful category. Another (h0ℓ) Fourier projection was produced (Figure 35) based on the new phases. However, it appeared that additional three-dimensional work would be needed to confirm the structure proposed.

The observed structure factors for the three-dimensional data are listed in Table 9 along with the calculated structure factors (no temperature correction was made) for the Fe positions in the disordered trigonal model. There appears to be some correlation of the large calculated structure factors with the observed data, especially with higher order reflections.

Table 8. Comparison of observed and calculated structure factors for (h0ℓ) data

Indices	$F^{T}_{calc.}$	$F_{obs.}$	Indices	$F^{T}_{calc.}$	$F_{obs.}$
	h0ℓ				
(00ℓ)			(50ℓ)		
2	-13.2	8.4	1	-26.4	14.2
4	-61.0	40.6	3	55.2	49.7
6	-11.2	4.6	5	19.8	33.5
(h00)			(60ℓ)		
2	- 9.4	10.7	4	5.0	13.2
4	-73.6	40.6			
6	-21.4	12.6	(70ℓ)		
8	-12.2	9.6	1	- 4.8	7.1
			3	- 5.8	9.6
(10ℓ)			5	-15.6	14.2
1	30.2	47.6	7	- 2.6	9.6
3	-51.0	21.8			
5	-23.6	44.7	(80ℓ)		
7	-10.6	20.3	2	- 5.0	8.1
			4	-14.2	14.2
(20ℓ)					
2	-104.0	140.1	(90ℓ)		
4	- 8.6	24.9	5	- 8.0	6.1
6	- 1.8	16.2			
8	- 5.6	12.2	(10·0·ℓ)		
10	10.4	11.7	2	11.8	13.2
(30ℓ)			(11·0·ℓ)		
1	-63.4	57.9	1	9.6	10.7
5	33.4	20.8			
7	-15.0	11.7			
(40ℓ)					
2	- 1.0	18.8			
4	76.8	83.7			
6	- 2.6	14.7			

Table 8. (Continued)

Indices	$F^{T}_{calc.}$	$F_{obs.}$	Indices	$F^{T}_{calc.}$	$F_{obs.}$
	$\bar{h}0\ell$				
$(\bar{1}0\ell)$			$(\bar{5}0\ell)$		
1	128.4	92.4	1	- 6.0	5.1
3	-47.4	15.2	3	9.8	15.2
5	14.2	9.6	5	- 1.0	9.1
7	19.4	22.8			
			$(\bar{6}0\ell)$		
$(\bar{2}0\ell)$			2	52.8	35.5
2	57.2	14.2	4	13.8	17.3
4	-20.2	16.7	6	-12.0	19.3
6	43.4	23.3			
8	- 0.4	13.2	$(\bar{7}0\ell)$		
			1	11.6	16.2
$(\bar{3}0\ell)$			3	25.8	25.9
1	-50.2	92.4	5	-11.0	9.6
3	-13.2	21.3			
7	22.4	30.5	$(\bar{8}0\ell)$		
9	- 7.6	7.1	4	6.4	12.2
			6	- 8.6	9.6
$(\bar{4}0\ell)$					
2	-13.2	19.3	$(\bar{9}0\ell)$		
4	-12.6	5.1	5	-14.4	9.6
10	-10.8	7.1			
			$(\bar{1}\bar{0}\cdot0\cdot\ell)$		
			2	-10.4	13.2
			4	- 6.6	6.1

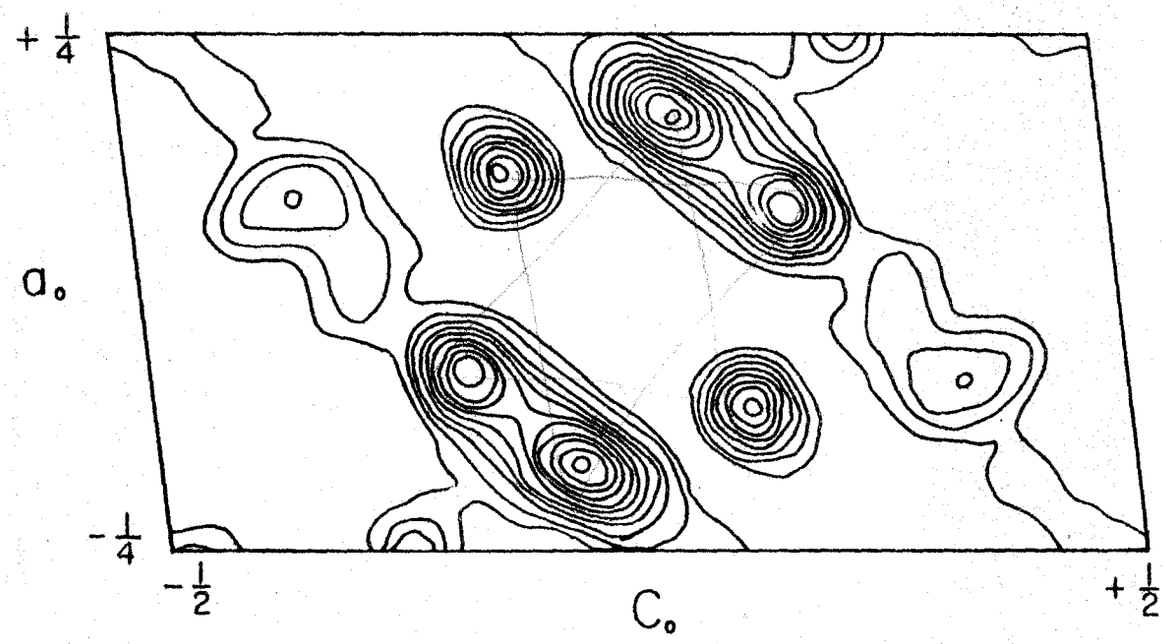

Figure 35. Fourier projection onto the (010) plane

Table 9. Observed structure factors for (hkℓ) data together with calculated structure factors for iron positions based on disordered trigonal model

Indices	$F_{calc.}$	$F_{obs.}$	Indices	$F_{calc.}$	$F_{obs.}$
	hOℓ				
(00ℓ)			(40ℓ)		
2	11.1	11.6	2	7.1	25.9
4	-44.6	56.0	4	82.6	115.5
6	7.3	6.3	6	7.6	20.3
8	-15.9		8	-28.9	
			10	13.7	
(h00)			(50ℓ)		
2	8.7	14.7	1	-27.5	19.6
4	-38.7	56.0	3	52.1	68.6
6	-18.8	17.4	5	37.8	46.2
8	-32.6	13.3	7	-40.1	
(10ℓ)			(60ℓ)		
1	52.7	65.8	2	-19.8	
3	-58.5	30.1	4	20.7	18.2
5	-33.6	61.6	6	-22.0	
7	-25.3	28.0			
(20ℓ)			(70ℓ)		
2	-39.7	193.2	1	-49.9	9.8
4	-16.2	34.3	3	-18.9	13.3
6	-17.8	22.4	5	-16.2	19.6
8	-11.1	16.8	7	0.7	13.3
10	49.0	16.1			
			(80ℓ)		
(30ℓ)			2	-19.5	11.2
1	-45.0	79.8	4	-17.1	19.6
3	20.4		6	3.8	
5	36.7	28.7			
7	-19.7	16.1	(90ℓ)		
9	18.9		1	12.8	
			3	10.7	
			5	-13.2	8.4

Table 9. (Continued)

Indices	$F_{calc.}$	$F_{obs.}$
$(10\cdot0\cdot\ell)$		
2	51.3	18.2
4	-10.7	
$(11\cdot0\cdot\ell)$		
1	50.1	14.7

$\bar{h}0\ell$

$(\bar{1}0\ell)$		
1	78.0	127.4
3	-36.4	21.0
5	24.9	13.3
7	47.3	31.5
$(\bar{2}0\ell)$		
2	-30.4	19.6
4	-20.8	23.1
6	75.7	32.2
8	31.6	18.2
10	-31.2	
$(\bar{3}0\ell)$		
1	-38.3	127.4
3	-52.9	29.4
5	7.2	
7	52.3	42.0
9	- 8.7	9.8
$(\bar{4}0\ell)$		
2	- 9.6	26.6
4	-30.7	7.0
6	- 4.8	
8	- 3.7	
10	-20.3	9.8
$(\bar{5}0\ell)$		
1	21.0	7.0
3	38.2	21.0
5	-28.1	12.6
7	-26.3	
$(\bar{6}0\ell)$		
2	77.8	49.0
4	32.2	23.8
6	-32.5	26.6
$(\bar{7}0\ell)$		
1	13.4	22.4
3	62.9	35.7
5	- 9.6	13.3
7	- 3.7	
$(\bar{8}0\ell)$		
2	11.7	
4	0.8	16.8
6	-25.5	13.3
$(\bar{9}0\ell)$		
1	-19.8	
3	-15.0	
5	-34.3	13.3
$(\overline{10}\cdot0\cdot\ell)$		
2	-21.5	18.2
4	-13.7	8.4
$(\overline{11}\cdot0\cdot\ell)$		
1	- 5.7	

Table 9. (Continued)

Indices	$F_{calc.}$	$F_{obs.}$	Indices	$F_{calc.}$	$F_{obs.}$
	hlℓ				
(01ℓ)			(31ℓ)		
1	100.7	120.4	1	4.8	29.0
2	-14.5	14.7	2	-21.5	47.9
3	-44.8	9.8	3	- 2.5	
4	7.2		4	45.1	28.3
5	-12.1		5	-12.6	
6	10.9	12.6	6	4.6	14.0
7	1.2				
8	- 0.1		(41ℓ)		
9	-24.9	10.8	1	-33.8	49.0
			2	8.8	20.3
(h10)			3	58.3	41.7
1	98.7	115.5	4	- 2.4	
2	13.3		5	56.6	44.9
3	-42.2	24.5	6	- 8.7	
4	- 4.3		7	-27.2	
5	-17.2	28.7			
6	- 7.0	21.7	(51ℓ)		
7	-32.3		1	4.4	33.5
8	- 4.6		2	7.1	
			3	12.9	
(11ℓ)			4	65.0	47.5
1	- 1.2	14.0	5	- 2.9	
2	-21.6		6	- 9.5	16.5
3	- 5.7				
4	-51.4	24.5	(61ℓ)		
5	2.2	30.1	1	-38.0	23.4
6	-22.5	41.7	2	11.5	
7	2.9		3	11.5	14.7
			4	7.6	
(21ℓ)			5	1.6	14.7
1	-18.8	16.0	6	- 3.8	
2	- 2.3	17.6			
3	-34.7	52.2	(71ℓ)		
4	- 8.6	11.8	1	- 0.9	9.0
5	- 8.5	13.3	2	-36.0	
6	- 5.6		3	5.6	
7	-23.8	31.1	4	-12.3	
			5	1.7	

Table 9. (Continued)

Indices	$F_{calc.}$	$F_{obs.}$
(81ℓ)		
1	-30.8	
$(10\cdot1\cdot\ell)$		
1	47.8	14.7
	$\bar{h}1\ell$	
$(\bar{1}1\ell)$		
1	-21.8	22.7
2	8.1	33.5
3	- 4.1	93.9
4	-20.1	
5	15.5	19.7
6	51.2	34.9
7	3.0	
$(\bar{2}1\ell)$		
1	4.1	9.0
2	-13.4	
3	-45.3	59.6
4	8.0	10.8
5	33.7	21.3
6	5.1	22.5
7	70.7	44.1
$(\bar{3}1\ell)$		
1	- 3.3	99.1
2	44.0	41.6
3	2.9	36.3
4	-35.0	34.3
5	3.3	
6	44.0	31.9
$(\bar{4}1\ell)$		
1	-17.6	25.1
2	10.5	
3	-20.0	13.3
4	3.0	22.5
5	-24.4	24.6
6	- 5.6	
7	5.4	
$(\bar{5}1\ell)$		
1	14.8	
2	48.1	27.0
3	5.7	
4	0.4	
5	- 3.6	
6	-33.9	
$(\bar{6}1\ell)$		
1	34.0	18.8
2	7.1	18.8
3	72.9	50.3
4	- 7.1	
5	-13.9	
6	- 0.2	
7	-21.8	16.5
$(\bar{7}1\ell)$		
1	5.6	
2	54.7	29.4
3	- 8.6	
4	29.8	14.0
5	- 7.8	
$(\bar{8}1\ell)$		
1	-14.4	9.0
$(\bar{10}\cdot1\cdot\ell)$		
1	- 9.5	9.9

Table 9. (Continued)

Indices	$F_{calc.}$	$F_{obs.}$	Indices	$F_{calc.}$	$F_{obs.}$
	h2ℓ				
(02ℓ)			(32ℓ)		
1	-24.5	23.0	1	-43.4	15.4
2	9.9		2	4.8	16.5
3	- 7.7		3	14.3	
4	-36.6	52.5	4	-17.8	
5	24.3	13.3	5	35.8	38.1
6	7.6		6	-18.6	
7	9.8				
8	-18.9	10.8	(42ℓ)		
9	- 6.2	6.3	1	7.2	
			2	4.8	
(h20)			3	10.9	
1	22.7	18.2	4	74.3	60.9
2	6.5	27.3	5	-17.0	
3	7.8	27.0	6	8.3	
4	-31.4	59.5	7	- 3.6	
5	-14.8	19.3			
6	-15.1		(52ℓ)		
7	-10.4		1	-21.8	
8	-33.5	24.2	2	24.9	9.0
			3	47.7	43.4
(12ℓ)			4	10.0	
1	40.7	33.5	5	32.6	29.4
2	-13.8	23.8	6	-11.3	
3	-54.4	41.7			
4	- 1.3	18.2	(62ℓ)		
5	-27.2	16.9	1	6.4	20.7
6	5.7		2	-15.3	21.7
7	-23.9	25.1	3	24.5	
			4	17.8	
(22ℓ)			5	1.3	
1	8.4				
2	-43.0	18.8	(72ℓ)		
3	-11.7		1	-45.0	
4	-14.7		2	7.8	
5	-16.4	21.7	3	-15.1	
6	-12.8		4	7.8	
7	- 0.8				

Table 9. (Continued)

Indices	$F_{calc.}$	$F_{obs.}$	Indices	$F_{calc.}$	$F_{obs.}$
(82ℓ)			($\bar{4}$2ℓ)		
2	-16.0	13.3	1	19.4	
			2	- 6.6	23.8
(10·2·ℓ)			3	13.3	
2	47.4	13.3	4	-33.2	59.8
			5	- 2.3	
	$\bar{h}k\ell$		6	- 6.9	
			7	-16.7	
($\bar{1}$2ℓ)			($\bar{3}$2ℓ)		
1	69.5	54.6	1	22.6	19.3
2	-34.4	16.1	2	24.5	24.6
3	-27.8	57.5	3	32.5	
4	18.9	48.3	4	- 1.6	
5	24.6	30.7	5	-29.5	24.6
6	21.9	27.6	6	- 6.0	
7	41.2	28.4			
			($\bar{6}$2ℓ)		
($\bar{2}$2ℓ)			1	21.6	31.5
1	-33.2	49.1	2	70.8	85.8
2	-21.8	39.1	3	- 2.8	
3	- 4.6	17.2	4	27.8	
4	-18.0	22.5	5	-11.0	26.2
5	19.7	32.9			
6	67.9	59.8	($\bar{7}$2ℓ)		
7	- 6.8		1	9.8	26.9
			2	- 1.0	
($\bar{3}$2ℓ)			3	57.2	50.3
1	-30.4	60.9	4	-23.0	
2	- 1.8	44.2			
3	-47.5	59.5	($\bar{8}$2ℓ)		
4	9.5		2	8.1	10.9
5	2.6				
6	- 5.4		($\bar{10}$·2·ℓ)		
7	48.2	34.3	2	-19.1	14.0

Table 9. (Continued)

Indices	$F_{calc.}$	$F_{obs.}$	Indices	$F_{calc.}$	$F_{obs.}$
	h3ℓ				
(03ℓ)			(33ℓ)		
1	73.7	27.7	1	9.5	30.1
2	-34.5	131.6	2	-27.9	20.3
3	-31.7	32.2	3	- 6.5	21.7
4	20.2	22.1	4	35.8	23.8
5	- 3.7	7.7	5	-33.1	23.0
6	28.2	26.6	6	10.5	
7	- 3.3				
8	- 0.6	7.7			
9	-28.4	13.3	(43ℓ)		
			1	-26.3	37.6
(h30)			2	21.8	40.0
1	71.0	29.4	3	44.4	23.8
2	31.4	48.4	4	- 5.9	
3	-31.2	14.0	5	47.8	25.1
4	-13.3	17.2			
5	- 6.5	21.3	(53ℓ)		
6	-17.5	19.7	1	11.0	19.7
7	-29.8		2	9.0	
			3	34.0	23.0
(13ℓ)			4	51.7	29.7
1	- 2.7	78.3			
2	-26.2	15.4	(63ℓ)		
3	-12.1	33.2	1	-26.3	
4	-38.8		2	31.6	23.1
5	6.3		3	12.2	9.8
6	-15.2				
			(73ℓ)		
(23ℓ)			1	- 0.8	
1	-25.7	23.8	2	-25.4	
2	- 5.6				
3	-36.8	15.4	(83ℓ)		
4	-21.1	18.8	3	- 5.1	6.3
5	- 0.6				
6	-16.1				
7	-17.0				

Table 9. (Continued)

Indices	$F_{calc.}$	$F_{obs.}$	Indices	$F_{calc.}$	$F_{obs.}$
	$\bar{h}3\ell$				
$(\bar{1}3\ell)$			$(\bar{6}3\ell)$		
1	-53.6	18.2	1	29.8	27.0
2	13.8	30.1	2	18.4	25.5
3	-10.6	31.9	3	58.3	42.0
4	- 9.5	19.7			
5	40.7	25.8	$(\bar{7}3\ell)$		
6	45.8	43.8	1	14.3	
			2	41.9	35.1
$(\bar{2}3\ell)$					
1	9.7	26.6	$(\bar{8}3\ell)$		
2	-35.0	58.7	3	16.2	10.8
3	-30.7	29.0			
4	19.3		$(\bar{9}3\ell)$		
5	26.5	21.7	3	-11.5	14.0
6	12.7				
7	57.7	43.1	$(\bar{10}\cdot 3\cdot\ell)$		
			3	- 9.4	10.8
$(\bar{3}3\ell)$					
1	- 7.7	12.6			
2	-28.4			$h4\ell$	
3	5.1				
4	-34.6	40.9			
5	8.1		(04ℓ)		
6	32.6	38.4	1	-35.2	10.8
			2	7.0	9.0
$(\bar{4}3\ell)$			3	- 8.6	34.7
1	- 5.9	18.2	4	-17.5	
2	26.3	20.7	5	41.0	34.3
3	-20.4	18.2	6	8.3	
4	7.1		7	14.5	9.8
5	-30.4	31.4	8	-26.0	16.0
$(\bar{5}3\ell)$			$(h40)$		
1	38.9	19.3	1	32.8	60.9
2	41.5	35.4	2	1.8	12.6
3	14.5	14.7	3	7.9	11.8
4	- 7.9	21.3	4	-13.8	13.3
			5	-25.6	17.2

Table 9. (Continued)

Indices	$F_{calc.}$	$F_{obs.}$	Indices	$F_{calc.}$	$F_{obs.}$
(14ℓ)			(74ℓ)		
1	15.6		1	-32.2	
2	-18.4		2	15.0	
3	-44.4	63.1	3	- 5.4	
4	1.6		4	10.5	
5	-11.9				
6	7.2		(84ℓ)		
			4	- 5.7	14.0
(24ℓ)					
1	10.5	20.3		$\bar{h}4\ell$	
2	-49.2	41.6			
3	-16.2	21.7			
4	-11.1				
5	-27.0				
6	- 0.4		($\bar{1}$4ℓ)		
			1	51.8	99.0
(34ℓ)			2	-52.7	58.4
1	-39.8	77.3	3	- 8.7	13.3
2	5.6		4	30.8	18.8
3	- 0.4		5	23.8	
4	-27.0	36.0	6	36.0	23.8
5	33.1	29.7			
			($\bar{2}$4ℓ)		
(44ℓ)			1	-50.1	29.4
1	7.5		2	- 3.2	
2	- 0.6		3	-11.0	26.6
3	17.8		4	-11.1	
4	54.0	46.6	5	31.2	29.0
5	-27.5		6	48.6	37.4
(54ℓ)			($\bar{3}$4ℓ)		
1	- 7.9	18.8	1	-10.5	14.7
2	40.8	35.4	2	- 5.6	
3	36.2	42.3	3	-34.7	17.8
4	17.1	14.0	4	12.0	21.7
5	19.2		5	- 8.5	
(64ℓ)					
1	12.6				
2	- 4.1				
3	41.3	30.0			
4	10.4				

Table 9. (Continued)

Indices	$F_{calc.}$	$F_{obs.}$	Indices	$F_{calc.}$	$F_{obs.}$
($\bar{4}4\ell$)			(h50)		
1	32.6	31.9	1	37.7	25.8
2	0.6	28.0	2	33.1	19.7
3	18.8		3	-16.6	14.7
4	-38.8	23.8	4	-22.9	16.0
5	- 3.1		5	8.7	
($\bar{3}4\ell$)			6	-20.0	19.7
1	25.8		(15ℓ)		
2	39.4	25.9	1	- 2.8	17.2
3	18.0		2	-31.3	19.7
4	- 2.2		3	- 8.2	
5	-32.2	23.4	4	-20.4	
($\bar{6}4\ell$)			5	9.5	9.0
1	34.6	29.0	6	- 3.0	
2	52.1	27.6	(25ℓ)		
3	- 4.9		1	-33.6	23.0
4	17.0		2	- 6.4	20.7
($\bar{7}4\ell$)			3	-38.6	32.2
1	0.8		4	-23.9	26.2
2	- 2.0		5	9.9	
3	42.1	34.0	(35ℓ)		
4	-38.5	9.0	1	4.7	
($\bar{9}4\ell$)			2	-35.6	33.2
4	-14.7	14.0	3	- 7.3	
			4	21.7	
			5	-42.7	23.0
	h5ℓ		(45ℓ)		
			1	-15.2	18.8
			2	24.2	24.2
(05ℓ)			3	23.4	20.3
1	40.6	28.7	4	- 6.5	
2	-37.5	28.4	5	33.7	23.4
3	-13.9		(55ℓ)		
4	30.4	7.7	1	12.4	
5	8.1	16.5	2	11.4	
6	35.3	23.0	3	44.5	23.8
7	- 9.7	7.7	4	30.9	

Table 9. (Continued)

Indices	$F_{calc.}$	$F_{obs.}$
(65ℓ)		
1	- 8.5	
2	43.8	27.3
3	12.8	
4	24.5	
5	-15.3	
(85ℓ)		
5	-10.4	13.3
	$\bar{h}5\ell$	
($\bar{1}$5ℓ)		
1	-62.3	42.7
2	20.5	
3	-13.4	19.3
4	5.2	14.7
5	52.8	31.6
6	31.0	23.8
($\bar{2}$5ℓ)		
1	16.4	
2	-46.6	30.0
3	- 9.9	25.1
4	20.1	
5	15.4	23.8
($\bar{3}$5ℓ)		
1	- 7.8	13.3
2	- 7.5	
3	- 0.6	
4	-33.1	17.2
5	8.9	
($\bar{4}$5ℓ)		
1	10.0	
2	30.8	21.3
3	-20.5	
4	6.5	
5	-38.0	14.0
($\bar{5}$5ℓ)		
1	50.6	34.0
2	30.7	23.4
3	17.1	29.7
4	-19.7	18.8
($\bar{6}$5ℓ)		
1	22.8	
2	23.0	20.7
3	34.9	
4	-22.5	
5	-10.2	15.4
	h6ℓ	
(06ℓ)		
1	-32.3	9.0
2	4.1	
3	- 1.7	14.0
4	2.7	16.0
5	47.4	32.2
6	8.6	
7	12.0	11.8
8	-32.6	13.3
(h60)		
1	31.1	34.9
2	- 2.5	20.3
3	- 1.0	
4	4.4	
5	-30.7	31.9
6	3.8	9.0
(16ℓ)		
1	- 7.2	10.9
2	-13.4	
3	-31.5	31.6
4	10.0	
5	6.1	
6	3.0	

Table 9. (Continued)

Indices	$F_{calc.}$	$F_{obs.}$	Indices	$F_{calc.}$	$F_{obs.}$
(26ℓ)			$\bar{h}6\ell$		
1	6.0	14.7			
2	-52.9	16.0			
3	-11.5		($\bar{1}$6ℓ)		
4	- 6.7		1	34.1	54.2
5	-29.2		2	-54.8	27.0
6	13.3		3	10.3	
			4	33.4	20.3
(36ℓ)			5	21.8	21.7
1	-34.3	30.7	6	39.4	23.0
2	1.4				
3	-15.4	20.3	($\bar{2}$6ℓ)		
4	-26.6	22.1	1	-50.7	34.0
5	28.6		2	14.5	
6	-37.7	20.7	3	-19.6	18.8
			4	- 3.5	17.2
(46ℓ)			5	31.6	
1	- 0.8		6	24.7	20.7
2	- 6.2				
3	19.0		($\bar{3}$6ℓ)		
4	28.1	23.0	1	8.4	
			2	-12.0	26.6
(56ℓ)			3	-19.8	
1	7.1		4	5.5	
2	44.1		5	-19.7	
3	21.9	21.7	6	- 8.4	
4	19.6				
5	3.3		($\bar{4}$6ℓ)		
			1	38.0	28.4
(66ℓ)			2	7.8	
1	18.5		3	13.8	
2	8.3	23.8	4	-42.7	19.3
3	46.1	25.1			
			($\bar{5}$6ℓ)		
			1	27.9	19.7
			2	41.4	34.6
			3	1.8	
			4	- 1.5	
			5	-33.6	21.2

Table 9. (Continued)

Indices	$F_{calc.}$	$F_{obs.}$
($\bar{6}6\ell$)		
1	35.8	
2	29.6	
3	- 5.9	
	h7ℓ	
(07ℓ)		
1	14.4	
2	-27.8	16.0
3	1.2	
4	37.4	28.4
5	17.7	15.4
6	31.2	12.6
7	-14.8	9.8
(h70)		
1	11.5	21.7
2	23.1	20.3
3	- 4.1	14.0
4	-32.7	17.2
5	21.1	9.0
(17ℓ)		
1	- 1.9	
2	-32.9	18.8
3	4.5	
4	- 3.5	
5	11.7	
6	8.1	
7	- 8.4	
(27ℓ)		
1	-37.5	13.3
2	- 5.1	
3	-36.8	19.7
4	-14.6	
5	18.3	
(37ℓ)		
1	- 8.0	
2	-39.2	34.0
3	- 5.5	
4	7.8	
5	-40.4	23.4
6	24.7	
7	-11.3	10.8
(47ℓ)		
1	- 4.9	18.2
2	16.7	
(57ℓ)		
1	8.7	
2	12.6	
3	43.2	
	$\bar{h}7\ell$	
($\bar{1}7\ell$)		
1	-55.0	28.7
2	24.2	14.0
3	-12.9	26.6
4	16.9	17.7
5	51.0	26.9
6	15.6	
7	9.5	15.4
($\bar{2}7\ell$)		
1	20.2	14.7
2	-50.0	30.7
3	7.5	
4	11.2	
5	4.8	20.3

Table 9. (Continued)

Indices	$F_{calc.}$	$F_{obs.}$
($\bar{3}7\ell$)		
1	- 4.1	
2	9.8	
3	-13.3	
4	-29.3	
5	5.4	
6	- 2.4	
($\bar{4}7\ell$)		
1	22.2	
2	24.5	16.5
($\bar{5}7\ell$)		
1	49.7	31.6
2	19.2	
3	13.5	23.8

h8ℓ

Indices	$F_{calc.}$	$F_{obs.}$
(08ℓ)		
1	-24.0	
2	1.8	
3	10.0	21.7
4	16.6	
5	44.8	18.8
6	7.8	9.0
7		
(h80)		
1	22.7	29.7
2	- 5.1	
3	-15.2	
4	16.6	
5	-31.0	21.7

Indices	$F_{calc.}$	$F_{obs.}$
(18ℓ)		
1	-20.8	18.8
2	- 2.6	14.0
3	-20.8	
4	21.6	
5	18.0	
(28ℓ)		
1	- 2.6	14.7
2	-49.9	24.6
3	- 0.7	
4	- 2.9	
5	-24.4	21.7
(38ℓ)		
1	-26.9	23.0
2	- 5.9	

$\bar{h}8\ell$

Indices	$F_{calc.}$	$F_{obs.}$
($\bar{1}8\ell$)		
1	19.6	29.4
2	-45.9	17.7
3	22.4	
4	29.0	16.6
5	17.9	18.8
($\bar{2}8\ell$)		
1	-40.9	31.6
2	24.6	14.0
3	-29.0	
4	2.2	
5	23.1	
($\bar{3}8\ell$)		
1	20.2	
2	-19.3	15.4

Table 9. (Continued)

Indices	$F_{calc.}$	$F_{obs.}$
($\bar{5}8\ell$)		
1	26.3	17.7
	h9ℓ	
(09ℓ)		
1	- 2.3	
2	-12.1	9.0
3	9.9	6.3
4	41.2	13.3
5	21.0	19.3
6	19.8	10.9
(h90)		
1	- 4.9	
2	7.5	17.7
3	3.9	
4	-41.1	18.3
5	25.5	
	$\bar{h}9\ell$	
($\bar{1}9\ell$)		
1	-39.8	19.7
	h·10·ℓ	
(0·10·ℓ)		
1	-12.4	7.7
2	0.3	
3	22.0	9.0
4	20.9	
(0·10·ℓ) (cont.)		
5	37.1	11.8
6	5.7	6.3
(h·10·0)		
1	12.1	
2	- 5.4	
3	-29.5	
4	19.9	
5	-28.1	18.8
	h·11·ℓ	
(0·11·ℓ)		
4	43.0	10.9
(h·11·0)		
1	-12.0	
2	- 7.6	
3	7.1	
4	-47.4	19.3
	h·12·ℓ	
(0·12·ℓ)		
3	30.3	11.8
	0kℓ	
(0k0)		
2	129.1	125.2
4	82.1	99.0
6	38.2	14.7
8	7.5	23.8
10	- 9.6	4.5
12	-15.2	6.3

Infrared spectral analysis

The infrared absorption spectrum of $[Fe(CO)_4]_3$ was examined in solution and in the solid state. The latter investigation included the KBr pellet method and single crystal infrared work with a polarizing microscope.

Sheline (20) had previously examined the infrared spectrum of $[Fe(CO)_4]_3$ from 830 cm.$^{-1}$ to 5000 cm.$^{-1}$, both as a saturated solution in toluene and as a fine powder. Throughout this entire region the only absorption detected, aside from some weak peaks, was in the CO stretching region. Here, Sheline found two strong carbon monoxide type carbonyl bands at 2020 cm.$^{-1}$ and 2043 cm.$^{-1}$ and a very weak band at 1833 cm.$^{-1}$ which he attributed to a bridge carbonyl. Cable and Sheline (1) later reported that the 1833 cm.$^{-1}$ band was a doublet with bridge carbonyl frequencies at 1830 cm.$^{-1}$ and 1860 cm.$^{-1}$. No explanation was given for the very weak intensities of the 1800 cm.$^{-1}$ bands in $[Fe(CO)_4]_3$ compared with the strong intensities of the bridge carbonyl bands reported for $Fe_2(CO)_9$, $Co_2(CO)_8$, and $[Co(CO)_3]_n$.

Therefore spectral studies of $[Fe(CO)_4]_3$ were undertaken in order to determine whether the so-called bridge carbonyl bands were real. The studies in solution were conducted with both a Baird Associates Model B double beam infrared

spectrophotometer and a Perkin-Elmer Model 13 double beam infrared recording spectrophotometer. Saturated solutions of $[Fe(CO)_4]_3$ in CCl_4, $CHCl_3$, and CS_2 gave essentially the same spectrum. Since intermolecular forces between solute molecules are destroyed in dilute solutions, the effect of dilution was also examined. The spectrum of a saturated solution of $[Fe(CO)_4]_3$ in CCl_4, together with the spectra of solutions prepared by successive two-fold dilutions of the saturated solution, and the solid KBr pellet spectrum are shown in Figures 36 and 37. The observed bands are listed in Table 10.

Table 10. Infrared frequencies ($cm.^{-1}$) of $[Fe(CO)_4]_3$

Solution		Solid (KBr pellet)	Intensity
2038		2018 - 2038	strong
2015			strong
1875		1860	weak
1853	?	1830	weak
1835			weak

Figure 36. Infrared carbonyl stretching frequencies of $[Fe(CO)_4]_3$ in CCl_4

Curve a. Saturated solution
Curve b. Two-fold dilution of the saturated solution
Curve c. Four-fold dilution of the saturated solution
Curve d. Background

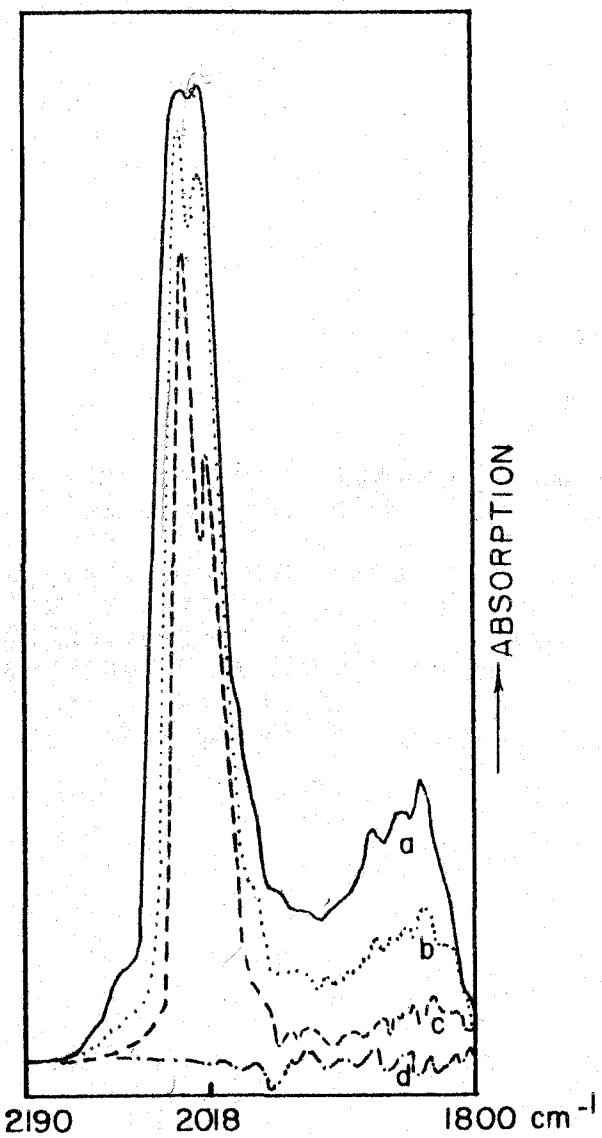
ABSORPTION
a
b
c
d
2190
2018
1800 cm⁻¹

Figure 37. Infrared carbonyl stretching frequencies of $[Fe(CO)_4]_3$ as solid in pressed KBr pellet. Concentration - 1 mg. sample/g. KBr

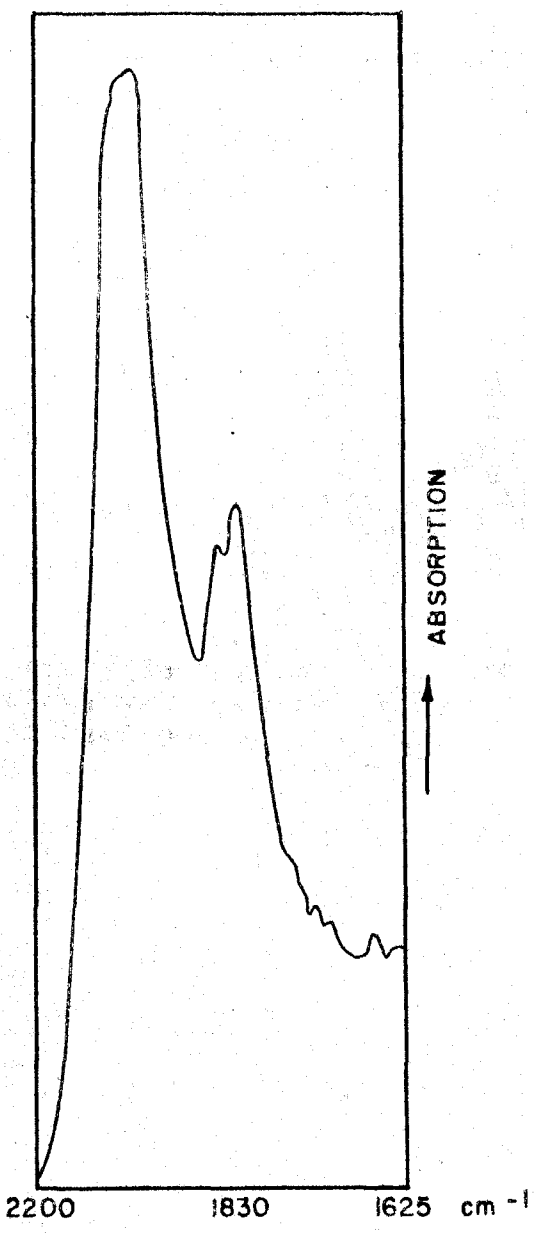
ABSORPTION
2200
1830
1625
cm -1

The two terminal carbonyl frequencies were well resolved in the solution spectra, but water vapor bands in the 1800-1900 cm.$^{-1}$ region given by the background curve in Figure 36 made it difficult to determine the number and peak positions of the weak bands. On dilution the intensities of the so-called bridge carbonyl bands decreased much faster than the intensities of the terminal carbonyl bands. The KBr pellet spectrum, however, clearly resolved two bands in the bridge carbonyl region and showed an increase in the intensity ratio of the weak bridge carbonyl bands compared to the strong terminal carbonyl bands. In an attempt to ascertain the total number of CO bands, a CaF_2 prism was substituted for the NaCl prism to increase the resolution of the spectrum. However, no further splitting of the bands was observed. Other infrared spectral analyses of $[Fe(CO)_4]_3$ (45, 46) have also given two terminal and two weak 1800 cm.$^{-1}$ absorption bands. Since the above evidence did not show conclusively whether or not $[Fe(CO)_4]_3$ contains bridge carbonyls, a study of the single crystal polarized spectrum of $[Fe(CO)_4]_3$ was undertaken.

In general a crystal resolves regular light into two components vibrating at right angles to each other. A non-cubic crystal gives two different refractive indices simultaneously, except when the incident light is polarized along

only one of the crystal's vibration directions. The refractive index of a crystal, therefore, depends on the vibration direction; the ellipsoidal three-dimensional graph of refractive indices is called the "indicatrix". For the monoclinic system the indicatrix is an ellipsoid with three unequal principal axes of refractive indices at right angles to each other. One axis of the indicatrix must coincide with the b_0 axis of the unit cell; the other two axes are located somewhere in the a_0c_0 plane normal to b_0.

When polarized infrared irradiation is passed through the crystal, the amount of absorption of a molecular vibration depends on the magnitude of the parallel projection of the transition moment vector on the electric vector of the incident polarized irradiation. Maximum absorption will occur when the electric vector is parallel to the transition moment vector, while minimum absorption will result when the vector directions are perpendicular.

For this reason polarization studies of single crystals can be useful in determining the bond orientation of particular groups.

The method of course depends on the crystal exhibiting pleochroism, that is, one of the polarized components of the incident irradiation is absorbed more strongly by a molecular vibration than the other.

Polarized infrared spectral studies of single crystals of $[Fe(CO)_4]_3$ were made with a Perkin-Elmer Model 112 single beam, double pass spectrograph equipped with a reflecting type microscope attachment and a AgCl polarizer. The optical path within the instrument was flushed with dry nitrogen.

It was hoped that pleochroism of the carbonyl bands might occur which would give information on the orientation of the CO bonds in the crystal. Thin specimens were needed to obtain good infrared absorption spectra. X-ray pictures of each crystal were taken to determine the orientation of the crystal axes.

Both $Fe_2(CO)_9$ and $[Fe(CO)_4]_3$ were examined; the terminal carbonyl and 1800 cm.$^{-1}$ absorption bands were clearly resolved by the microscope. Figure 38 gives the infrared polarized spectrum of an $Fe_2(CO)_9$ single crystal with the electric vector normal to the six-fold axis. Since the $Fe_2(CO)_9$ crystals are hexagonal as described previously in the Introduction no infrared pleochroism was observed on rotation of the electric vector normal to the hexagonal axis.

A number of $[Fe(CO)_4]_3$ crystals were examined, although difficulty was encountered in obtaining thin single crystals suitable for the work. With three crystals the carbonyl band at 1860 cm.$^{-1}$ was observed to be somewhat preferentially absorbed with the electric vector along the b_0 axis and

Figure 38. Infrared single crystal spectrum of the carbonyl stretching frequencies of $Fe_2(CO)_9$ with the electric vector normal to the six-fold axis

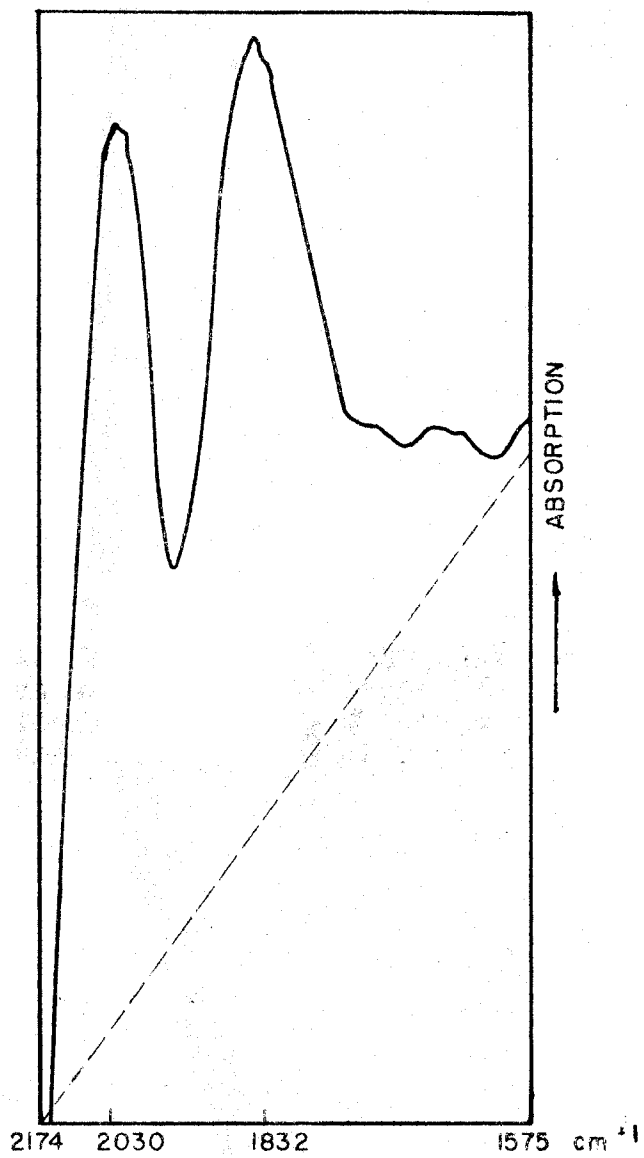
ABSORPTION
2174
2030
1832
1575
cm⁻¹

somewhat less absorbed with this vector along the c_B axis (Figure 39). Whether this difference is significant is difficult to decide, but in any event it was concluded that there is no polarization parallel or perpendicular to b_0 for the terminal carbonyl bands. The intensity ratio of the band at 1875 $cm.^{-1}$ to the band at 2040 $cm.^{-1}$ also increased greatly over the intensity ratios found in solution and with the KBr pellet method. This sharp difference in intensity of the compound measured in the solid as compared to solution is difficult to understand.

One explanation which can be given for the solution and KBr pellet spectra is that the molecule contains no bridge carbonyl bands, and the frequencies in the solid and solution are overtones or combination bands of iron-carbon stretching and iron-carbonyl bending frequencies. (This conclusion was also reached independently by Schufler, Sternberg, and Friedel (45) and Wilkinson and Cotton (46)). The increase of intensity in the solid spectrum may be attributed to an increase in perturbation of the molecule. Another explanation is that $[Fe(CO)_4]_3$ might dissociate in solution to non-bridging monomers, which might be paramagnetic. A magnetic susceptibility measurement of $[Fe(CO)_4]_3$ in CCl_4 was attempted, but was unsuccessful due to the slow decomposition of the compound and the limited solubility in the solvent.

Figure 39. Polarized infrared single crystal spectrum of the carbonyl stretching frequencies of $[Fe(CO)_4]_3$

Solid line--the electric vector is parallel to b_B

Dotted line--the electric vector is parallel to c_B

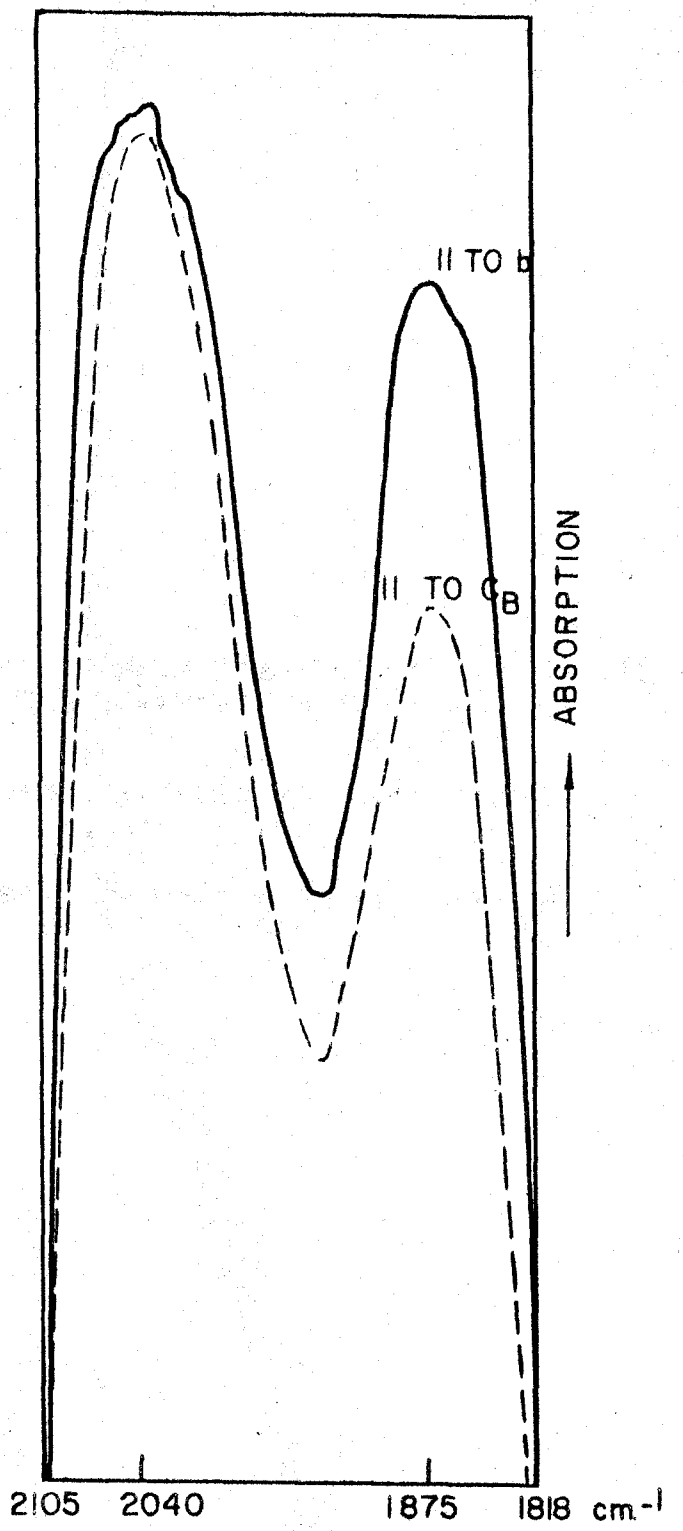
II TO b
II TO C_B
ABSORPTION
2105
2040
1875
1818
cm.-1

The solution data, hence, indicate that if $[Fe(CO)_4]_3$ contains bridge carbonyl bonds, the number is relatively few. The single crystal spectrum, however, strongly indicates association of the CO's with more than one metal in the crystalline state, although not necessarily the formation of a symmetrical bridge bond. The intensity of the 1800 cm.$^{-1}$ band in the crystal appears much too strong to be attributed simply to overtone or combination bands. However, the fact that only two terminal carbonyl frequencies are observed means that the molecular symmetry must be quite high.

A partial vibrational infrared analysis revealed that the D_{2d} structure (Figure 4b) favored by Brill (27) and Sheline (20) as the probable structure for $[Fe(CO)_4]_3$ would require three infrared-active terminal CO stretching frequencies, 1 B_2 and 2 E_1, and two bridge carbonyl stretching frequencies, 1 B_2 and 1 E_1. The apparent disagreement between the predicted number of terminal frequencies and the number in the observed spectrum is no doubt the reason that a vibrational analysis of the D_{2d} structure was not given by Sheline (20) in his infrared analysis of the compound.

The D_{3d} structure (Figure 4a) would give two terminal CO stretching frequencies, 1 A_{2u} and 1 E_u, and two bridge CO stretching frequencies, 1 A_{2u} and 1 E_u in apparent agreement with the observed spectrum. However, both structures

were eliminated by the three-dimensional Patterson and Fourier maps. Vibrational analysis of different CO arrangements for the trigonal model were inconclusive. It appears that the partial vibrational type analysis in this case is of limited value in the determination of the configuration of the CO ligands.

Inequalities

In an attempt to determine the phases of the structure factors directly, the method of inequalities was applied.

In 1948 Harker and Kasper (47) derived a number of inequalities for a centrosymmetric crystal which impose limitations on the magnitudes and phases of the structure factors. In some cases the restrictions are sufficient to determine the signs (phases) of all the important structure factors; in other cases a series of probable sign relationships is obtained. These inequalities depend on the fact that the electron-density is always positive and, moreover, is approximately a superposition of spherically-symmetric atoms. By a method similar to that used for the determination of "sharpened" Pattersons, unitary structure factors are defined as:

$$U(hk\ell) = \frac{F(hk\ell)}{F(000)\sqrt{f}} ,$$

where $|U(hk\ell)| < 1.00$ and $U(000) = 1.00$. Here, $U(hk\ell)$ is the unitary structure factor, $F(hk\ell)$ the structure factor, $F(000)$ the total number of electrons in the unit cell (i.e. $\sum_{j=1}^{N} Z_j$), and $\hat{f}$ the unitary scattering factor. The division of $F(hk\ell)/F(000)$ by $\hat{f}$ corresponds to correcting the observed structure factors to those of a crystal in which the electron-density of each atom is reduced to a point charge at its nucleus. If it is assumed that the atomic scattering factor f_j of the jth atom in a crystal is related to the unitary atomic scattering factor by the expression $f_j = Z_j \hat{f}$, where Z_j is the atomic number of the jth atom, the unitary structure factor equation reduces to the following:

$$U(hk\ell) = \frac{F(hk\ell)}{\sum_{j=1}^{N} f_j} .$$

Unitary structure factors were calculated from the above equation for each observed reflection, but the Harker-Kasper inequalities, as expressed in more applicable form by Grison (48), failed to give even probable sign relationships. Since this lack of success was attributed to the high temperature factor of the crystal, the unitary structure factors were made more powerful by the application of an inverse temperature factor $U(hk\ell) \exp (B \sin^2 \theta / \lambda^2)$, that is, each atom

was made to correspond to a "cold" point charge. An arbitrary value of B = 4.2 was chosen, as it was felt that the value B = 5.8 obtained from applying Wilson's method (43) to the three-dimensional data was too high. Unfortunately, the scale factor obtained from the equation

$$\overline{U(hk\ell)^2} = \frac{\sum_{j=1}^{N} Z_j^2}{(\sum_{j=1}^{N} Z_j)^2}$$

was found to be unreliable. The failure of the statistical method of scaling in this case was again attributed to the large number of accidentally absent reflections. The (404) reflection, therefore, was arbitrarily given a unitary structure value of 0.80. Sayre's equality (49; 50) and Harker-Kasper's inequalities (51) lead to the equation

$$S(hk\ell) = S(h'k'\ell')\, S(h + h', k + k', \ell + \ell')$$

where $S(hk\ell)$ refers to the sign of the $(hk\ell)$ reflection (i.e. + or -), $S(h'k'\ell')$ the sign of the $(h'k'\ell')$ reflection, and $S(h + h', k + k', \ell + \ell')$ the sign of the $(h + h', k + k', \ell + \ell')$ reflection. For a centrosymmetric crystal the above equation gives the probable sign relation if the corresponding

three structure factors are large. The Harker-Kasper inequalities together with the expression given above were used in the derivation of the following sign relationships:

1. $S(404)$ is +
2. $S(808)$ is +
3. $S(\bar{6}22) = S(\bar{2}26)$
4. $S(424) = S(020)$
5. $S(514) = S(\bar{2}37)S(\bar{7}23)$
6. $S(202) = S(505)S(707)$
7. $S(503) = S(\bar{7}23)S(\bar{2}26)$
8. $S(\bar{2}37) = S(\bar{6}22)S(415)$
9. $S(\bar{7}32) = S(\bar{2}26)S(514)$
10. $S(\bar{7}43) = S(\bar{2}37)S(5\bar{1}4)$
11. $S(\bar{7}23) = S(\bar{3}27)$
12. $S(\bar{2}26) = S(424)S(2010)$
13. $S(1002) = S(2010)$
14. $S(514) = S(\bar{1}\bar{1}0)$
15. $S(415) = S(0\bar{1}\bar{1})$
16. $S(820) = S(\bar{4}24)$
17. $S(820) = S(\bar{6}22)S(202)$
18. $S(028) = S(\bar{4}24)$
19. $S(028) = S(\bar{2}26)S(202)$

Indirect support of the trigonal structure was given by these sign relationships since all of them were consistent

with the signs calculated for the disordered trigonal structure.

Discussion

An inference as to the molecular structure of $[Fe(CO)_4]_3$ can be made from the crystal structures of the dimethylphosphinoborine and the dimethylphosphinodichloroborine trimers. The former compound, $[(CH_3)_2PBH_2]_3$, was found by Hamilton (52) to possess the orthorhombic space group, Pnma, with four molecules per unit cell. The molecule has a cyclohexane-like ring of alternating phosphorus and boron atoms arranged in a chair form, with two methyl groups attached to each phosphorus and two hydrogens to each boron. Schaeffer (53) determined the space group and lattice constants of $[(CH_3)_2PBCl_2]_3$ and found it to be essentially isomorphous with $[(CH_3)_2PBH_2]_3$. Crystals of $[(CH_3)_2PBCl_2]_3$, which were obtained from Dr. Schaeffer, are colorless bipyramids similar in habit to $[Fe(CO)_4]_3$. The B-centered lattice of $[Fe(CO)_4]_3$ also contains four trimers per unit cell. On interchange of the b_p (= b_B) and a_B axes of the B-centered lattice of $[Fe(CO)_4]_3$, the orientation of the axes of the two compounds was found to be the same. (The a_o and c_o axes are diagonal across the top of the bipyramid with the b_o axis normal to

the $a_o c_o$ plane.) Their lattice constants together with those of $[(CH_3)_2PBH_2]_3$ are as follows:

$[Fe(CO)_4]_3$	$[(CH_3)_2PBCl_2]_3$	$[(CH_3)_2PBH_2]_3$
$a_o = b_o = 11.33$ Å	$a_o = 11.59$ Å	$a_o = 11.16$ Å
$b_o = a_B = 12.93$ Å	$b_o = 13.75$ Å	$b_o = 13.16$ Å
$c_o = c_B = 11.44$ Å	$c_o = 11.86$ Å	$c_o = 10.53$ Å

There appears to be a correlation among the lattice constants of the three compounds, which suggests that the $[Fe(CO)_4]_3$ molecule might have a similar shape and therefore might pack in the same way as the two phosphorus-boron compounds.

If the three iron atoms are arranged at the corners of an equilateral triangle and placed in the unit cell in a manner corresponding to the molecular packing of $[(CH_3)_2PBH_2]_3$, it is found that in order to conform to the systematic extinctions observed for $[Fe(CO)_4]_3$, there must be a disorder in which the equilateral triangle is randomly placed in one of two orientations differing from one another by a rotation of 60° about the three-fold axis. This same conclusion had previously been made from a study of the Patterson map. This gives an apparent center of symmetry to the molecule, and, moreover, provides the only reasonable explanation for the six intense vectors of hexagonal symmetry and of length

1.5 to 1.6 Å around the origin of the three-dimensional "sharpened" Patterson. Actually the hexagon of peaks is the result of iron-iron vectors from an equilateral triangle in one unit cell to an equilateral triangle in the alternate position in another unit cell.

This model accounts very well for other large peaks in the "sharpened" three-dimensional Patterson. The complete hexagon of peaks around the origin is explained in terms of intramolecular and intermolecular iron-iron vectors; the complete hexagon of peaks about $\frac{1}{2},\frac{1}{2},\frac{1}{2}$ is the result of intermolecular iron-iron vectors.

On the other hand, no linear arrangement of iron atoms can explain the hexagon of peaks around the origin and $\frac{1}{2},\frac{1}{2},\frac{1}{2}$ in terms of iron-iron vectors; the peaks must be interpreted as coincidences of mainly iron-carbon and iron-oxygen vectors. This explanation was attempted for such structures as the D_{3d} and D_{2d} models (Figures 4a and 4b) with no success. Packing considerations alone definitely eliminated the D_{2d} structure from lying along the C_B or b_p axes. A deconvolution of the "sharpened" three-dimensional Patterson showed that no linear structure could reasonably explain the peak heights experimentally found. If the structure were linear, it seems very reasonable that the "sharpened" three-dimensional Patterson would have immediately given the iron-iron vectors.

The representation of the electron-density function and the Patterson function by a suitable Fourier series assumes that the electron-density is periodic in the crystal for the unit cell chosen. Since the observed intensities on the film correspond to the average electron-density of all the unit cells, the result of the disorder would be equivalent to placing twelve half-iron atoms, forty-eight half-carbon atoms, and forty-eight half-oxygen atoms in the unit cell. For the space group $P2_1/n$ with four-fold general positions, this would give the discouraging number of 81 parameters to be determined.

Steric considerations of the CO ligands restrict the disorder to be of a one-dimensional type along the b_o axis, with the trigonal arrangement in a particular $a_o c_o$ plane ordered in one of the two positions. There is no evidence of diffuse scattering, which means that the nature of the disorder is that of a true statistical distribution. A long exposure of the ($h0\ell$) zone shows six darker diffuse areas of hexagonal symmetry (probably the result of thermal motion of the molecule), which might be an indication of such a disorder.

An alternative choice of iron positions satisfying the "sharpened" three-dimensional Patterson exists, in which the two iron triangles are related by a two-fold axis in the b_p

direction rather than by a center of symmetry. This possibility seemed less likely since the probable space group $P2_1/n$ indicates a centrosymmetric molecule.

If a molecule crystallizes in the monoclinic space group $P2_1/n$ with two molecules in the unit cell, it ordinarily follows that the center of the molecule has to lie in the two-fold position which requires a center of symmetry. There are other known structures, however, that apparently are disordered in such a manner that the average symmetry corresponds to that of a center of symmetry. Three such examples are recorded in which the space group $P2_1/n$ or its "equivalent" (i.e. $P2_1/a$ or $P2_1/c$) is involved. Lund (54) found the compound 1e,2e,dichloro-4e,5e,dibromocyclohexane and the corresponding tetrachloro- and tetrabromo- compounds to be isomorphous and yet to crystallize in the space group $P2_1/n$ with two molecules per unit cell. Two-dimensional Fourier projections appeared to support the hypothesis of a statistical disorder. This same type of disorder was apparently found by Hendriks (55) for p-chloro-bromobenzene and also by Hassel and Vihovde (56) for trans 1,4-chloro-bromocyclohexane, although in the latter case there was some question as to whether the distribution was truly statistical. The crystal structure of $\left[Fe(CO)_4\right]_3$ represents the first known case of a random disorder for a transition metal complex.

Another indication of the iron positions is obtained directly from the intensities of the reflections on the film. An (010) Laue picture of $[Fe(CO)_4]_3$ indicates nearly orthorhombic symmetry along the B-centered axes with $\beta_B \sim 90°$ (i.e. $\beta_B = 93° 45'$). The extinctions of the B-centered lattice are:

$(h_B k l_B)$	$h_B + l_B = 2n + 1$	absent
$(h_B 0 l_B)$	$h_B = 2n + 1$	absent
$(0 k_B 0)$	$k_B = 2n + 1$	absent

which on interchange of the b_B and c_B axes become:

(hkl)	$h + k = 2n + 1$	absent	C-centered lattice
$(hk0)$	$h = 2n + 1$	absent	a_c glide plane
$(00l)$	$l = 2n + 1$	absent	2_{1_c} screw axis

If it is assumed that the iron atoms are related by orthorhombic symmetry, the only orthorhombic space groups compatible with the above systematic absences are Cmca (full symmetry C 2/m 2/c 2_1/a) and C2ca. Further support of this assumption is given by the presence of strong (hk0) intensities only for k = 2n, which by the interchange of the b_p and c_B axes indicates an approximate c_b glide plane in agreement with both orthorhombic space groups. The symmetry positions of the space group C2ca are given in Figure 40. The

Figure 40. Symmetry positions in the space group C2ca

Point positions: $(000;\ \frac{1}{2}\frac{1}{2}\frac{1}{2})+$

4: (a) x00; $x\frac{1}{2}\frac{1}{2}$

8: (b) xyz; $x,\frac{1}{2}+y,\frac{1}{2}-z$

$x\bar{y}\bar{z}$; $x,\frac{1}{2}-y,\frac{1}{2}+z$

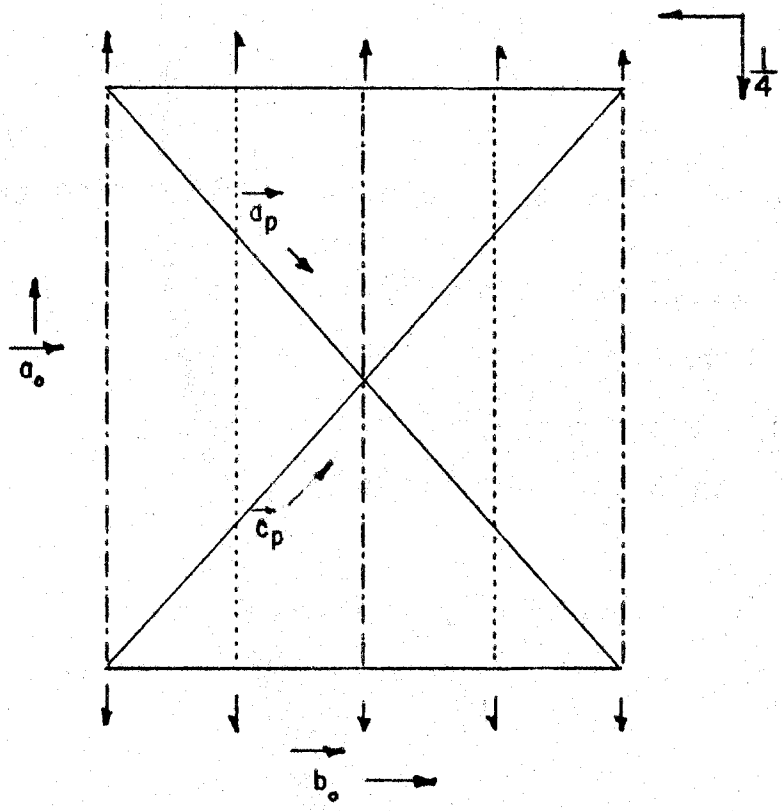
1/4
$\vec{a}_p$
$\vec{c}_p$
a_o
b_o

orientation of the primitive unit cell relative to the B-centered cell is included in the projected unit cell diagram.

Since there are twelve Fe atoms in the B-centered cell, if no disorder is assumed, the Fe atoms must be placed on three sets of special positions (a) or on one set of special positions (a) and on one set of general positions (b) given in Figure 40. It is easily seen that if the trigonal iron arrangement is not disordered, the iron atoms are related by the two-fold axis in the a_o direction with one iron lying on the two-fold axis. For any linear structure, the three iron atoms are restricted to lie along the a_o direction or approximately normal to it.

The space group Cmca, the symmetry positions of which are given in Figure 41, further restricts the three iron atoms of a linear structure to be on a two-fold axis in the a_o or b_o direction with the central iron located on a center of symmetry. It is felt that all possibilities corresponding to these limits have been investigated by Fourier projections and have been shown to be incompatible with the data.

An interpretation of the disordered trigonal structure can be made (corresponding to twenty-four half-iron atoms) with the space group Cmca. The eight-fold set $(0,0,0;\frac{1}{2},\frac{1}{2},0)$ + (d) and the sixteen-fold set $(0,0,0;\frac{1}{2},\frac{1}{2},0)$ + (g) of

Figure 41. Symmetry positions in the space group Cmca

Point positions: $(000;\ \frac{1}{2}\frac{1}{2}0)$ +

4: (a) $000;\ 0\frac{1}{2}\frac{1}{2}$ (b) $\frac{1}{2}00;\ \frac{1}{2}\frac{1}{2}\frac{1}{2}$

8: (c) $\frac{1}{4}\frac{1}{4}0;\ \frac{1}{4}\ 3/4\ 0;\ \frac{1}{4}\frac{1}{4}\frac{1}{2};\ \frac{1}{4}\ 3/4\ \frac{1}{2}$

(d) $x00;\ \bar{x}00;\ x\frac{1}{2}\frac{1}{2};\ \bar{x}\frac{1}{2}\frac{1}{2}$

(e) $\frac{1}{4}y\frac{1}{4};\ 3/4\ \bar{y}\ 3/4;\ 3/4\ y\ \frac{1}{4};\ \frac{1}{4}\ \bar{y}\ 3/4$

(f) $0yz;\ 0\bar{y}\bar{z};\ \frac{1}{2},y,\frac{1}{2}-z;\ \frac{1}{2},\bar{y},\frac{1}{2}+z$

16: (g) $xyz;\ x\bar{y}\bar{z};\ x,\frac{1}{2}+y,\ \frac{1}{2}-z;\ x,\frac{1}{2}-y,\ \frac{1}{2}+z$

$\bar{x}\bar{y}\bar{z};\ \bar{x}yz;\ \bar{x},\frac{1}{2}-y;\ \frac{1}{2}+z;\ \bar{x},\frac{1}{2}+y,\ \frac{1}{2}-z$

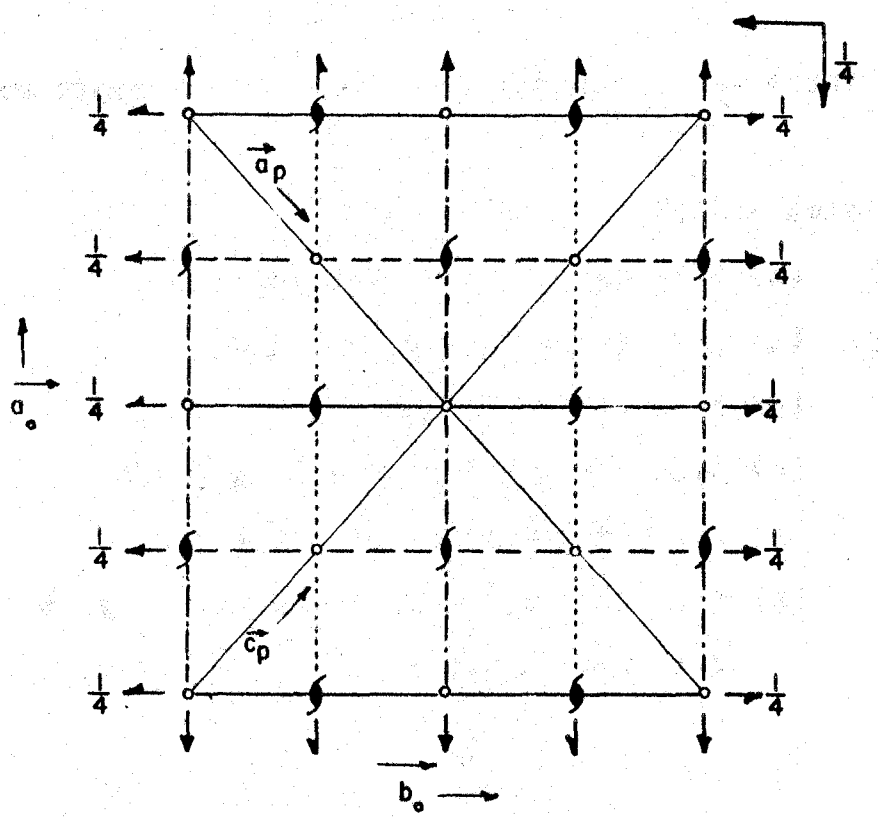
1/4
1/4
1/4
1/4
1/4
1/4
1/4
1/4
1/4
1/4
$\vec{a}_p$
$\vec{c}_p$
a_o
b_o

Cmca (Figure 41) approximately agree with the positions chosen previously.

The configuration of the CO ligands still needs to be determined. Unfortunately, as indicated by the large number of parameters, the complete solution of the structure demands the services of a big computor with which different trial structures can be quickly tested. Trigonal structures with either (a) four terminal CO ligands on each of the three iron atoms (i.e. no bridge CO's), (b) nine terminal CO ligands (three on each iron) and three bridge carbonyls, and (c) six terminal CO ligands and six bridge CO's are all compatible with the closed electronic shell rule, if iron-iron bonds from each iron atom to the other two iron atoms are assumed. It may be that the iron atoms in $[Fe(CO)_4]_3$ are not all equivalent. For example, bridge bonds may be formed between only two Fe atoms with metal-metal bonds linking the third iron atom to the other two. Since a number of CO arrangements are possible, no postulation of the probable CO configuration of the molecule is made. The spectral data strongly indicate some association in the solid state, although the solution spectrum definitely suggests no bridge carbonyls.

In addition to the iron-iron vectors, the three-dimensional Pattersons (both "unsharpened" and "sharpened")

and the three-dimensional electron-density Fourier strongly suggest that at least one terminal group per iron is approximately perpendicular to the plane made by the equilateral triangle of iron atoms. There is also definite indication that at least one terminal CO ligand per iron extends outward in approximately the same plane as the iron atoms. The iron-iron distance is approximately 2.75 to 2.85 $\mathring{A}$, which on comparison with the Fe-Fe distance of 2.46 $\mathring{A}$ for $Fe_2(CO)_9$, suggests that there are no bridge carbonyls or that the number of bridge carbonyl bonds is not greater than three. There is also the possibility that the bridge carbonyl bonds are not symmetric.

STRUCTURES OF RHENIUM PENTACARBONYL AND MANGANESE PENTACARBONYL

Review of Literature

Two polynuclear carbonyls of the Group VIIa transition metals, rhenium pentacarbonyl and manganese pentacarbonyl, have recently been isolated and characterized. Rhenium pentacarbonyl was first prepared by Hieber and Fuchs (57) from Re_2O_7, $KReO_4$, or Re_2S_7 at CO pressures of at least 200 atmospheres and temperatures of approximately 250°C. Unlike most other polynuclear carbonyls it cannot be synthesized from the halocarbonyl (in this case the halopentacarbonyl) by the action of halogen-binding metals or directly from the metal at elevated CO pressures and high temperatures. The molecular weight, determined (57) by cryoscopic measurements in camphene, showed rhenium pentacarbonyl to be dimeric (i.e. $Re_2(CO)_{10}$). Rhenium pentacarbonyl forms colorless and odorless crystals which are stable in air and resistant to dilute acids and bases and to concentrated HCl. It melts at 177°C. in a closed tube, but can be sublimed at 140° C. The crystals are not wet by water but are somewhat soluble in inert solvents such as dioxane and hexane where they

dissolve in concentrations up to 10^{-1} moles/l. at room temperature (58).

In 1954 Brimm, Lynch, and Sesny (18) synthesized manganese pentacarbonyl in small quantities by reducing MnI_2 with Mg in diethylether at room temperature under a CO pressure of 68-204 atmospheres. The molecular weight, determined by cryoscopic measurements in cyclohexane (18), revealed that manganese pentacarbonyl is also dimeric (i.e. $Mn_2(CO)_{10}$). Manganese pentacarbonyl forms golden-yellow, transparent crystals which melt at 154-155° C. in a sealed tube. In the absence of carbon monoxide $Mn_2(CO)_{10}$ begins to decompose at 110° C. Although stable for prolonged periods under an atmosphere of CO, it slowly turns brown in air at room temperature. It is not wet by water and is soluble in common organic solvents.

Morphologically similar to $[Fe(CO)_4]_3$, $Re_2(CO)_{10}$ crystallizes as pseudotetragonal, monoclinic, prismatic crystals. The axial ratios determined by Sternberg (57) are $a_o:b_o:c_o$ = 1.045:1:2.045 with β = 103° 32'.

X-ray single crystal Laue and rotation pictures of $Mn_2(CO)_{10}$ by Brimm et al. (18) showed the unit cell to be monoclinic with axial ratios $a_o:b_o:c_o$ = 1.036:1:0.5054 with β = 105°, and lattice constants a_o = 14.68 Å, b_o = 14.16 Å, and c_o = 7.16 Å.

Hieber and Fuchs (57) proposed a structure for $Re_2(CO)_{10}$ (Figure 42a) involving the coordination of two octahedra at a common edge; the rhenium atoms are therefore bonded to each other by two bridge carbonyls. An infrared analysis of both compounds by Brimm et al. (18), however, revealed no evidence of bridge carbonyl absorption. Three absorption bands were observed for both compounds in the region characteristic of the terminal carbonyl stretching frequencies. Hence, it was concluded that the dimerization occurs through the formation of direct metal-metal bonds.

Cable and Sheline (1) from a partial vibrational analysis of the spectra reported by Brimm et al. (18) postulated similar structures of D_{4h} symmetry for both molecules; the D_{4h} structure involves the junction of two octahedra at an apex such that the CO ligands are arranged in an eclipsed configuration (Figure 42b).

A closer examination of the infrared spectra by Cotton, Liehr, and Wilkinson (19) confirmed the observed spectra reported by Brimm et al. (18). However, from a partial vibrational analysis Cotton et al. (19) eliminated four postulated structures with direct metal-metal bonding including the D_{4h} structure favored by Cable and Sheline. Instead, they proposed as the only other reasonable alternative, structures with a pseudo-ring of CO groups between the

Figure 42. Proposed structures of $Re_2(CO)_{10}$ and $Mn_2(CO)_{10}$

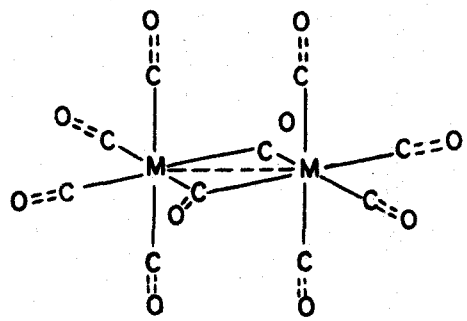

FIG. 42a

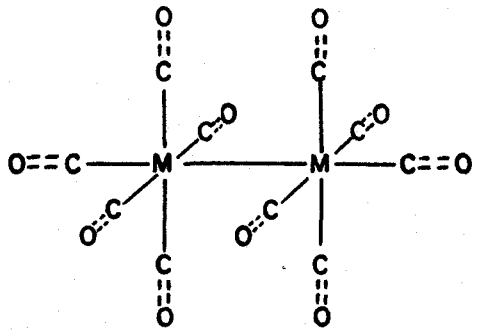

FIG. 42b

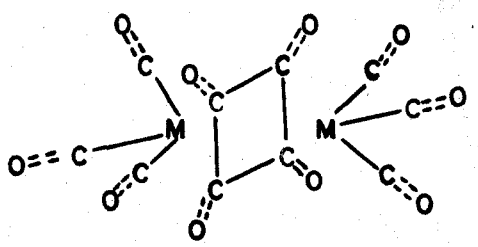

FIG. 42c

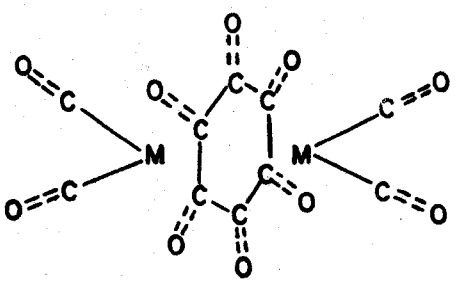

FIG. 42d

metal atoms. Two possible models were suggested as being consistent with the observed spectra--one has each of the terminal groups of CO ligands possessing C_{3v} local symmetry with a planar four-membered ring (D_{4h} symmetry) between the metal atoms (Figure 42c); the other has a planar six-membered ring between the metal atoms (Figure 42d). The diamagnetism of $Mn_2(CO)_{10}$ and $Re_2(CO)_{10}$ was explained for the pseudo-ring structures by the assumption that an odd number of electrons from the ring contribute to the orbitals of each metal atom.

Experimental Procedure and Results

Preparation and identification

The $Re_2(CO)_{10}$ and $Mn_2(CO)_{10}$ compounds were prepared by Dr. E. O. Brimm of Linde Air Products Company and were made available through the generosity of Professor G. Wilkinson[1].

The characteristic shapes and colors of the compounds were observed to be identical with their descriptions as contained in the section "Review of Literature".

---

[1]Present address: Chemistry Department, Imperial College of Science and Technology, London, S. W. 7, England.

Diffraction data

Single-crystal X-ray investigations showed $Re_2(CO)_{10}$ and $Mn_2(CO)_{10}$ to possess monoclinic symmetry. The lattice constants which were obtained from precession photographs, together with the intensity data, established the two compounds to be isomorphous. The lattice constants are as follows:

$Re_2(CO)_{10}$

$a_o = 14.70$ Å, $b_o = 7.15$ Å, $c_o = 14.91$ Å, $\beta = 106^\circ$

$Mn_2(CO)_{10}$

$a_o = 14.16$ Å, $b_o = 7.11$ Å, $c_o = 14.67$ Å, $\beta = 105^\circ$

The number of dimers per unit cell is four (i.e. the unit cell contains eight metal atoms, forty carbon atoms, and forty oxygen atoms), since eight $Mn(CO)_5$ species per unit cell give $d_{calc.} = 1.82$ g./cc. compared with the experimental value $d_{exp.}^{25^oC.} = 1.75$ g./cc. reported by Brimm et al. (18). The experimental value may be somewhat in error as it represents the average density as determined by the displacement of water rather than by the flotation method.

Intensity data for rhenium pentacarbonyl

The intensity data for $Re_2(CO)_{10}$ were taken first. The indexed data revealed the following systematic absences:

1. (h0ℓ) absent for h = 2n + 1, ℓ = 2n + 1
2. (h1ℓ) absent for h + ℓ = 2n
3. (h2ℓ) absent for h + ℓ = 2n + 1
4. (hk0) absent for h + k = 2n + 1

Therefore the probable space group is I2/a or Ia. The Internationale Tabellen zur Bestimmung von Kristallstructuren (38, pp. 102 and 96) lists the "equivalent" space groups C2/c and Cc which are based on an alternative unit cell. The alternative C-centered cell, defined by the choice of a diagonal axis as the new a_o lattice constant, has the same volume as the I-centered cell but is less convenient because its monoclinic angle is greater.

For the (h1ℓ) zone the intensities of the reflections h = 2n + 1, ℓ = 2n were very much stronger than the other reflections. For (h2ℓ), only the reflections h = 2n, ℓ = 2n appeared with but one exception. Since the Re atom is so much heavier than the rest of the atoms (atomic number of Re = 75), its intensity contribution to each reflection in general overwhelmed the intensity contributions from the other atoms. For the space group I2/a the additional

intensity information given above indicated a y parameter $\sim \frac{1}{4}$ for the eight-fold set of Re positions. This conclusion was also reached by the observation of a normal decline of intensities along the b_o axis for the (hk0) data. An x parameter for Re of 0.154 was estimated directly from the (hk0) photographs by calculation of the approximate intensities of a number of reflections for a range of parameters. From the (h0ℓ) and (h1ℓ) photographs, two z parameters were found to be equivalent; they are: (a) the value $z_1 = 0.180$, corresponding to a dimeric molecule with a center of symmetry at $\frac{1}{4},\frac{1}{4},\frac{1}{4}$, (b) the value $z_2 = z_1 - \frac{1}{4} = 0.930$ corresponding to a dimer symmetric about the two-fold axis at $\frac{1}{4},0,0$.

Intensity data of the (h0ℓ) and (hk0) zones were obtained for $Re_2(CO)_{10}$ using the precession camera with Mo irradiation. The number of independently observed reflections was 126 for the (h0ℓ) zone; 68 for the (hk0) zone.

Structure factors based on the Re parameters x = 0.154, y = 0.250, and z = 0.930 were calculated for the (h0ℓ) and (hk0) zones, from which phases were obtained for the observed structure factors. The calculated structure factors were given a temperature correction (for the (h0ℓ) zone, B = 3.73; for the (hk0) zone, B = 3.68), and the observed structure factors were placed on an absolute scale. The reliability index, R(hkℓ), with the unobserved reflections omitted was

found to be 22.0% for the (h0ℓ) zone; 14.8% for the (hk0) zone. A comparison of the observed and temperature-corrected calculated structure factors for the (h0ℓ) and (hk0) zones is given in Table 11.

Fourier projections of rhenium pentacarbonyl

Fourier electron-density projections onto the (010) and (001) planes were made (Figures 43 and 44). The Re peak positions determined for both zones by the application of Booth's method (44) indicated no shift in the x, y, and z parameters (determined to the nearer 0.001). The projections, also, suggested octahedral bonding for the CO ligands, since the electron-density for the (010) projection was concentrated about a line drawn through each Re position and approximately normal to the line connecting the Re atoms. Both the (010) and (001) projections showed evidence of an end CO bond almost collinear with the Re-Re bond.

Intensity data for manganese pentacarbonyl

In order to ascertain the molecular symmetry of $Re_2(CO)_{10}$, $Mn_2(CO)_{10}$ was next investigated. The (hk0), (0kℓ), and (h0ℓ) intensity data were taken by the precession camera with Mo

Table 11. Comparison of observed and temperature-corrected calculated structure factors for $Re_2(CO)_{10}$

Indices	$F_{calc.}$ 8	$F_{obs.}$ 8	Indices	$F_{calc.}$ 8	$F_{obs.}$ 8
	h0ℓ				
(h00)			(h04)		
2	-25.1	18.8	0	-12.4	12.6
4	-45.4	42.1	2	55.5	58.2
6	44.6	30.1	4	-24.9	30.2
8	4.5	7.7	6	-24.7	26.2
10	-29.9	28.7	8	30.1	37.4
12	13.2	9.8	12	-16.0	20.3
14	9.1	9.6	14	8.9	6.6
16	-11.3	12.9	16	3.5	6.4
(h02)			($\bar{h}$04)		
0	45.1	44.7	$\bar{2}$	-52.6	37.0
2	32.0	35.5	$\bar{4}$	45.7	40.0
4	-54.6	81.9	$\bar{6}$	14.1	13.0
6	9.8	11.0	$\bar{8}$	-42.9	31.0
8	30.3	32.7	$\bar{10}$	13.9	9.7
10	-22.5	15.4	$\bar{12}$	17.0	18.5
12	- 5.4	7.0	$\bar{14}$	-16.6	17.5
14	14.6	16.6	$\bar{18}$	8.5	9.8
16	5.6	3.4			
18	- 4.7	6.0	(h06)		
			0	-45.0	36.9
($\bar{h}$02)			2	35.5	25.1
2	-65.4	56.2	4	13.3	16.4
$\bar{4}$	2.3	6.5	6	-33.1	42.1
$\bar{6}$	47.5	3.6	8	9.9	12.5
$\bar{8}$	-28.7	23.7	10	14.3	17.1
$\bar{10}$	-14.0	16.2	12	-12.9	17.2
$\bar{12}$	24.3	23.1	14	- 0.9	2.7
$\bar{16}$	- 9.9	11.5	16	6.8	9.9
$\bar{18}$	7.4	7.2			

Table 11. (Continued)

Indices	$F_{calc.}$ / 8	$F_{obs.}$ / 8	Indices	$F_{calc.}$ / 8	$F_{obs.}$ / 8
($\bar{h}$06)			($\bar{h}$·0·10)		
$\bar{2}$	- 7.2	2.5	$\bar{2}$	33.1	24.5
$\bar{4}$	47.8	38.4	$\bar{4}$	-13.2	9.1
$\bar{6}$	-24.9	16.3	$\bar{6}$	-21.8	20.7
$\bar{8}$	-21.7	19.1	$\bar{8}$	24.9	20.7
$\bar{10}$	29.2	27.4	$\bar{10}$	1.4	3.8
$\bar{12}$	- 2.6	3.9	$\bar{12}$	-17.9	14.7
$\bar{14}$	-15.6	17.6	$\bar{14}$	9.0	7.0
$\bar{16}$	9.3	7.1	$\bar{16}$	5.6	6.5
$\bar{18}$	3.2	4.8	$\bar{18}$	- 7.8	8.2
(h08)			(h·0·12)		
0	-37.4	28.0	0	12.5	11.5
4	29.7	33.9	2	-20.4	17.6
6	-17.1	15.0	4	2.9	2.9
8	- 9.7	11.3	6	12.6	16.5
10	15.4	20.8	8	- 9.0	8.0
12	- 2.7	3.4	10	- 2.7	5.6
14	- 6.7	10.5	12	6.3	9.1
16	4.6	6.2			
($\bar{h}$08)			($\bar{h}$·0·12)		
$\bar{2}$	28.5	18.8	$\bar{2}$	15.0	15.0
$\bar{4}$	18.2	9.8	$\bar{4}$	-24.2	19.9
$\bar{6}$	-37.5	29.5	$\bar{8}$	19.5	13.6
$\bar{8}$	8.6	6.1	$\bar{10}$	-13.8	8.1
$\bar{10}$	21.9	22.0	$\bar{12}$	- 5.9	5.0
$\bar{12}$	-17.8	15.4	$\bar{14}$	12.3	11.8
$\bar{14}$	- 3.4	4.7	$\bar{18}$	- 5.3	5.6
$\bar{16}$	11.9	11.7			
			(h·0·14)		
(h·0·10)			0	16.8	15.6
0	- 9.7	6.1	2	- 7.2	5.9
2	-22.0	22.5	4	- 8.5	9.4
4	20.9	17.2	6	9.9	11.0
6	3.2	4.0	10	- 5.8	8.8
8	-15.2	20.8			
10	6.4	6.2			
12	5.3	6.8			
14	- 5.9	6.0			

Table 11. (Continued)

Indices	$F_{calc.}$	$F_{obs.}$
	8	8
($\bar{h}$·0·14)		
$\bar{2}$	- 4.3	3.0
$\bar{4}$	-15.3	11.5
$\bar{6}$	14.8	11.5
$\bar{8}$	3.9	4.2
$\bar{10}$	-14.6	14.2
$\bar{12}$	5.8	1.0
$\bar{14}$	6.6	7.1
16	- 7.3	5.3
(h·0·16)		
0	10.2	6.4
2	3.8	4.2
4	- 9.0	9.2
8	4.3	6.6
10	- 3.7	1.9
($\bar{h}$·0·16)		
2	-11.6	9.9
6	12.6	11.2
8	- 7.4	6.7
10	- 6.0	5.6
12	9.4	8.9
16	- 5.2	7.7
(h·0·18)		
0	- 5.1	3.0
2	6.9	7.4
4	- 3.8	5.0
($\bar{h}$·0·18)		
$\bar{2}$	- 8.2	7.2
$\bar{4}$	3.4	4.7
$\bar{6}$	3.8	3.0
$\bar{8}$	- 8.9	7.6
$\bar{12}$	5.6	5.9
$\bar{14}$	- 5.1	4.0
($\bar{h}$·0·20)		
$\bar{4}$	6.9	6.8

hk0

Indices	$F_{calc.}$	$F_{obs.}$
	8	8
(h00)		
2	-25.0	18.8
4	-45.4	45.7
6	44.7	38.3
8	4.5	9.3
10	-30.0	32.5
12	13.4	11.8
14	9.2	10.1
16	-11.5	12.5
18	1.1	3.9
(h20)		
0	-64.2	55.6
2	20.9	6.3
4	39.0	39.1
6	-39.2	42.4
8	- 4.0	6.6
10	27.0	33.8
12	-12.1	11.3
14	- 8.4	10.9
16	10.5	13.3

Table 11. (Continued)

Indices	$F_{calc.}$ / 8	$F_{obs.}$ / 8	Indices	$F_{calc.}$ / 8	$F_{obs.}$ / 8
(h40)			(h30)		
0	40.6	35.4	1	41.5	32.7
2	-14.2	9.4	3	11.1	12.2
4	-26.8	26.1	5	-41.0	44.2
6	27.7	31.4	7	16.5	16.9
8	2.9	4.0	9	18.2	23.2
10	-19.8	23.2	11	-19.9	21.1
12	9.0	8.1	15	10.7	14.3
14	6.4	7.5	17	- 5.4	6.7
16	- 8.1	8.3			
(h60)			(h50)		
0	-23.6	17.0	1	-25.8	27.3
2	8.2	5.1	3	- 7.0	5.2
4	15.8	11.3	5	25.7	25.4
6	-16.7	13.0	7	-10.7	9.4
10	12.4	12.2	9	-12.2	12.2
12	- 5.8	5.4	11	13.7	13.1
14	- 4.2	4.3	15	- 7.5	10.2
			17	3.9	3.7
(h80)			(h70)		
0	12.1	9.8	1	14.0	9.2
4	- 8.3	5.0	5	-14.6	11.5
6	8.8	6.4	7	6.0	4.5
10	- 6.7	4.7	9	7.0	7.0
			11	- 8.0	7.3
(h10)					
1	-57.3	56.9			
3	-14.9	19.1			
5	53.6	53.8			
7	-21.0	20.4			
9	-22.9	24.7			
11	24.6	26.6			
15	-12.8	16.6			
17	6.5	7.5			
19	4.6	5.6			

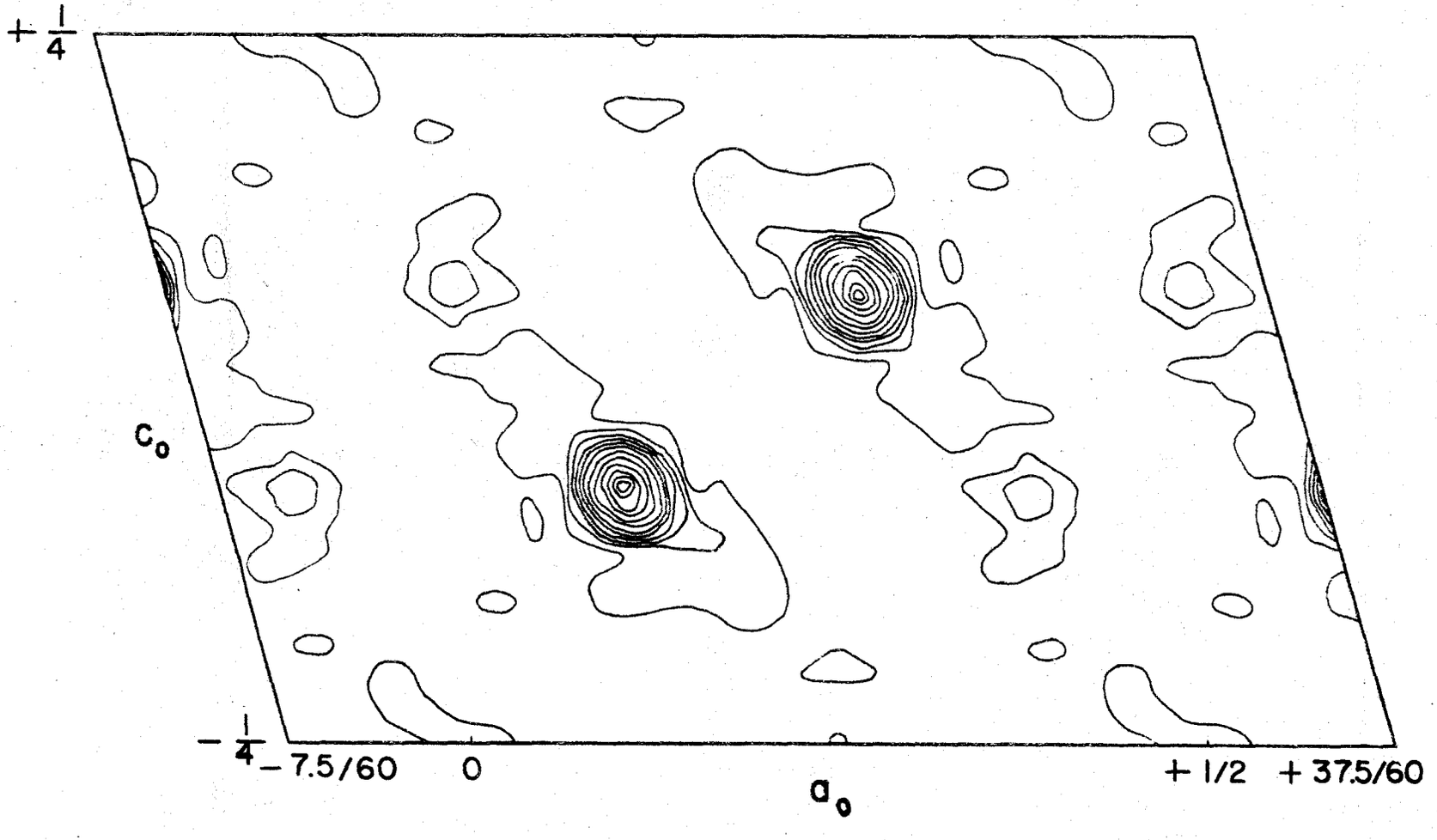

Figure 43. Fourier projection of $Re_2(CO)_{10}$ onto the (010) plane

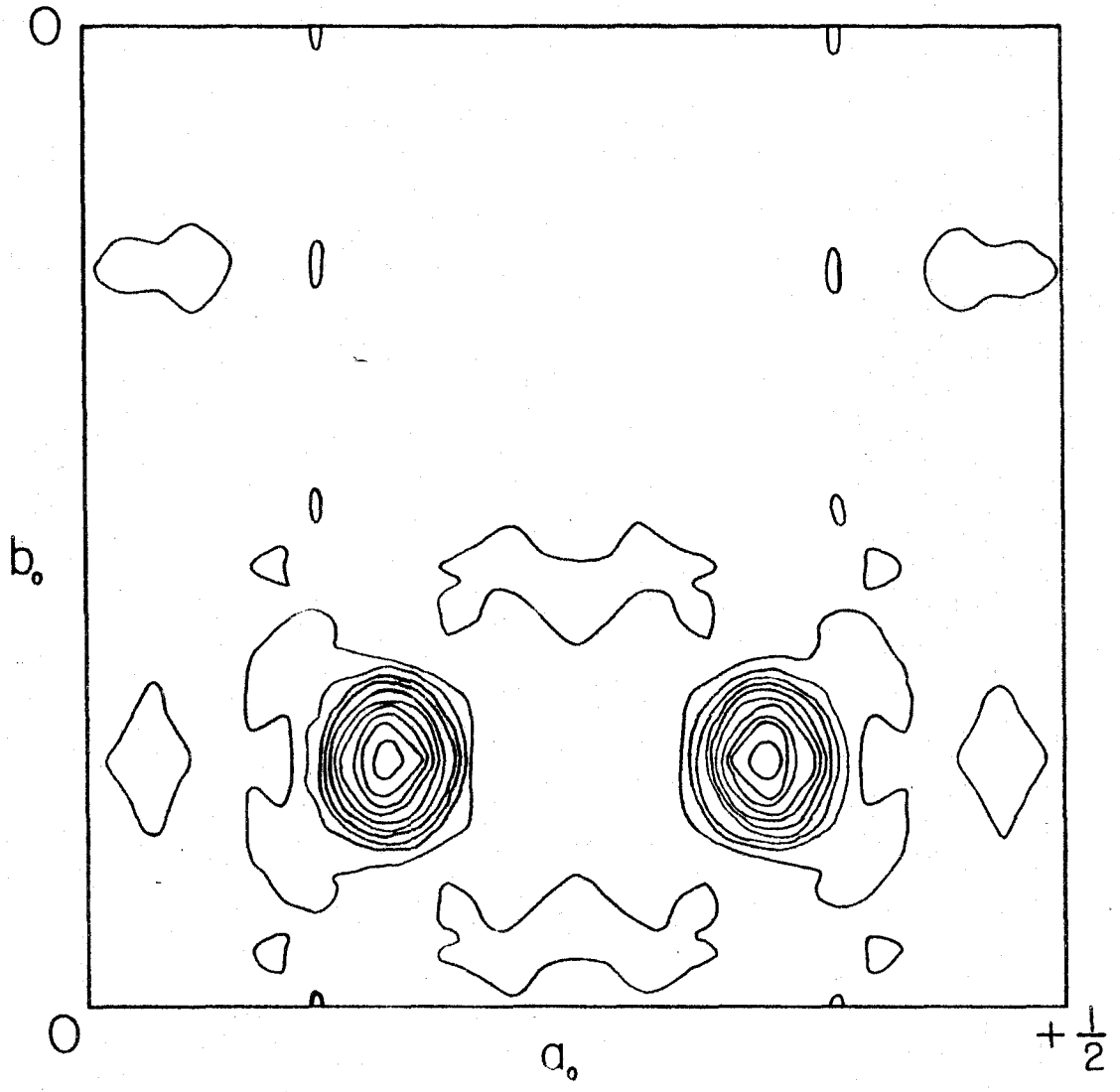

Figure 44. Fourier projection of $Re_2(CO)_{10}$ onto the (001) plane

irradiation. The intensities of the three zones were placed on the same scale by correlation of the axial reflections. The number of independently observed reflections for the (h0ℓ) zone was 115; for the (hk0) zone, 50; and for the (0kℓ) zone, 66. Some three-dimensional data were obtained including the (h1ℓ), (h2ℓ), and (1kℓ) zones. Unfortunately, the crystals either decomposed after a few days in the X-ray beam or disintegrated by cleavage along planes perpendicular to the b_o axis.

Although an intensity distribution study (33) of the (h0ℓ) zone for $Mn_2(CO)_{10}$ favored I2/a, a similar study of the (0kℓ) and (hk0) zones indicated to some extent a non-centrosymmetric distribution.

For the centrosymmetric space group I2/a, for which the symmetry positions are shown in Figure 45, the probable arrangement of the carbon and oxygen atoms in the general eight-fold set gave 33 parameters to be determined. This number was increased to 66 parameters for the space group Ia. Hence, for a first approximation the space group I2/a was assumed. Fortunately, the heavy atom technique and the isomorphism of the Mn and Re compounds greatly simplified the phase determination for each reflection.

Figure 45. Symmetry positions in the space group I2/a

Point positions: $(000;\ \frac{1}{2}\frac{1}{2}\frac{1}{2})+$

4: (a) $000;\ \frac{1}{2}00$ (b) $0\frac{1}{2}0;\ \frac{1}{2}\frac{1}{2}0$

(c) $\frac{1}{4}\frac{1}{4}\frac{1}{4};\ 3/4\ 3/4\ \frac{1}{4}$ (d) $\frac{1}{4}\ 3/4\ \frac{1}{4};\ 3/4\ \frac{1}{4}\frac{1}{4}$

(e) $\frac{1}{4}y0;\ 3/4\ \bar{y}\ 0$

8: (f) $xyz;\ \frac{1}{2}+x,\bar{y},z;$

$\bar{x}\bar{y}\bar{z};\ \frac{1}{2}-x,y,\bar{z};$

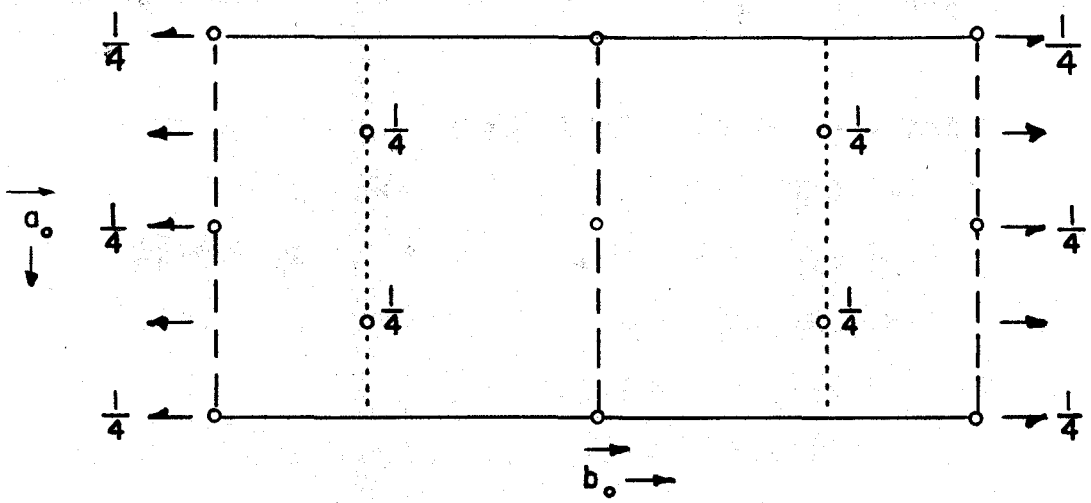
1/4
1/4
1/4
1/4
1/4
1/4
1/4
1/4
1/4
1/4
a₀
b₀

Patterson projections of manganese pentacarbonyl

The Re and Mn positions were assumed to be located in the eight-fold general set (f) given in Figure 45 for I2/a; the Patterson metal-metal vectors which were obtained are as follows:

Vector	Multiplicity	Vector	Multiplicity
$0,0,0$	8		
$\frac{1}{2},\frac{1}{2},\frac{1}{2}$	8		
$2x,2y,2z$	2	$\frac{1}{2}+2x,\frac{1}{2}+2y,\frac{1}{2}+2z$	2
$2\bar{x},2\bar{y},2\bar{z}$	2	$\frac{1}{2}-2x,\frac{1}{2}-2y,\frac{1}{2}-2z$	2
$2x,2\bar{y},2z$	2	$\frac{1}{2}+2x,\frac{1}{2}-2y,\frac{1}{2}+2z$	2
$2\bar{x},2y,2\bar{z}$	2	$\frac{1}{2}-2x,\frac{1}{2}\ \ 2y,\frac{1}{2}-2z$	2
$\frac{1}{2},2y,0$	4	$0,\frac{1}{2}+2y,\frac{1}{2}$	4
$\frac{1}{2},2\bar{y},0$	4	$0,\frac{1}{2}-2y,\frac{1}{2}$	4
$2x,\frac{1}{2},\frac{1}{2}+2z$	4	$\frac{1}{2}+2x,0,2z$	4
$2\bar{x},\frac{1}{2},\frac{1}{2}-2z$	4	$\frac{1}{2}-2x,0,2\bar{z}$	4

For $y=\frac{1}{4}$ these vector positions reduced to a set summarized as follows:

Vector	Multiplicity	Vector	Multiplicity
0,0,0	8		
$\frac{1}{2},\frac{1}{2},\frac{1}{2}$	8		
$2x,\frac{1}{2},2z$	4	$\frac{1}{2}+2x,0,\frac{1}{2}+2z$	4
$2\bar{x},\frac{1}{2},2\bar{z}$	4	$\frac{1}{2}-2x,0,\frac{1}{2}-2z$	4
$\frac{1}{2},\frac{1}{2},0$	8	$0,0,\frac{1}{2}$	8
$2x,\frac{1}{2},\frac{1}{2}+2z$	4	$\frac{1}{2}+2x,0,2z$	4
$2\bar{x},\frac{1}{2},\frac{1}{2}-2z$	4	$\frac{1}{2}-2x,0,2\bar{z}$	4

Both "unsharpened" and "sharpened" Patterson projections of $Mn_2(CO)_{10}$ were produced using IBM equipment. These are shown in Figures 46, 47, 48, 49, and 50. An analysis of the Patterson projections was made using the vector set given above. The only Mn parameters compatible with the analysis were the same as those already found for the Re compound. The Mn-Mn vectors, therefore, unlike the iron-iron vectors in $[Fe(CO)_4]_3$ were easily resolved from the Patterson projections, especially from the "sharpened" Patterson projections.

Structure determination of manganese pentacarbonyl

The intensity data for $Mn_2(CO)_{10}$ were placed on an absolute scale by the application of Wilson's method (43).

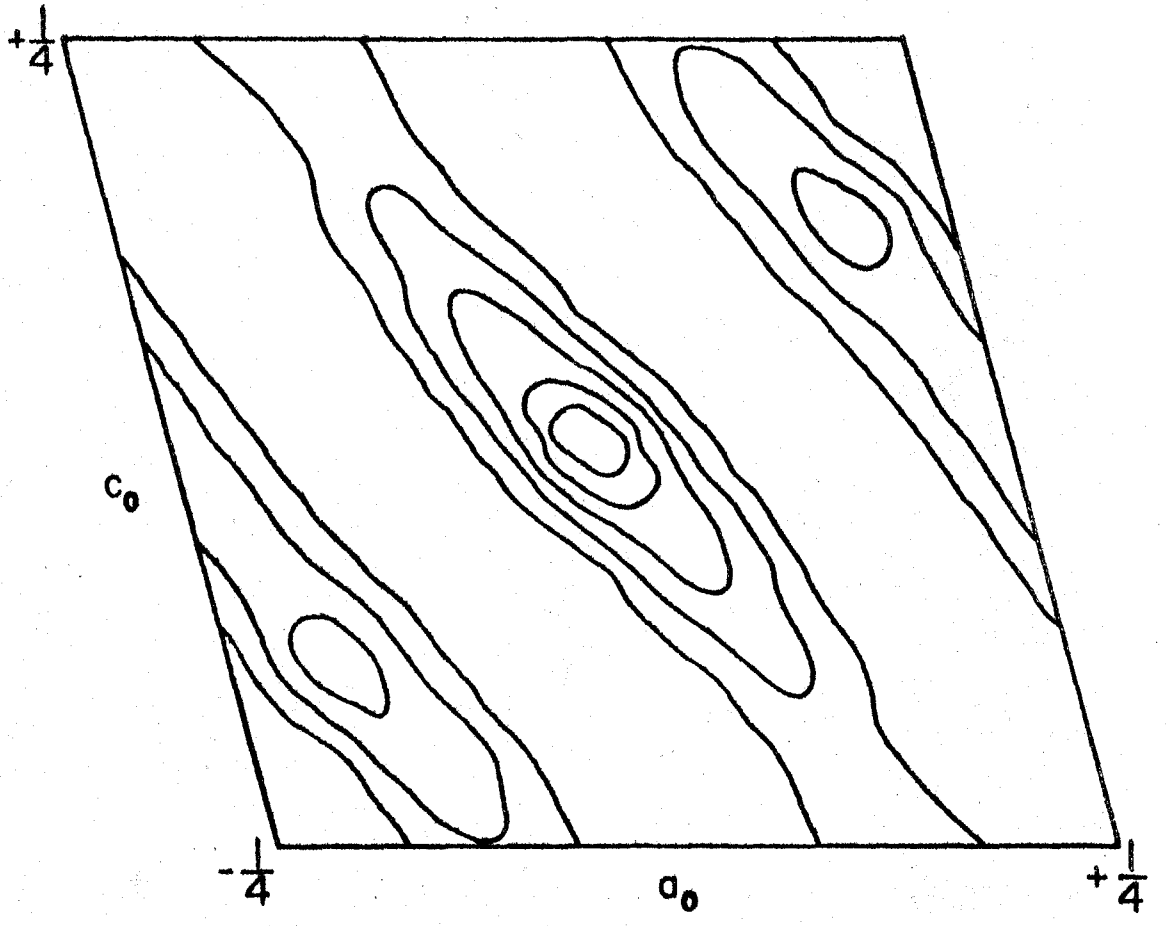

Figure 46. Patterson projection of $Mn_2(CO)_{10}$ onto the (010) plane

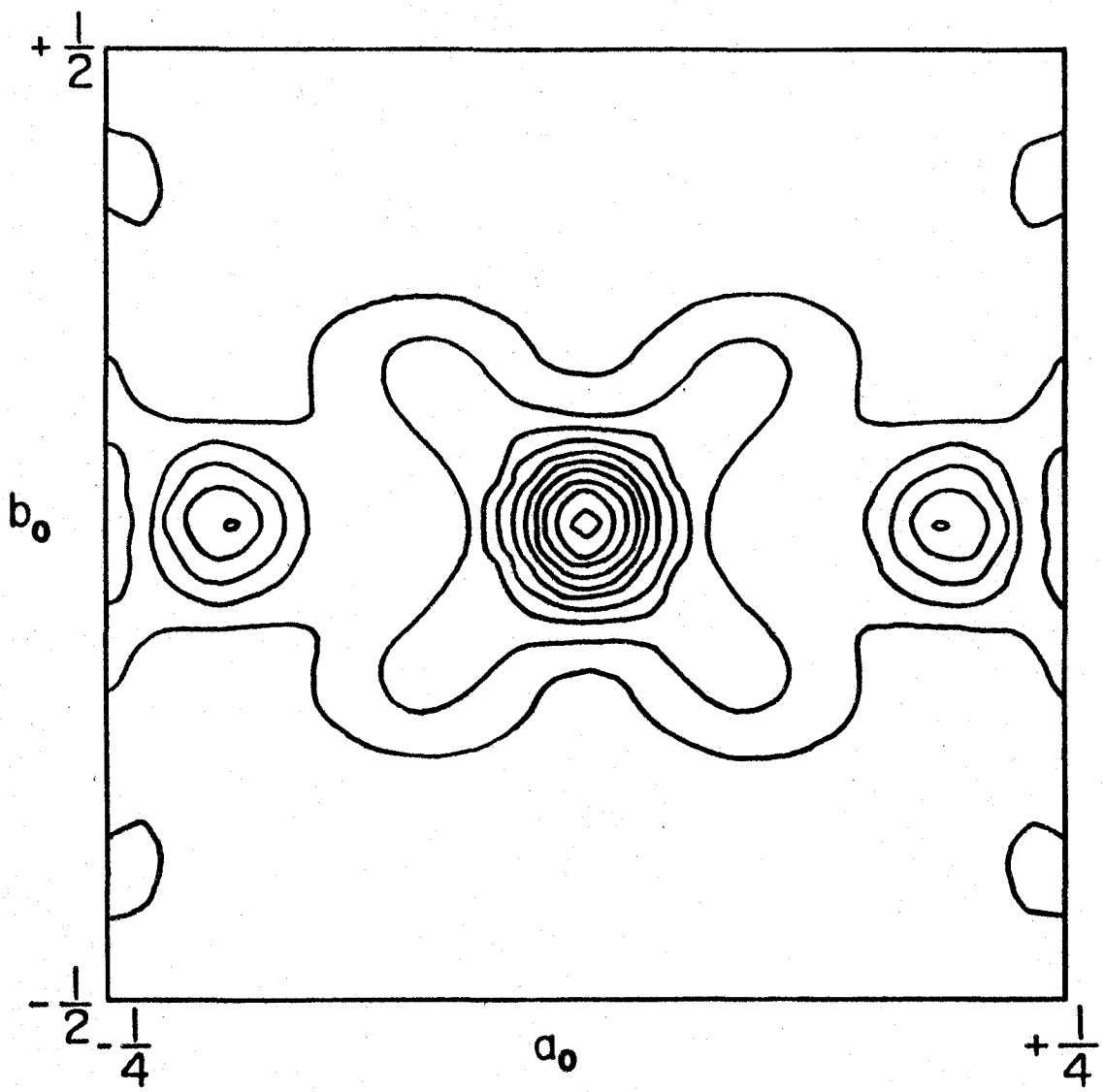

Figure 47. Patterson projection of $Mn_2(CO)_{10}$ onto the (001) plane

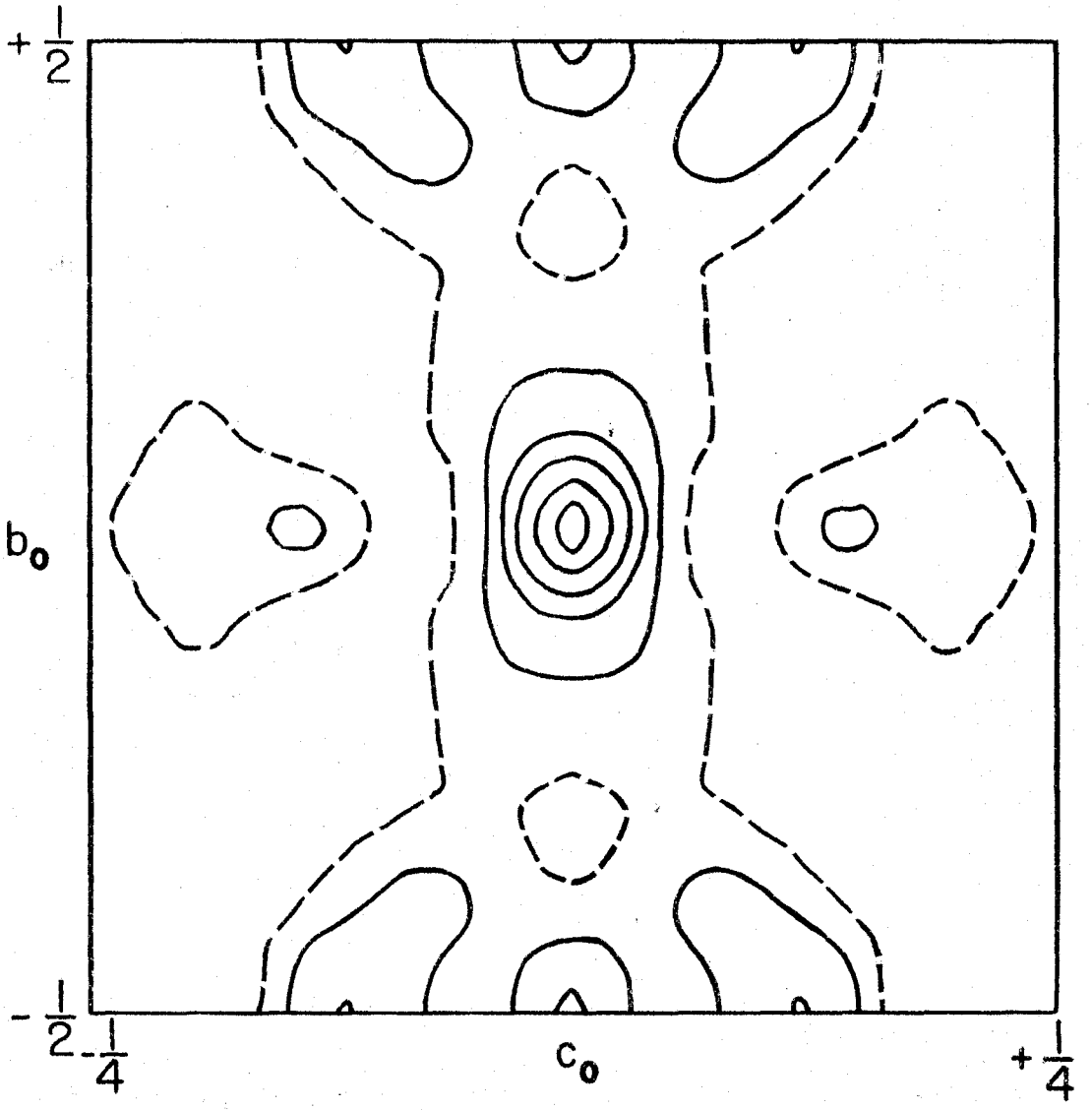

Figure 48. Patterson projection of $Mn_2(CO)_{10}$ onto the (100) plane

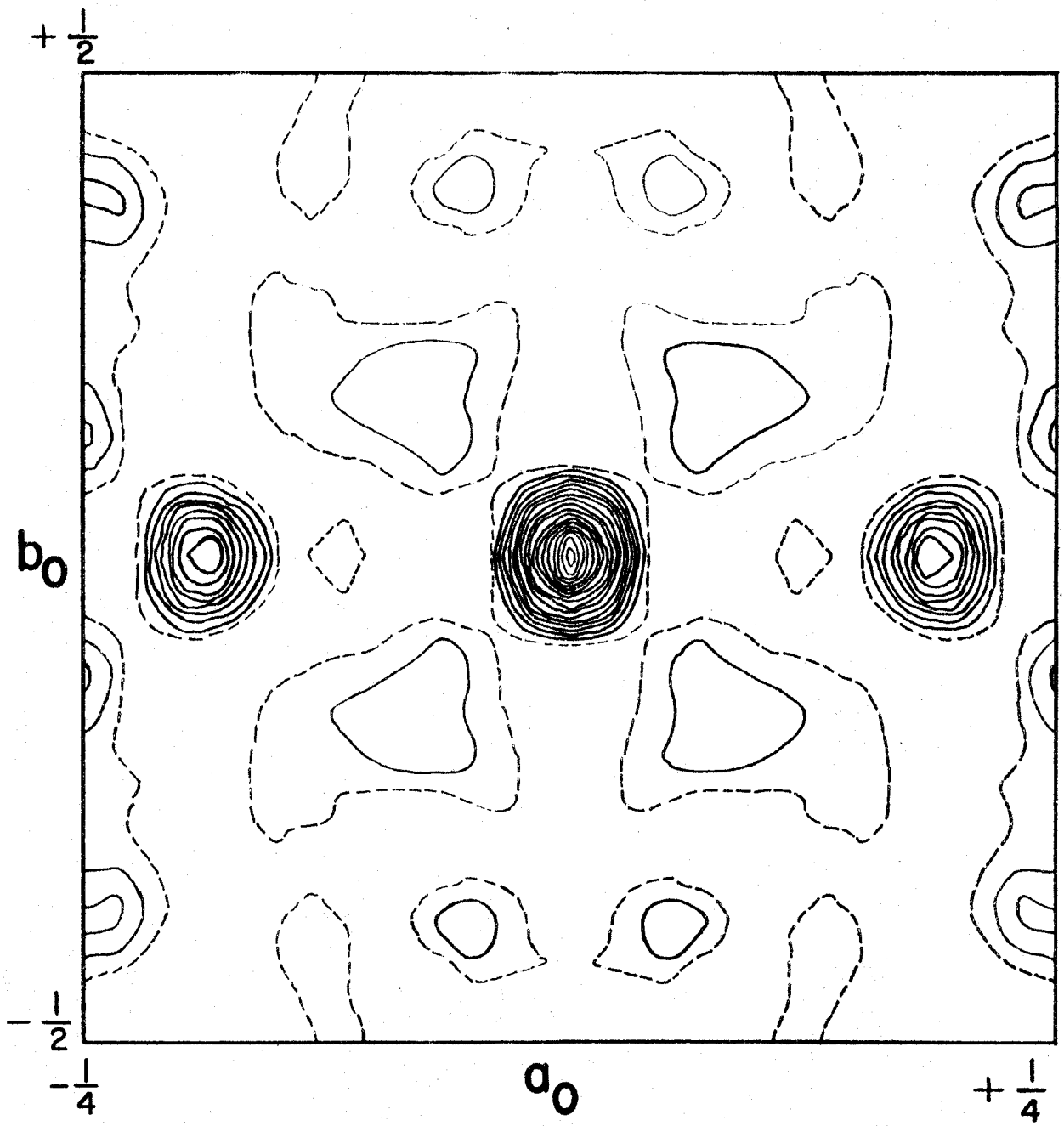

Figure 49. "Sharpened" Patterson projection of $Mn_2(CO)_{10}$ onto the (001) plane

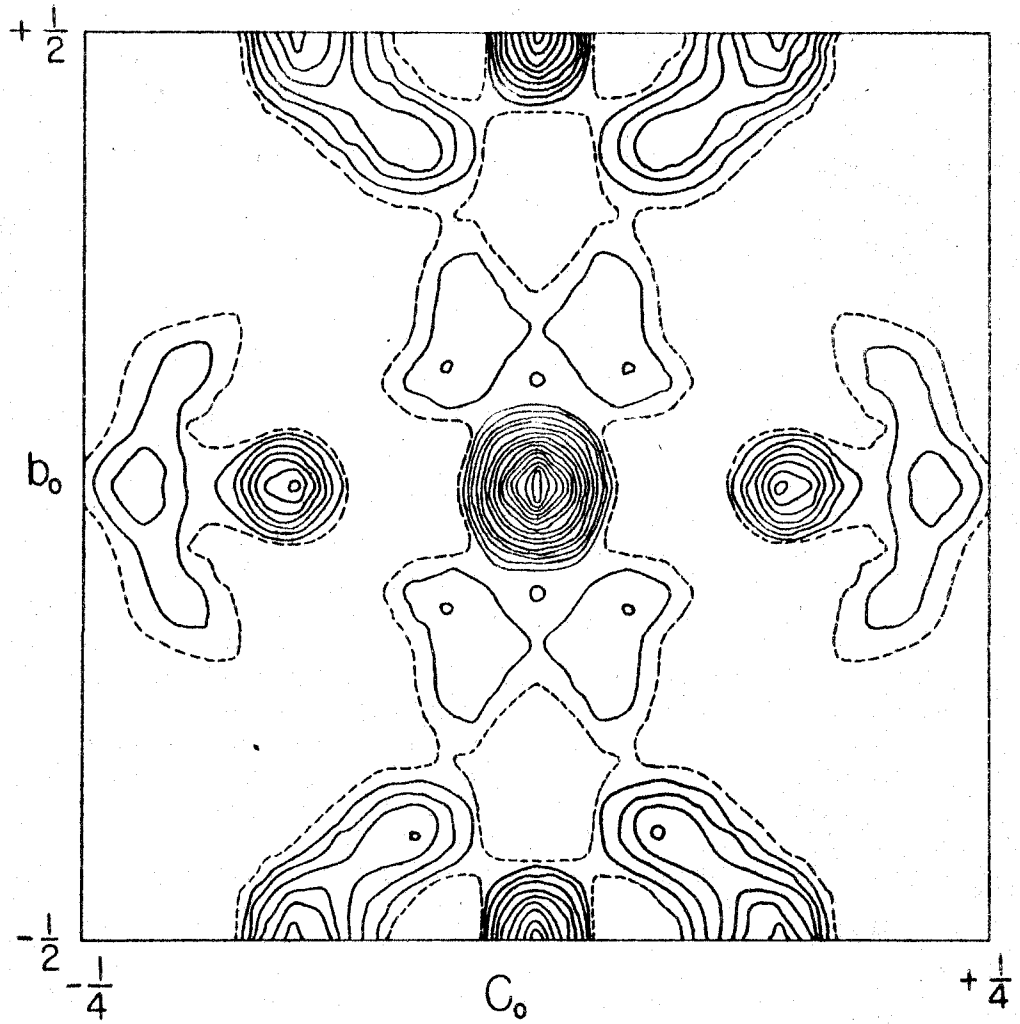

Figure 50. "Sharpened" Patterson projection of $Mn_2(CO)_{10}$ onto the (100) plane

The difference between the observed and temperature-corrected calculated structure factors (i.e. $\Delta F = F_o - F_c^T$) for each reflection of the Re compound was assumed to be the result of the carbon-oxygen contribution. The Mn positions were assumed to be identical with the Re positions, and structure factors were calculated for the (h0ℓ) and (hk0) reflections of $Mn_2(CO)_{10}$. The ΔF obtained for the Re compound was then added to the result. The ΔF ideally should be about the same for both compounds since the compounds are isomorphous. In this way the phases of many more (h0ℓ) and (hk0) reflections were unambiguously determined for the Mn compound. The electron-density Fourier projections of $Mn_2(CO)_{10}$ onto the (010) and (001) planes (the final Fourier projections are shown in Figures 51 and 52) definitely indicated direct metal-metal bonding with two octahedra joined together at a common apex. The end-CO bond was clearly shown to be collinear with the Mn-Mn bond. Moreover, the spacial arrangements of the CO's verified that the correct z parameter for the metal was approximately 0.930. Considerations of the packing due to the CO arrangement as shown by the (h0ℓ) Fourier eliminated the D_{4h} structure (an eclipsed configuration of CO bonds), which was suggested by Cable and Sheline (1), and instead strongly supported a molecular structure of approximately D_{4d} symmetry (a staggered arrangement of

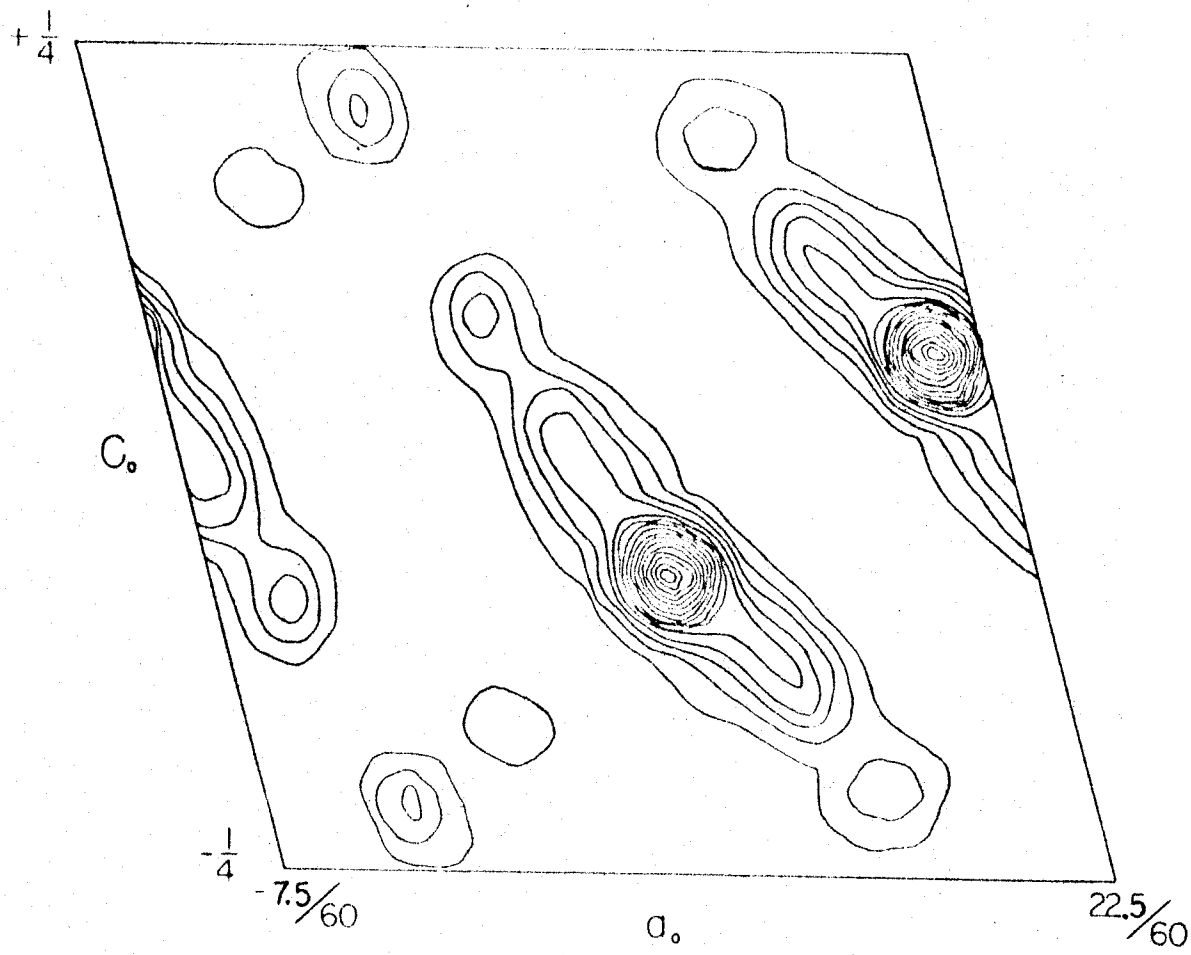

Figure 51. Fourier projection of $Mn_2(CO)_{10}$ onto the (010) plane

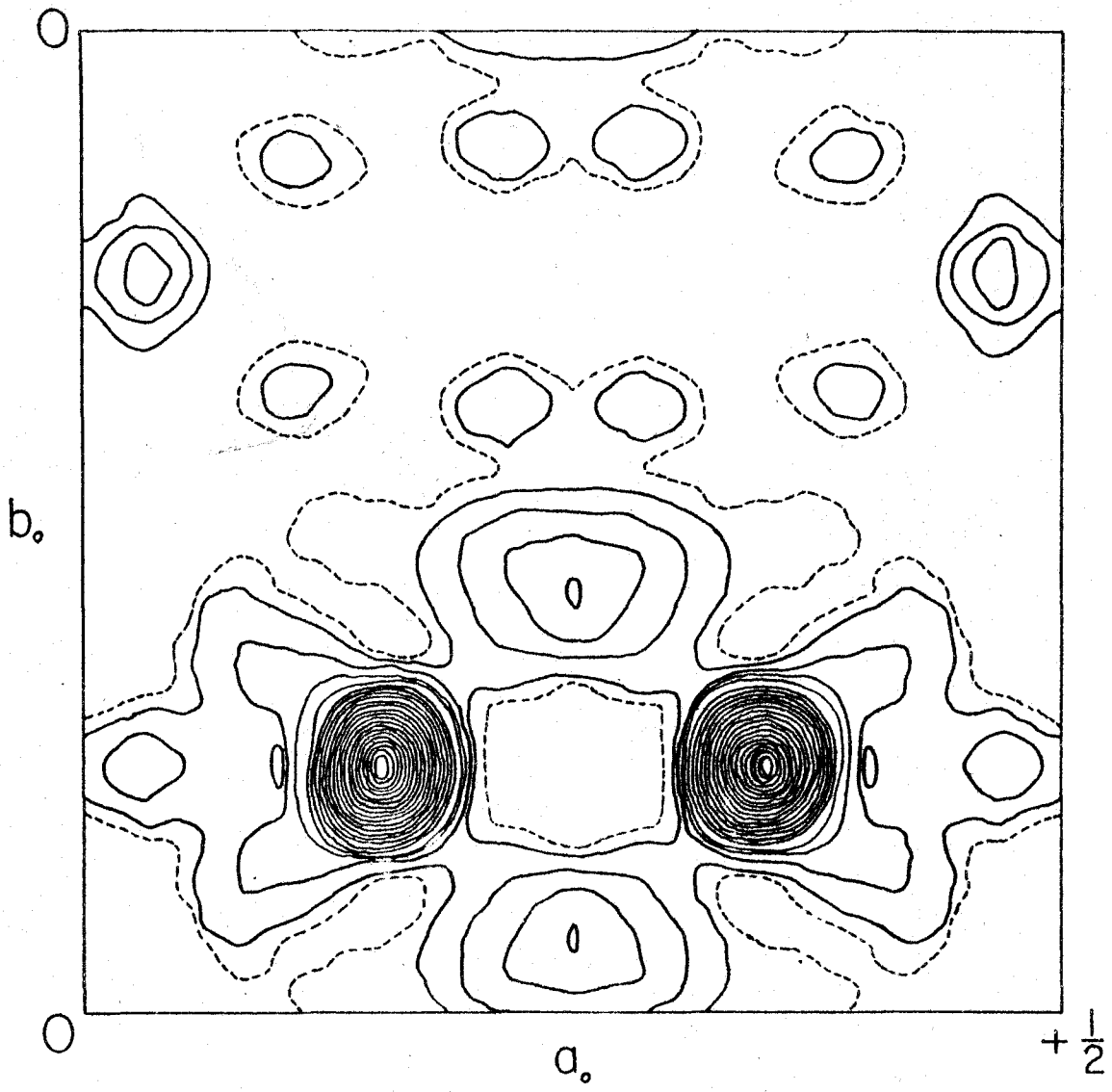

Figure 52. Fourier projection of $Mn_2(CO)_{10}$ onto the (001) plane

CO's). This same conclusion was also reached from the symmetry of the space group Ia.

The reliability index, R(hkℓ), for temperature-corrected structure factors of manganese only was 43.5% for the (hOℓ) zone; 24.4% for the (hkO) zone (observed reflections only). The much lower R value for the (hkO) zone was attributed to the overlapping of the Mn positions or Re positions for $Re_2(CO)_{10}$ on the (001) projection. Temperature-corrected calculated structure factors for all the atoms gave a much lower R value of 26.4% for the (hOℓ) zone and a slightly lower R value of 23.0% for the (hkO) zone.

In order to sharpen the carbon and oxygen peaks, structure factors, $F'_{obs.}$, corresponding to the sum of the carbon-oxygen contributions were obtained by subtraction of the temperature-corrected structure factors, F^T_{Mn}, for the Mn atoms from the observed structure factors (i.e. $F'_{obs.} = F_{obs.} - F^T_{Mn}$). Partial difference Fourier syntheses onto the (010) and (001) planes were computed from the $F'_{obs.}$; only $F'_{obs.}$ reflections to which signs could be assigned were used. The coefficients $F'_{obs.}$ were included for a number of accidentally absent reflections (i.e. for which $F_{obs.} = 0$). The partial difference Fourier projections, shown in Figures 53 and 54, gave much better carbon-oxygen peaks. Temperature-corrected structure factors were calculated from the new

Figure 53. Partial difference Fourier projection of $Mn_2(CO)_{10}$ onto the (010) plane

(The temperature-corrected manganese structure factors have been subtracted from the observed structure factors.)

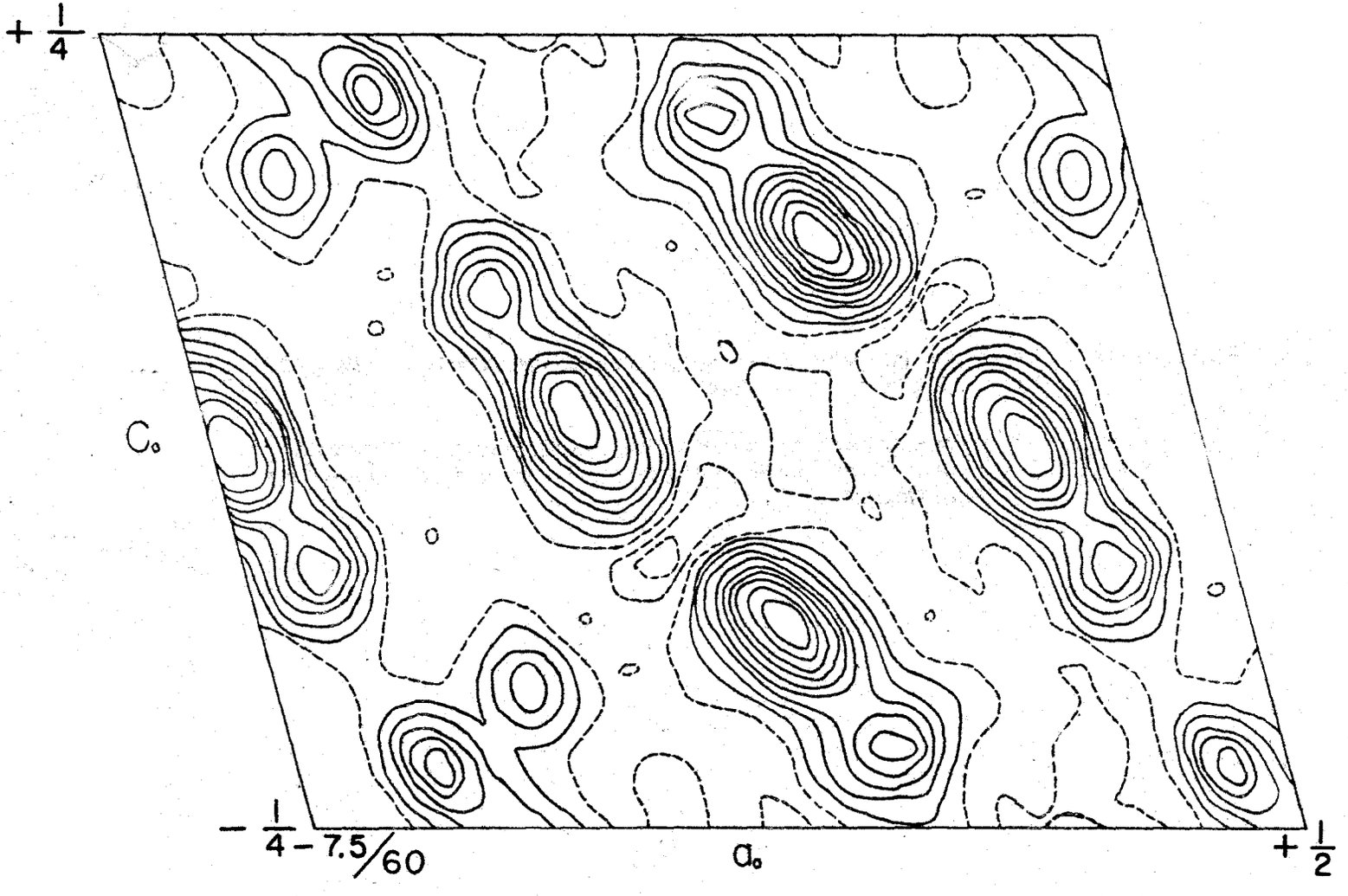
+ 1/4
C₀
1446
− 1/4 − 7.5/60
a₀
+ 1/2

Figure 54. Partial difference Fourier projection of $Mn_2(CO)_{10}$ onto the (001) plane

(The temperature-corrected manganese structure factors have been subtracted from the observed structure factors.)

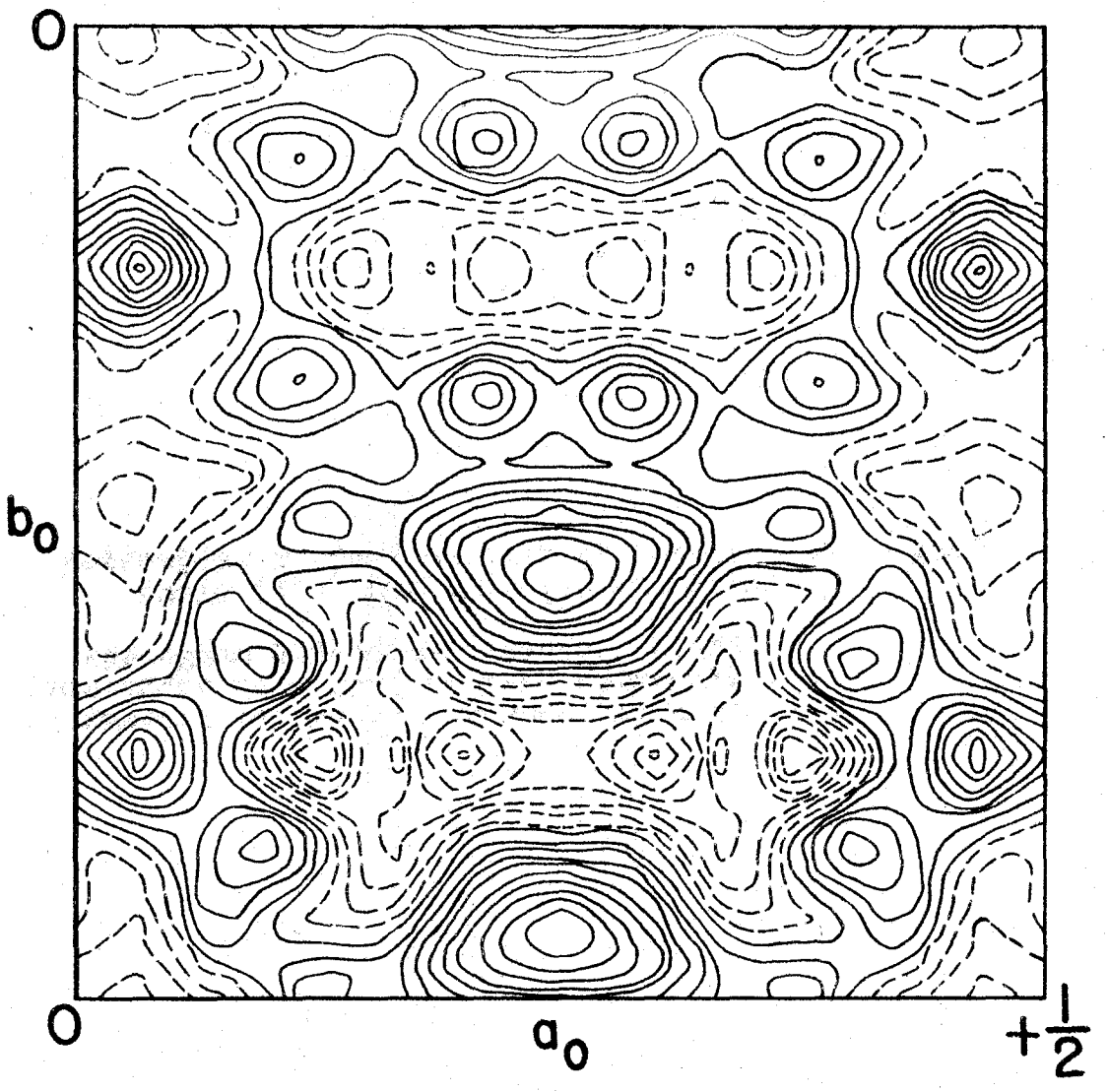
0
b_0
0
a_0
$+\frac{1}{2}$

parameters, and the resulting R(hkℓ) value dropped considerably, to 21.5% for the (h0ℓ) zone and to 21.8% for the (hk0) zone. Several (h0ℓ) and (hk0) difference Fourier syntheses (i.e. $\triangle F = (F_{obs.} - F^{T}_{calc.})$) were computed in an effort to refine the positions, especially the positions of the unresolved atoms. There was evidence on the (010) Fourier difference syntheses of anisotropic thermal motion (36, p. 306; 59) of the apical CO. Refinement of the parameters by difference syntheses reduced the R(hkℓ) value to 20.8% for the (h0ℓ) zone; 20.9% for the (hk0) zone.

The (0kℓ) data for the Mn compound were analyzed next. During the refinement of the parameters obtained from the (h0ℓ) and (hk0) data, several (0kℓ) structure factor sets were calculated, but the correlation of the (0kℓ) data with the observed data was still poor. The observed (0kℓ) data included 29 reflections with the indices k = 2n + 1, ℓ = 2n + 1, for which a Mn parameter of y = 0.250 gave no structure factor contribution (i.e. the odd k indices are dependent only on the carbon-oxygen parameters for $y_{Mn} = \frac{1}{4}$). For these reflections the R(0kℓ) value was 53.5% compared to an R(0kℓ) value of 24.8% for the indices k = 2n, ℓ = 2n. The total R value for the (0kℓ) zone was 33.4% at this point. This indicated that the Mn positions were probably not located exactly at y = 0.250, and an arbitrary value y = 0.237 for

Mn(1), C(1), and O(1) decreased the total R(0kℓ) value to 25.2% (for the even k indices R = 21.9%; for the odd k indices R = 32.9%). The phases of most of the calculated structure factors were then assigned to the observed structure factors, and the resulting (100) Fourier electron-density projection (Figure 55) revealed a shift of the y parameter for Mn(1), C(1), and O(1) to y = 0.232. Temperature-corrected structure factor calculations for the three zones based on an analysis of the Fourier projections and difference syntheses together with the known intramolecular distances gave a final R(hkℓ) value of 20.5% for the (h0ℓ) zone; 20.0% for the (hk0) zone; and 22.2% for the (0kℓ) zone. Table 12 lists the final parameters obtained for $Mn_2(CO)_{10}$. A comparison of the observed and temperature-corrected calculated structure factors for the three principal zones of $Mn_2(CO)_{10}$ is given in Table 13.

Description of the structures

The isomorphous compounds, $Re_2(CO)_{10}$ and $Mn_2(CO)_{10}$, have been found to possess a molecular structure of approximately D_{4d} symmetry. Each metal atom is octahedrally coordinated by five CO ligands and the other metal atom in

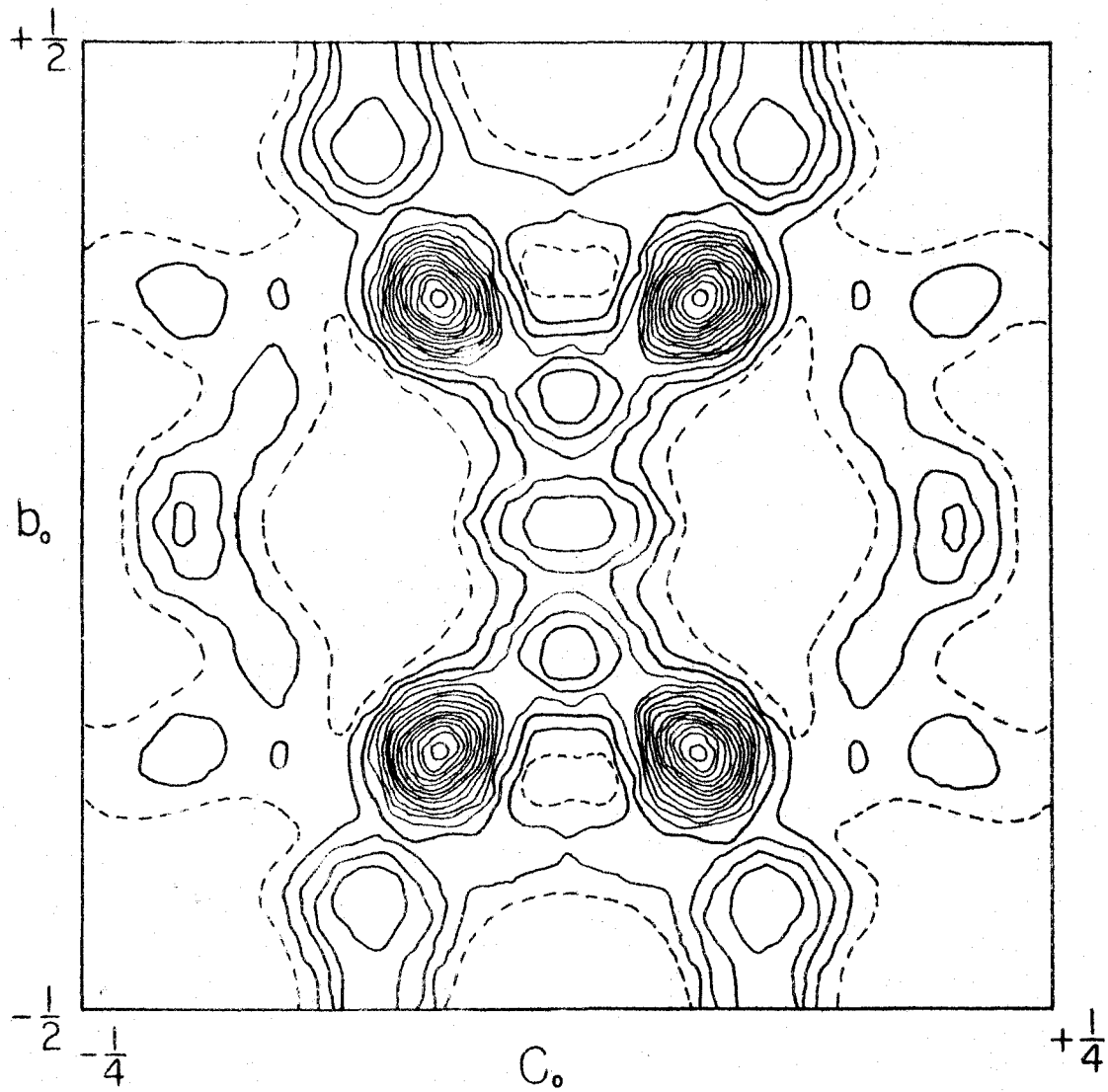

Figure 55. Fourier projection of $Mn_2(CO)_{10}$ onto the (100) plane

Table 12. Eight-fold sets of parameters for $Mn_2(CO)_{10}$

Atom	Parameters		
	x	y	z
Mn	0.1538	0.2322	0.9322
C(1)	0.0352	0.2322	0.8388
O(1)	0.9635	0.2322	0.7905
C(2)	0.1075	0.3363	0.0300
O(2)	0.0787	0.4017	0.0858
C(3)	0.2158	0.1167	0.8523
O(3)	0.2517	0.0450	0.8030
C(4)	0.1352	0.0083	0.9733
O(4)	0.1224	0.8607	0.0000
C(5)	0.1870	0.4683	0.9017
O(5)	0.2130	0.6188	0.8783

Table 13. Comparison of the observed and temperature-corrected calculated structure factors for the three principal zones of $Mn_2(CO)_{10}$

Indices	$F_{calc.}$	$F_{obs.}$	Indices	$F_{calc.}$	$F_{obs.}$
	h0l				
(00l)			(40l)		
2	177.6	156.8	0	-94.6	87.4
4	-33.0	34.2	2	-412.9	346.0
6	-49.9	57.9	4	-169.6	136.3
8	-69.2	59.8	6	26.1	25.5
12	14.1	13.8	8	65.2	71.8
14	36.2	29.8	10	29.1	24.2
16	9.8	11.2	16	-16.3	13.4
(20l)			($\bar{4}$0l)		
0	-115.7	93.3	2	-55.4	50.5
2	105.0	103.8	4	46.8	61.9
4	174.6	166.8	6	96.8	66.9
6	34.6	34.6	8	-34.9	13.0
10	-35.3	40.3	12	-57.3	45.6
12	-27.3	32.9	14	-24.2	17.5
14	-12.9	15.2	20	10.2	9.0
18	14.5	10.2			
			(60l)		
($\bar{2}$0l)			0	41.4	46.3
2	-192.6	157.4	2	79.4	50.6
4	-48.3	41.9	4	-39.7	43.4
6	8.3	11.9	6	-114.2	113.1
8	- 3.5	21.4	8	- 7.9	18.3
10	49.2	41.1	12	18.6	23.3
12	50.4	46.2	14	17.3	20.2
16	-22.4	16.6			
18	-11.9	12.3	($\bar{6}$0l)		
20	- 7.9	7.4	2	45.9	36.0
			4	32.4	15.5
			8	-88.9	70.0
			10	-64.5	62.6
			14	16.1	13.4
			16	26.4	20.7
			18	15.6	14.2

Table 13. (Continued)

Indices	$F_{calc.}$	$F_{obs.}$	Indices	$F_{calc.}$	$F_{obs.}$
(80ℓ)			($\overline{12}$·0·ℓ)		
0	31.2	14.6	2	36.8	41.7
2	69.5	65.6	4	27.7	26.6
4	136.3	125.4	6	-15.9	11.8
6	69.0	46.6	8	-38.8	25.8
10	-33.6	39.4	10	-10.6	15.0
12	-15.3	21.2	12	-10.1	11.4
16	6.7	7.0	14	- 2.1	8.8
			16	16.8	14.5
($\overline{8}$0ℓ)			18	5.2	9.0
2	-24.7	42.2			
4	-51.8	43.7	(14·0·ℓ)		
6	- 9.3	20.0	0	9.8	11.4
10	73.2	47.9	2	27.1	23.6
12	22.4	18.4	4	1.9	15.5
18	-14.8	13.2	10	-11.5	15.1
20	- 4.7	5.8			
			($\overline{14}$·0·ℓ)		
(10·0·ℓ)			4	-35.4	31.5
0	-58.8	44.8	6	-37.1	31.0
2	4.1	17.6	8	- 1.5	10.2
6	4.0	12.2	10	2.8	8.9
8	49.1	46.1	12	26.1	25.2
10	8.0	15.2	14	15.4	12.1
14	- 6.4	10.7			
			(16·0·ℓ)		
($\overline{10}$·0·ℓ)			0	-18.2	21.4
2	-24.8	17.2	6	12.2	13.9
4	-11.9	13.0			
6	65.8	59.8	($\overline{16}$·0·ℓ)		
8	55.1	50.1	2	-10.8	12.7
10	5.1	10.7	8	11.9	12.6
12	-10.6	11.3	14	- 8.5	9.8
14	-36.1	28.5	16	- 5.9	4.4
16	-14.8	14.9			
			(18·0·ℓ)		
(12·0·ℓ)			2	- 6.8	7.0
0	- 1.0	11.8			
4	-30.8	30.3			
6	-43.1	41.4			
8	-24.1	16.1			
12	10.2	14.7			

Table 13. (Continued)

Indices	$F_{calc.}$	$F_{obs.}$
$(\bar{1}8 \cdot 0 \cdot l)$		
2	15.1	14.6
4	10.9	14.0
10	-17.2	14.7
12	-11.5	8.7
hk0		
(h00)		
2	-115.7	93.3
4	-95.0	87.4
6	41.7	46.3
8	31.7	14.6
10	-60.2	44.8
12	- 1.1	11.8
14	10.2	11.4
16	-19.4	21.4
(h10)		
1	-166.4	144.5
3	-46.9	40.2
5	104.7	95.4
7	-24.0	33.4
9	-28.4	38.5
11	60.8	63.0
15	-23.4	26.2
(h20)		
0	-127.0	108.4
2	-79.5	60.6
4	76.6	78.7
6	-104.7	91.0
10	53.6	63.4
12	- 2.6	21.1
16	27.1	29.7
(h30)		
1	53.1	61.4
3	17.3	34.8
5	-129.4	104.6
7	34.1	43.6
9	38.3	41.2
11	-20.1	35.8
15	17.3	22.8
17	-11.0	11.6
(h40)		
0	62.4	50.8
4	-25.1	41.6
6	82.2	79.0
10	-61.4	53.5
12	16.3	17.8
16	- 9.2	13.6
(h50)		
1	-80.2	66.8
5	46.1	45.7
7	- 9.2	23.2
9	-26.4	22.5
11	23.7	25.6
15	- 6.1	16.0
(h60)		
0	-44.7	35.0
6	-20.0	29.7
8	10.1	10.1
10	22.0	25.2
12	- 9.0	15.5
(h70)		
5	-18.6	21.4
7	9.9	10.1
9	4.1	14.3
11	-12.0	15.0
(h80)		
0	29.1	26.4

Table 13. (Continued)

Indices	$F_{calc.}$	$F_{obs.}$	Indices	$F_{calc.}$	$F_{obs.}$
	0kℓ		(08ℓ)		
			0	28.7	23.5
(00ℓ)			2	12.4	9.2
2	177.6	153.4	4	- 4.1	7.5
4	-33.0	35.8	6	- 4.3	5.8
6	-49.9	58.6	12	2.6	3.3
8	-69.2	61.4	(01ℓ)		
12	14.1	13.0	1	12.1	12.2
14	36.2	26.6	3	16.4	18.7
16	9.8	10.6	5	145.9	118.6
18			7	15.9	16.0
			9	-16.8	23.8
(02ℓ)			11	- 2.7	7.1
0	-126.8	118.2	13	5.4	6.5
2	-49.6	54.6	15	13.1	10.2
6	54.6	62.0			
8	70.9	69.8	(03ℓ)		
10	40.0	40.9	1	-20.7	20.8
12	-15.5	18.1	3	- 6.6	10.9
14	-36.1	31.4	5	15.3	17.4
16	-14.9	14.6	7	9.2	10.6
			9	7.3	20.8
(04ℓ)			13	-26.9	14.0
0	62.3	48.1	15	-10.1	8.6
2	- 0.6	17.4			
4	13.4	7.1	(05ℓ)		
6	-50.4	51.1	1	51.9	41.9
8	-77.9	58.6	3	- 2.9	10.9
10	-14.2	10.2	5	-20.8	17.8
12	3.0	12.2	7	-36.9	22.8
14	12.8	15.0	9	-10.0	13.3
16	4.1	8.6	15	6.9	10.9
			17	1.6	5.1
(06ℓ)					
0	-44.4	30.3	(07ℓ)		
4	23.9	20.1	1	-16.6	13.6
6	32.7	28.3	5	11.1	13.0
8	31.6	24.6	7	23.5	17.4
10	7.2	7.1	9	12.0	8.9
12	- 7.2	10.6			
14	-14.2	14.3	(09ℓ)		
16	- 5.2	5.4	1	13.5	10.9
			3	4.6	6.8
			7	- 5.6	6.2

such a way that the CO groups are arranged in a staggered configuration.

If strict D_{4d} symmetry is assumed, the orientation of the molecule in the unit cell is limited by the molecular packing. The Mn-CO angle of tilt from an $a_o c_o$ plane which contains two dimeric Mn atoms should be approximately 22.5° for two of the four CO ligands on each Mn atom (i.e. one ligand should be tipped upward 22.5° and the other one tilted downward 22.5°). The other CO's would then be at an angle of approximately 67.5° with respect to the same $a_o c_o$ plane. Unfortunately, the four CO's in the plane approximately normal to the Mn-Mn bond appeared to be considerably distorted. The Mn-CO(2) and Mn-CO(3) bonds, which seemed to be clearly resolved on the (010) Fourier projection, are apparently bent inward toward the other half of the molecule. The angle of tilt from the $a_o c_o$ plane containing the Mn atoms was found to be approximately 23° for the Mn-CO(2) bond; about 29° for the Mn-CO(3) bond.

These values are not completely reliable as the calculations are based up on the validity of the centrosymmetric space group, I2/a, which limits the dimeric Mn atoms to the same $a_o c_o$ plane. If the non-centrosymmetric space group Ia is assumed, a y-tilt of the Mn-Mn bond is possible. Evidence for a slight y-tilt is shown in Figure 56 which

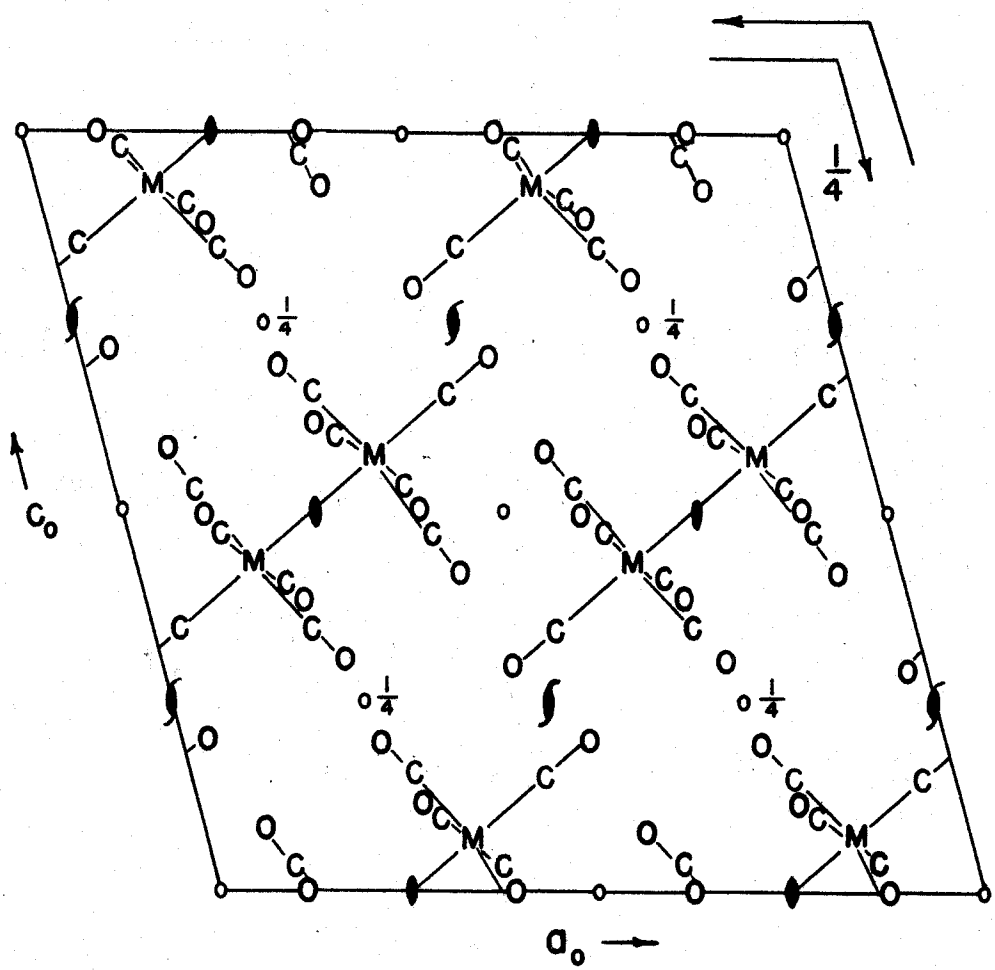

Figure 56. The arrangement of the $Mn_2(CO)_{10}$ molecules in the unit cell

illustrates the projection of the dimeric molecules of $Mn_2(CO)_{10}$ onto the (010) plane. The (001) difference Fourier projections for $Mn_2(CO)_{10}$, which were used in a partial refinement of the parameters, also suggested a slight y-tilt of the molecule. The positions given in Table 12 would then approximately represent the average of the non-centrosymmetric positions. The approximation of centrosymmetry would account for at least part of the apparent distortion of the dimeric molecule. Verification of the orientation of the metal-metal bonds can be obtained easily from (0kℓ) data for $Re_2(CO)_{10}$; unfortunately X-ray pictures of this zone were not taken.

The large overlap of the atoms on the three principal projections made it difficult to refine the two-dimensional data. With the possible exception of the apical carbonyl group the CO parameters are still not known with sufficient accuracy for the intramolecular M-C and M-O distances and angles to be meaningful. The Re-Re and Mn-Mn distances and the intramolecular distances involving the apical carbonyl group are given in Table 14, along with the nearest intermolecular oxygen-oxygen distances. The latter distances involve the four CO ligands around each Mn atom which are approximately normal to the Mn-Mn bond. Because of the large overlap of atoms, these distances are subject to

Table 14. Intramolecular and intermolecular bond distances for $Re_2(CO)_{10}$ and $Mn_2(CO)_{10}$

Atoms	Distance Å
Re-Re	3.02
Mn-Mn	2.93
Mn-C(1)	1.88
Mn-O(1)	2.95
C(1)-O(1)	1.08
O(4)-O(5)'	3.00
O(2)-O(1)'	3.31
O(3)-O(3)'	3.30

considerable error. Again, it should be pointed out that the calculations are based upon the assumption of the validity of the space group I2/a. The experimental carbon-oxygen distance of 1.08 Å, determined for the apical carbonyl of $Mn_2(CO)_{10}$, compared to a carbon-oxygen distance of 1.15 ± 0.04 Å (Table 2) for the other known mononuclear metal carbonyls certainly indicates that the y-tilt of the molecules, if any, is small. The purpose of this investigation has been to ascertain the molecular structure of the compounds, and the R values indicate that the structure is

correct except for refinement. It is hoped that three dimensional data for $Mn_2(CO)_{10}$ can be obtained from which a least squares refinement can be made on a computer of sufficient capacity.

Infrared spectral analysis

The infrared spectra of the rhenium and manganese carbonyls in solution and in the gaseous and solid (KI pellet) states, have been found to be substantially identical. Three strong absorption bands observed in the 2000 $cm.^{-1}$ region were assigned as carbonyl stretching frequencies (18; 19), and two absorption bands around 600 $cm.^{-1}$ were designated as metal-carbon stretching frequencies (19). Cotton, Liehr, and Wilkinson (19) eliminated the D_{4h} and D_{4d} configurations as probable structures, since the number of metal-carbon frequencies should equal the number of CO frequencies, and this was apparently inconsistent with the observed spectra. They predicted only two infrared-active terminal carbonyl bands for the D_{4h} and D_{4d} models, whereas three such bands were observed. However, a vibrational analysis by this author revealed that the D_{4h} structure requires three terminal CO stretching frequencies, 2 A_{2u} and 1 E_u, and the D_{4d} structure gives 2 B_2 and 1 E_1. If it is

assumed that the method of local symmetry (19) is valid in this case (i.e. the CO groups on each metal are non-interacting vibrational groups), the C_{4v} symmetry around each Re (or Mn) atom, also, leads to the prediction of three infrared-active CO stretching frequencies, 2 A_1 and 1 E_1.

Thus, the infrared data are consistent with the D_{4d} structure except for the two MC stretching frequencies. Since separations in the 600 cm.$^{-1}$ region are small, it may be that they are not resolved. If the method of local symmetry is not valid, any lower molecular symmetry would be expected to produce more than the three CO stretching bands observed. For example, a vibrational analysis of a structure of molecular symmetry D_{2h}, formed by staggering the four CO's about one Mn atom at an angle other than 45° or 90° with respect to the four CO's around the other Mn atom, predicts four infrared-active CO stretching frequencies ($2B_{1u}$, 1 B_{2u}, and 1 B_{3u}). The infrared spectrum of $Mn_2(CO)_{10}$ in the solid state, therefore, suggests that the molecular structure has approximately D_{4d} symmetry.

Discussion

The structures of $Re_2(CO)_{10}$ and $Mn_2(CO)_{10}$ represent the first real evidence for a direct metal-metal bond between

two transition metals in which the metal-metal bond alone permits the existence of the dimer. The X-ray structure determination of nickel dimethylglyoxime by Godycke and Rundle (60) led them to postulate that weak Ni-Ni bonds (a nickel-nickel distance of 3.25 Å was found) were responsible for the extreme insolubility of the nickel compound as compared to that of the copper derivative. The partial X-ray structural analysis of nickel bis-acetylacetone by Bullen (61) indicated a trimeric molecule composed of nearly collinear Ni-Ni bonds approximately 2.8 Å apart. The proximity of the nickel atoms implied an interaction between neighboring nickels or the less likely possibility of a bridging of neighboring nickels by other atoms.

A dimer structure held together by only a metal-metal link was postulated for the isomorphous compounds, $(C_5H_5W)_2(CO)_6$ and $(C_5H_5Mo)_2(CO)_6$. Wilson and Shoemaker (62) found the shortest metal-metal distance from Patterson projections to be 3.24 Å in the tungsten compound and 3.28 Å in the molybdenum compound. The prediction of a metal-metal bond was in accord with the observed diamagnetism of these compounds and with the molecular weights in solution. Fourier projections onto the (010) plane were reported to indicate a model in which each half of the molecule possesses three carbonyl groups and one cyclopentadienyl group

disposed around the metal atom in very roughly tetrahedral directions with only a metal-metal bond linking the two halves.

The rhenium and manganese carbonyl structures also substantiate the assumption of direct metal-metal bonding proposed to account for the observed diamagnetism of $Fe_2(CO)_9$ and $Co_2(CO)_8$. Jensen and Asmussen (63) made the alternative suggestion that the diamagnetism of $Fe_2(CO)_9$ could be accounted for by resonance between bridge structures without the assumption of a metal-metal bond. Ewens (64), however, indicated that such resonance states are equivalent to a metal-metal bond with ionic character.

In the $Mn_2(CO)_{10}$ crystal there definitely is restricted rotation about the metal-metal bond as evidenced by the close intermolecular oxygen-oxygen distances between the neighboring dimers. Carbonyl-carbonyl repulsions probably explain the fact that the molecular symmetry in the crystal is D_{4d} rather than D_{4h} (i.e. a staggered arrangement of CO's rather than an eclipsed arrangement).

It is difficult to understand the large distortion that appears to exist in the dimer. The distortion, however, seems to be the result of the influence of the CO's of neighboring molecules, since the M-CO's are bent such that the intermolecular oxygen-oxygen distances have been increased. Hence, the packing seems to distort the molecule instead of

the undistorted molecules determining the packing. Of course, as previously mentioned in the "Description of the structures", the calculations and Fourier projections are based on the validity of the centrosymmetric space group I2/a. There is some indication of a slight y-tilt of the dimeric molecule. This might well account for at least part of the apparent distortion.

The Re-Re and Mn-Mn distances computed from their covalent radii (8) are 2.34 Å and 2.56 Å respectively as compared to the experimentally determined metal-metal distances of 2.93 Å and 3.02 Å. The large difference can be attributed mainly to the negative charge localized on the metal atom through coordination with the CO ligands. If it is assumed that each of the five terminal CO ligands contributes two bonding electrons to the metal, a symmetrical sharing of electrons would result in a formal charge of -5 on each metal atom. Certainly, the actual charge distribution is not nearly so extreme as such a simple schematic picture indicates. Some partial double bond character is obtained by utilization of the d-orbital electrons of the metal in π-bonding. On the basis of a carbonyl bond order of about 2.5 Cable and Sheline (1) predicted a metal-carbon bond order of about 1.5 for the metal carbonyls. However, King and Lippincott (65) from a calculation of the Fe-C and Ni-C bond

energies estimated a M-C bond order only slightly larger than one, since the Fe-C and Ni-C bond energies were found to be of the same order of magnitude as the bond energies calculated for Sn-C and Pb-C.

A bridge carbonyl group which is assumed to contribute only one bonding electron to each metal atom removes a greater negative charge from the metal atom than a terminal carbonyl group. The formal charge contribution to the central metal is zero for a bridge carbonyl bond and -1 for a terminal carbonyl bond. This probably accounts for an iron-iron distance of 2.46 Å in the $Fe_2(CO)_9$ structure (2) which is only slightly greater than the calculated covalent Fe-Fe distance of 2.33 Å (8). For $Fe_2(CO)_9$ the formal charge on each iron is -3.

No doubt a much better representation of the electronic charge distribution is given by the molecular orbital description, in that such a treatment permits the delocalization of the so-called "bonding electrons" contributed to the metal by the ligands. However, the qualitative picture as given by the "closed electronic shell rule" appears to be in agreement with the experimental results, and furthermore for the rhenium and manganese compounds there still must be some negative charge localized on the metal in order to increase the M-M distance by approximately half an Angstrom over the distance predicted from the covalent radii.

It is somewhat surprising that $Re_2(CO)_{10}$ and $Mn_2(CO)_{10}$ do not possess bridge carbonyl bonds, expecially since other dimers of Re have been suggested to possess bridge-type bonds. Hieber and Schuster (66) have prepared the compound potassium-μ-dioxohydrogen-octacarbonyl dirhenate by the reaction of $Re(CO)_5$ or $Re(CO)_5Cl$ with KOH. A bridge structure (given below) which can be viewed as the junction of

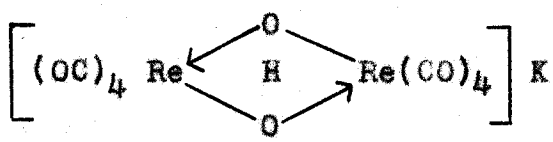

two octahedra at an edge (D_{2h} symmetry) was formulated for the compound. The proton was postulated to form a H-bridge between the two oxygens.

A corresponding thiophenol complex was prepared with a similar configuration predicted, as given below:

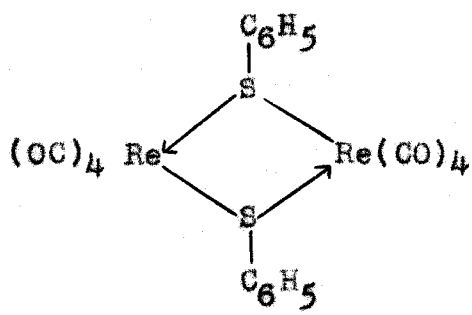

In both cases an inert gas structure was assumed to account for the observed diamagnetism. From precedent the formulation of bridge bonds for the above two compounds is much

more reasonable than a structure similar to that of $Re_2(CO)_{10}$. An infrared spectral analysis of both compounds should quickly substantiate the correct structure.

An explanation for the occurrence of such an unusual type of structure for $Re_2(CO)_{10}$ and $Mn_2(CO)_{10}$ is, of course, difficult without some type of quantitative calculations. A reasonable but admittedly crude attempt toward the prediction of the molecular structures of other polynuclear carbonyls has been made by Cable and Sheline (1). A molecular orbital type calculation as employed by Richardson (67) might be very illuminating in the determination of the electron distribution between the metal and ligand in $Mn_2(CO)_{10}$. The D_{4d} coordination should be of sufficient molecular symmetry to make the calculation tractable. One feature of the Richardson procedure is a requirement of self-consistency with respect to charge distribution. Hence, a more "educated guess" of the actual charge distribution can be made and compared with the "formal charge estimation" as given by the "closed electronic shell rule". An appraisal of the amount of π-bond interaction would also help clarify the conflicting estimates of the M-C bond character.

SUMMARY

A structural investigation of the polynuclear metal carbonyls--$[Fe(CO)_4]_3$, $Re_2(CO)_{10}$, and $Mn_2(CO)_{10}$--was undertaken by means of X-ray diffraction techniques.

Iron tetracarbonyl was found to possess monoclinic symmetry; the lattice constants based on a primitive unit cell are:

$$a_p = 8.88\ \text{Å} \qquad b_p = 11.33\ \text{Å} \qquad \beta_p = 97^\circ\ 9.5' \qquad c_p = 8.35\ \text{Å}$$

There are six $Fe(CO)_4$ species per unit cell. Systematic absences indicated the centrosymmetric space group $P2_1/n$, which would ordinarily require a trimeric molecule to possess a center of symmetry, and would thereby make the iron atoms collinear. The iron atoms should then be located easily by Patterson projections, but this did not turn out to be the case.

The structural analysis proceeded through a complete three-dimensional Patterson and three-dimensional "sharpened" Patterson. The only model at all compatible with this analysis and other evidence, involves a disordered structure in which the iron atoms are arranged at the corners of an equilateral triangle and are randomly placed in each unit cell

in one of two orientations approximately differing from one another by a rotation of 60° about the three-fold axis. An iron-iron distance of approximately 2.75 to 2.85 Å was found. The configuration of the CO ligands still needs to be determined, since it was very difficult to find the carbonyl positions due to the disorder in the structure. An infrared spectral study strongly indicated some association of the carbonyls in the solid state, although the solution spectrum definitely suggested that there are no bridge carbonyls. Three-dimensional Fourier sections computed on X-RAC at Pennsylvania State University appeared to verify the trigonal model, although additional three-dimensional work will be needed to confirm the proposed structure.

On the other hand, no linear arrangement of iron atoms, including the widely accepted D_{2d} structure, can explain the three-dimensional Pattersons. In fact, none of the structures postulated on the basis of the theory of directed valence or on an analysis of the vibrational spectrum appear to be correct.

The rhenium and manganese carbonyls were found to be monoclinic and isomorphous. The lattice constants are as follows:

$$Re_2(CO)_{10}$$

$$a_o = 14.70\ \text{Å},\ b_o = 7.15\ \text{Å},\ c_o = 14.91\ \text{Å},\ \beta = 106^\circ$$

$Mn_2(CO)_{10}$

$a_o = 14.16$ Å, $b_o = 7.11$ Å, $c_o = 14.67$ Å, $\beta = 105^o$

The space group was determined to be I2/a or Ia; there are four dimers per unit cell. A two-dimensional Fourier analysis of $Mn_2(CO)_{10}$ revealed that each manganese atom is octahedrally coordinated by five CO ligands and a direct metal-metal bond with another manganese atom, in such a way that the dimeric molecule possesses approximately D_{4d} symmetry (staggered CO's).

These compounds are the first polynuclear carbonyls known to be held together by metal-metal bonds, and, moreover, represent the first real evidence of a metal-metal bond in transition metal complexes stabilized by only metal-metal bonds.

An explanation was given for the long metal-metal distances found (i.e. 2.93 Å for $Mn_2(CO)_{10}$ and 3.02 Å for $Re_2(CO)_{10}$) for the compounds as compared to the relatively short iron-iron distance of 2.46 Å for $Fe_2(CO)_9$.

An infrared vibrational analysis was found to be in agreement with the D_{4d} structure. The molecular structures indicate the validity of the assumption that the 1800 $cm.^{-1}$ infrared absorption band is due to bridge carbonyl absorption,

since, as the infrared analysis predicted, no absorption bands were observed in this region.

However, there are limitations in the utilization of the partial vibrational infrared analysis in predicting the correct internuclear structures for the metal carbonyls. Although other investigators used such a method to postulate different rhenium and manganese structures, no one predicted the correct structure. The failure of this spectral method in predicting internuclear structures for iron tetracarbonyl is another example of its limitations.

LITERATURE CITED

1. Cable, J. W. and Sheline, R. K., Chem. Revs., 56, 1 (1956).

2. Powell, H. M. and Ewens, R. V. G., J. Chem. Soc., 1939, 286.

3. Brockway, L. O., Ewens, R. V. G., and Lister, M. W., Trans. Faraday Soc., 34, 1350 (1938).

4. Rudorf, W. and Hofmann, V., Z. physik. Chem., B 28, 351 (1935).

5. Ewens, R. V. G. and Lister, M. W., Trans. Faraday Soc., 35, 681 (1939).

6. Ladell, J., Post, B., and Fankuchen, I., Acta Cryst., 5, 795 (1952).

7. Brockway, L. E. and Cross, P. C., J. Chem. Phys., 3, 828 (1935).

8. Pauling, L., J. Am. Chem. Soc., 69, 542 (1947).

9. Sheline, R. K. and Pitzer, K. S., J. Am. Chem. Soc., 72, 1107 (1950).

10. Hawkins, N. J., Mattraw, H. C., Sabol, W. W., and Carpenter, D. R., J. Chem. Phys., 23, 2422 (1955).

11. Shufler, S. L., Sternberg, H. W., and Friedel, R. A., J. Am. Chem. Soc., 78, 2687 (1956).

12. Friedel, R. A., Wender, I., Shufler, S. L., and Sternberg, H. W., J. Am. Chem. Soc., 77, 3951 (1955).

13. Crawford, B. L. and Cross, P. C., J. Chem. Phys., 6, 525 (1938).

14. Margoshes, M., Fillwalk, F., Fassel, V. A., and Rundle, R. E., J. Chem. Phys., 22, 381 (1954).

15. Sheline, R. K., J. Am. Chem. Soc., 72, 5761 (1950).

16. Cotton, F. A., Liehr, A. D., and Wilkinson, G., J. Inorg. Nucl. Chem., 1, 175 (1955).

17. Cable, J. W., Nyholm, R. S., and Sheline, R. K., J. Am. Chem. Soc., 76, 3373 (1954).

18. Brimm, E. O., Lynch, M. A., and Sesny, W. J., J. Am. Chem. Soc., 76, 3831 (1954).

19. Cotton, F. A., Liehr, A. D., and Wilkinson, G., J. Inorg. Nucl. Chem., 2, 141 (1956).

20. Sheline, R. K., J. Am. Chem. Soc., 73, 1615 (1951).

21. Hieber, W., Muhlbauer, F., and Ehmann, E. A., Ber., 65, 1090 (1932).

22. Klemm, W., "Inorganic Chemistry", Part 2, Office of Millitary Government for Germany, Field Information Agencies, Technical, British, French, United States, 1948.

23. Freudlich, H. and Cuy, E. J., Ber., B 56, 2264 (1923).

24. Berkman, S. and Zocher, H., Z. physik. Chem., 124, 318 (1926).

25. Cutforth, H. G. and Selwood, P. W., J. Am. Chem. Soc., 65, 2414 (1943).

26. Hieber, W. and Becker, E., Ber., 63B, 1405 (1930).

27. Brill, R. Z., Z. Krist., 77, 36 (1931).

28. Klemm, W., Jacobi, H., and Tilk, W., Z. anorg. u. allgem. Chem., 201, 1 (1931).

29. Sidgwick, N. W. and Bailey, R. W., Proc. Roy. Soc. (London), 144A, 521 (1934).

30. Florio, J. and Rundle, R. E., Private communication, Department of Chemistry, Iowa State College (1951).

31. Speyer, E. and Wolf, H., Ber., 60, 1424 (1927).

32. Hieber, W., Z. anorg. Chemie, 204, 165 (1932).

33. Howells, E. R., Phillips, D. C., and Rogers, D., Acta Cryst., 3, 210 (1950).

34. Lu, C., Rev. Sci. Instr., 14, 331 (1943).

35. Patterson, A. L., Phys. Rev., 46, 372 (1934).

36. Lipson, H. and Cochran, W., "The Determination of Crystal Structures", Vol. 3, G. Bell and Sons Ltd., London, 1953.

37. James, R. W., "The Optical Principles of the Diffraction of X-Rays", Vol. 2, G. Bell and Sons Ltd., London, 1954.

38. "Internationale Tabellen zür Bestimmung von Kristallstrukturen", Rev. Ed., Band 1, Gebrüder Borntraeger, Berlin, 1935.

39. Berghuis, J., Haanappel, M., Potters, M., Loopstra, B. O., MacGillavry, C. H., and Veenendaal, A. L., Acta Cryst., 8, 478 (1955).

40. Pepinsky, R., "Computing Methods and the Phase Problem in X-Ray Crystal Analysis", X-Ray Crystal Analysis Laboratory, The Pennsylvania State College, State College, Pennsylvania, 1952.

41. Takeuchi, Y. and Pepinsky, R., Unpublished research, Department of Physics, Pennsylvania State University (1956).

42. Robertson, J. M. and Shearer, H. M., Nature, 177, 885 (1956).

43. Wilson, A. J., Nature, 150, 152 (1942).

44. Booth, A. D., "Fourier Technique in X-Ray Organic Structure Analysis", University Press, Cambridge, 1948.

45. Shufler, S. L., Sternberg, H. W., and Friedel, R. A., Unpublished research, Bureau of Mines, Synthetic Fuels Research Branch, Bruceton, Pennsylvania (1956).

46. Wilkinson, G. and Cotton, F. A., Unpublished research, Chemistry Department, Massachusetts Institute of Technology (1956).

47. Harker, D. and Kasper, J. S., Acta Cryst., 1, 70 (1948).

48. Grison, E., Acta Cryst., 4, 489 (1951).

49. Sayre, D. M., Acta Cryst., 5, 60 (1952).

50. Cochran, W., Acta Cryst., 5, 65 (1952).

51. Zachariasen, W. H., Acta Cryst., 5, 68 (1952).

52. Hamilton, C. W., Acta Cryst., 8, 199 (1955).

53. Schaeffer, R., Private communication, Department of Chemistry, Iowa State College (1956).

54. Lund, E. W., Acta Chem. Scand., 8, 1378 (1954).

55. Hendriks, S. B., Z. Krist., 84, 85 (1933).

56. Hassel, O. and Vihovde, E. H., Acta Chem. Scand., 7, 1164 (1953).

57. Hieber, W. and Fuchs, H., Z. anorg. u. allgem. Chem., 248, 256 (1941).

58. Schuh, R., Z. anorg. u. allgem. Chem., 248, 276 (1941).

59. Jeffrey, G. A. and Cruickshank, D. W. J., Quart. Revs. (London), 7, 335 (1953).

60. Godycke, L. E. and Rundle, R. E., Acta Cryst., 6, 487 (1953).

61. Bullen, G. J., Nature, 177, 537 (1956).

62. Wilson, F. C. and Shoemaker, D. P., Naturwissenschaften, 43, 57 (1956).

63. Jensen, K. A. and Asmussen, R. W., Z. anorg. Chem., 252, 233 (1944).

64. Ewens, R. V. G., Nature, 161, 530 (1948).

65. King, F. T. and Lippincott, E. R., J. Am. Chem. Soc., 78, 4192 (1956).

66. Hieber, W. and Schuster, L., Z. anorg. u. allgem. Chem., 285, 205 (1956).

67. Richardson, J. W., Ph.D. Thesis, Iowa State College Library (1956).

ACKNOWLEDGEMENTS

The author's indebtedness to Dr. R. E. Rundle for his interest, suggestions, and encouragement cannot be adequately expressed. The author is deeply grateful for having had the privilege of being guided by one whose research outlook is that of a true scientist.

The author wishes to thank Dr. R. Pepinsky and his staff at Pennsylvania State University for the use of their computing facilities and also for their helpful suggestions concerning iron tetracarbonyl.

The valuable assistance of Mr. Etsuro Ishishi in the work involving rhenium and manganese carbonyls is gratefully appreciated. Thanks are due to Mr. F. H. Hollenbeck for his aid in the calculations and the drawing of the many projections. Last, but not least, the author wishes to acknowledge the work of his wife, June, in helping assemble this thesis.